Technical Report: 026511-3-T

MICROWAVE PROPAGATION THROUGH CULTURAL VEGETATION CANOPIES

Ahad Tavakoli
Kamal Sarabandi
Fawwaz T. Ulaby

JPL Contract C-958437 (NASA Prime)
Principal Investigator: Fawwaz T. Ulaby

July, 1991

ABSTRACT

MICROWAVE PROPAGATION THROUGH CULTURAL VEGETATION CANOPIES

The need to understand the interaction of microwaves with vegetation canopies has markedly increased in recent years. This is due to advances made in remote sensing science, microwave technology, and signal processing circuits. One class of the earth's vegetation cover is man-made canopies, such as agricultural fields, orchards, and artificial forests. Contrary to natural vegetation terrain, location, spacing, and density of plants in a man-made vegetation canopy are deterministic quantities. As a result, the semi-deterministic nature of cultural vegetation canopies violate the random assumption of the radiative transfer theory and leads to experimented results that are in variance with model calculations. Hence, an alternative approach is needed to model the interaction of microwaves with such canopies.

This thesis examines the propagation behavior through a canopy of corn plants. The corn canopy was selected as a representative of cultural vegetation canopies that are planted in parallel rows with an approximately fixed spacing between adjacent plants. Several experimental measurements were conducted to determine the transmission properties of a corn canopy in the 1-10 GHz range. The measurements which included horizontal propagation through the canopy as well as propagation at oblique incidence, were performed for defoliated canopies and for canopies with leaves.

Through experimental observations and model development, the propagation behavior was found to be strongly dependent on the wavelength and the path length. At a wavelength in the neighborhood of 20 cm, for example, it was found that scattering by the

stalks was coherent in nature for waves propagating horizontally through the canopy, which necessitated the development of a coherent-field model that uses Bragg scattering to account for the observed interference pattern in the transmitted beam. As the wavelength is made shorter, the semi-random spacing between plants becomes significant relative to the wavelength, thereby destroying the coherent properties of the propagating field, in which case propagating wave becomes partially incoherent in nature.

Because of the short path lengths associated with oblique propagation through the canopy, Bragg scattering need not be considered and a much simpler formulation was found to provide good agreement with experimental observations.

TABLE OF CONTENTS

LIST OF FIGURES

Figure

LIST OF TABLES

Table

CHAPTER I

INTRODUCTION

1.1 Background

The need to understand the interaction of electromagnetic waves with vegetation canopies has markedly increased in recent years. Sensors mounted on spaceborne platforms offer enormous scientific potential for studying the earth's surface on a global scale that was impossible before. Electromagnetic sensors operating in various parts of the electromagnetic spectrum have been used for numerous applications. The more common instruments operate in the optical, thermal-infrared, millimeter, and microwave regions of the electromagnetic spectrum. Each band of the spectrum provides new information about the target by virtue of its spectral properties.The ability of microwave energy to penetrate clouds over a wide range of frequencies has made microwave remote sensing an attractive tool for observing the Earth's surface [Ulaby, *et al.*, 1982]. A device operating in the microwave region of the spectrum has the all-weather capability that is not shared by others. Microwaves can penetrate a variety of land-covers, thus providing subsurface information about the illuminated target. Furthermore, because radars provide their own source of illumination, incidence angle and polarization are additional parameters that can be used along with frequency to retrieve information about the earth's surface. Monitoring the Earth's vegetation cover is one of the objectives of todays microwave remote sensing research, which has been examined by several researchers [Bush and Ulaby, 1978; Eyton,

1979; Brisco and Protz, 1980]. Agricultural applications of microwave remote sensing include crop classification, and quality and quantity prediction of the final yield.

Besides remote sensing applications, horizontal wave propagation over the earth's surface has also been of interest to researchers. With increased use of communication devices, line of sight propagation of microwaves through forested areas has gained increased consideration [Brown and Curry, 1980; Low, 1988]. Additionally, information about plant biomass and other features of the vegetation canopies can be obtained by measuring horizontal wave propagation through forests [Stutzman, *et al.*, 1979]. In order to utilize all these potentials, an understanding of the interaction between microwave energy and vegetation canopies is necessary.

1.2 Models of the Earth's Vegetation Canopies

Earth's vegetation cover can be classified into two groups, natural terrain and man-made canopies. Location, spacing, and density of plants in a natural vegetation cover tend to be random in character. On the other hand, in man-made vegetation canopies such as agricultural fields, orchards, and artificial forests, location, spacing, and density of plants are deterministic quantities.

The randomness in natural vegetation covers provides justification for treating the vegetation canopy as a statistically homogeneous medium and using random media approaches to model propagation through and backscatter from vegetation-covered areas. Traditionally, all volume scattering models developed for vegetation cover have considered the canopies to be random in character. Solution of scattering from random media can be pursued in a number of ways. Continuous and discrete random-medium techniques are the two major approaches that are used to model natural vegetation canopies. In the continuous case, the vegetation canopy is modeled by assuming that its dielectric constant ε (x,y,z) is a random variable whose moments are known [Fung and Ulaby, 1978; Fung, 1979; Lee and

Kong, 1985]. The analysis of the problem is carried out in two ways, the wave approach [Lang, 1981; Eom and Fung, 1984] and the radiative transfer approach [Tsang and Kong, 1978; Tsang, *et al.*, 1985; Ulaby, *et al.*, 1986; Ulaby, *et al.*, 1990]. If the density of scatterers in the medium is low, single-scattering theory is applied to model the wave-vegetation interaction [Engheta and Elachi, 1982; Lang and Sidhu, 1983; Karam, *et al.*, 1987].

Models for man-made vegetation canopies are also needed for situations where the location and density of plants are deterministic quantities, with some random fluctuations. Many cultural vegetation canopies are planted in a row arrangement. For example, row spacing is fixed, but within a given row the orientation, size and location of the constituent particles could be either random or deterministic. For such a vegetation cover, which includes orchards, row crops, plantations, and artificial forests, the random-medium techniques may not be applicable over the entire microwave spectrum. We need a hybrid model that treats the scattering problem in a semi-random fashion. That is, the electromagnetic interaction between the constituent particles within a row can be obtained using random or nonrandom-media techniques, but the interaction between the periodic rows should be treated deterministically. So far, no report has been found that takes this deterministic or semi-deterministic characteristic of man-made vegetation covers into consideration in model development.

Most vegetation canopies are composed of trunks (or stalks), branches and leaves. A model representation of each plant constituent is needed to be employed in scattering models. In the literature, leaves are usually assumed to be small dipoles, spheres, or planar dielectric disks, and stalks, trunks, and branches are modeled as circular homogeneous dielectric cylinders.

1.3 The Purpose of Experiments

Experimental measurements not only can be used to check the validity of a model, but they also can provide insight to guide the development of the theoretical representation of the medium. Also, it is possible to conduct experiments that will help separate the scattering contributions of the different constituents of a plant, thereby eliminating some of the guess-work associated with modeling wave scattering in a vegetation canopy. Hence, in this study, a series of experiments were performed first, and then the theoretical models based on the experimental observations were developed.

Modeling the vegetation cover independently of the soil surface contribution will reduce the complexity of the problem. Propagation measurements are one way of achieving this goal and many investigators have attempted to measure the attenuation of microwave energy by vegetation. Horizontal propagation at 16 GHz through a wheat canopy were reported for both vertical and horizontal polarizations by Story *et al.* [1970]. Two-way attenuation measurements for potatoes, oats, barley, and wheat at X-band, using a 45° incidence angle and vertical polarization were reported by Attema and Kuilenburge [1974]. Kastern and Smit [1977] have also reported attenuation measurements of a potato field at X-band at six different locations within the field with inconsistent results. Lopes [1983] has documented horizontal attenuation through wheat stalks at 9 GHz for both vertical and horizontal polarizations, and Ulaby and Jedlica [1984 reported one-way attenuation values through corn and soybean canopies on a temporal basis at 10.2 GHz and 52° incidence angle for vertical polarization. Allen and Ulaby [1984] reported height profile attenuation measurements for a wheat canopy at 10.2 GHz and 52° incidence angle for a vertically polarized wave and separated the head contributions of the attenuation from the stalk's contribution. They also measured one-way attenuation of soybean at 10.2 GHz and 37° incidence angle using a vertically polarized wave. The first result of multi-angle, multi-frequency, and dual-polarized measurements were reported by Ulaby and Wilson [1984].

They have reported attenuation loss measurements for wheat and soybean canopies at L-, C-, and X-band frequencies, 24° and 56° incidence angle, and for both polarizations. These attenuation measurements show that the statistical distributions of the constituents of a plant canopy, size, shape, and their dielectric properties determine the propagation loss factor at a specific frequency, polarization, and incidence angle.

Because atmospheric losses are low in the L- to X- band frequencies, many remote sensing probes operate in this frequency range. Furthermore, in terms of the dimensions of canopy constituents, this 10:1 frequency range provides the opportunity to infer extensive information about the canopy by observing its scattering properties at multiple frequencies. As mentioned previously, a series of propagation measurement were made in this frequency range for this study.

A canopy planted in corn was selected for conducting the experiments in support of this study because a corn canopy is a useful representative of many types of row-structured vegetation. The corn plants (Fig. 1.1) include a vertically oriented cylinder (the stalk) and semi-randomly oriented leaves. In the above frequency range, the constituents of a corn canopy exhibit weak scattering properties at the lower end of the range and strong scattering properties at the higher end. A model that can explain the propagation properties of a corn canopy should prove applicable to other vegetation canopies as well. Two separate sets of experiments were conducted to measure the signal transmitted through a corn canopy. The purpose of the first set of experiments was to study the effect of polarization, frequency, and incidence angle on the propagating wave through the canopy and its relation to the canopy parameters. The wave was transmitted at oblique incidence with respect to the nadir and power attenuation measurements and polarization phase difference measurements were performed. The experiments were performed over a wide frequency range (1.5 GHz, 4.75 GHz, and 10.2 GHz), at many incidence angles (20°, 40°, 60°, and 90° from nadir), and for various canopy conditions (full and defoliated) at both vertical and horizontal polarizations. The second series of measurements were aimed at

investigating the effect of row direction on horizontal propagation and its relation to the propagating beam and canopy parameters. Beam patterns of the transmitted power and phase were measured when both transmit and receive antennas were located at the same height above the ground surface and the wave was transmitted horizontally. Frequencies of 1.5 GHz and 4.75 GHz were selected for these measurements, and the experiments were performed for look directions both parallel and perpendicular to the row.

Measurements performed for this study have many advantages over the previous attenuation measurements reported in the literature. To name a few, they include a wide span of frequencies and incidence angles, measurements of the polarization phase, extensive canopy parameter measurements, and horizontal-propagation beam patterns of power and phase.

1.4 Propagation Models

In order to take advantage of the many uses of microwave sensors, the physics of the wave-vegetation interaction must first be understood. This understanding can be gained through theoretical electromagnetic investigations and extensive experimentation. The former provides explanations for certain observations in the experiments, whereas the latter verifies or refutes the proposed theories. Through these efforts theoretical models evolve. The success of each model depends on how well the simulated data matches the experimental measurements and the degree to which the guess work related to estimating the canopy parameters has been eliminated. In microwave remote sensing, soil conditions, plant constituent sizes, plant density, and plant dielectric constant are among the canopy parameters needed for successful verification of the proposed models.

Figure 1.1 A corn plant composed of a stalk, leaves and cobs

The role of the soil in radar backscattering has been studied extensively by several researchers [Batlavala and Ulaby, 1977; Ulaby *et al.*, 1982; Dobson *et al.*, 1986]. The relations between the water content of the plant constituents and their dielectric constant have also been examined [Ulaby and El-Rayes, 1987; Sarabandi *et al.* 1988]. The area that needs much further research is the interaction of the electromagnetic wave with the vegetation canopy. One of the first theoretical models to successfully relate radar backscatter to vegetation parameters [Attema and Ulaby, 1978] used experimental data to estimate some of the model parameters. As models become more elaborate, their dependence on experimental data for modeling purposes diminishes and the experimental tasks are then only performed to check the validity of the theoretical models.

The microwave attenuation coefficient of a vegetation canopy is one of the key inputs in volume scattering models. Propagation models are also needed when direct transmission through the canopy is of interest. There are many approaches to characterizing attenuation by vegetation canopies. In 1984, Ulaby *et al.* [1984] considered leaves to be thin layers of a lossy dielectric material, and then proceeded to model the scattering along two approaches. In the first approach, the dimensions of the leaves were assumed to be much larger than the wavelength and the leaves were assumed to be horizontally aligned. The coherent transmissivity through a leaf layer was calculated and a multi-layer transmissivity approach was adopted to account for all the leaves in the volume. The second approach treated the leaves as small (compared to the wavelength), lossy, disk-shaped inclusions of finite thickness, and a dielectric mixing formula was used to obtain the effective dielectric constant of the volume. The second approach was further extended by Allen and Ulaby [1984] and Ulaby and Wilson [1984] to model the attenuation of vertical stalks of wheat. The stalks were assumed to be very thin compared to the wavelength and oriented vertically. Dielectric mixing models for needles oriented vertically in air were adopted to obtain the effective dielectric constant of the medium. These approaches, even

though successful at certain frequencies and for certain vegetation types, can not be extended to the entire microwave spectrum and other crop types.

In radiative transfer theory, the extinction matrix characterizes the attenuation of the Stokes parameters due to absorption and scattering [Ulaby *et al.*, 1986]. The extinction cross section, σ^p_{ext} (p= V or H), can be calculated by applying the optical theorem and is given by

$$\sigma^p_{ext} = \frac{4\pi}{k_0} \mathrm{Im}[S_{pp}(\theta_i, \phi_i; \theta_i, \phi_i)]$$

where $S_{pp}(\theta_i, \phi_i, ;\theta_i, \phi_i)$ is the forward scattering amplitude of a single scatterer. The extinction coefficient, κ_p is obtained through $\kappa_p = N < \sigma^p_{ext} >$, where N is the number of particles per unit volume and < > denotes ensemble average over sizes and orientations. Since in radiative transfer theory the wave propagates incoherently, phase information of the propagating wave is not incorporated in the model. Recently, backscatter phase measurements have been shown to contain useful information about the target, which indicates the need to develop models that predict the phase properties of the scattered wave [Ulaby, *et al.*,1987].

In summary, previous propagation models have many limitations. First, phase information is not considered in most models. Second, those models that incorporate phase are only applicable in the Rayleigh region where the size of the scatterers are small compared to the wavelength and only absorption loss is taken into account [Ulaby *et al.*, 1984]. Finally, these models are only applicable to wave propagation in random-media and their applicability to wave propagation in man-made semi-deterministic media has not been investigated. The goal of this thesis is to develop propagation models for semi-deterministic vegetation media. Both propagation at oblique incidence and horizontal propagation through periodic structures are considered. Through model development and experimentation, it was concluded that for the case of oblique incidence a random-medium approach is quite satisfactory. This result can be attributed to several reasons. The plant

constituents are different at various canopy heights, therefore, the wave does not go through identical environments in different rows. Another reason is that the propagating wave travels through a very limited number of rows and, as a result, row periodicity does not exercise much influence on the propagating wave. A general random-medium model that takes both absorption and scattering losses into consideration is developed and presented in chapter II, along with the corresponding experiments. Then, for modelling purposes, stalks are modeled as infinitely long dielectric cylinders. Two frequency regions for modelling the leaves are considered. At low frequencies, where leaf surface dimensions are small compared to the wavelength, leaves are modeled as randomly oriented circular disks and dielectric mixing models are used to represent them. When the surface dimensions of the leaves are much larger than the wavelength, leaves are modeled as randomly oriented dielectric slabs of arbitrary shapes. By application of the resistive sheet model, together with the physical optics approximation, the scattering properties of leaves are then calculated.

Chapter III contains experimental procedures and model developments for horizontal propagation through man-made vegetation canopies. The corn canopy under investigation was planted in a row arrangement with plants periodically distributed in each row. Through experimentation, we found that a deterministic approach that accounts for the periodicity of the rows and plants is needed in order to characterize wave propagation through such canopies. In the developed model, stalks are represented as infinite cylinders and a two-dimensional deterministic wave approach is used to model wave propagation in the defoliated canopy. The effect of leaves when their surface dimensions are much smaller than a wavelength is further incorporated in the model.

When the leaf surface dimensions are comparable to or larger than a wavelength, their presence in the canopy makes the coherent wave approach impractical. Strong incoherent scattering by the leaves takes over the coherent scattering by the stalks. As a result, the periodicity between plants in each row becomes unimportant, but row periodicity

is still important. A two-dimensional periodic radiative transfer technique is developed for this situation. Stalks are modeled as infinitely long dielectric cylinders again, and leaves are presented as resistive strips. Chapter IV contains a brief review of the radiative transfer formulation and the development of the two-dimensional model. Chapter IV also includes comparison of this model with the measured data of chapter III. The conclusion chapter, chapter V, contains a summary of the results of the research presented in this dissertation and a list of topics recommended for future work.

CHAPTER II

MICROWAVE PROPAGATION CONSTANT FOR A VEGETATION CANOPY WITH RANDOMLY POSITIONED PLANTS

2.1 Introduction

In microwave remote sensing, the energy backscattered from a vegetation canopy consists of three major sources: direct backscattering from plants, direct backscattering from the soil attenuated twice by the canopy, and multiple scattering due to plant-soil interactions. Hence, models representing the attenuation loss factor of the canopy must be developed and incorporated into the canopy backscattering models. Information about wave transmission through vegetation media is also needed when line of sight propagation is considered. Some natural vegetation canopies consist of randomly located plants each having a vertical trunk and randomly oriented leaves. In contrast, many man-made vegetation canopies are planted in a row arrangement, but also with plants made of vertical stalks surrounded by randomly oriented leaves. The purpose of this study was to characterize wave propagation at oblique incidence on a man-made vegetation canopy. Through model development and experimentation, it was concluded that a random-medium approach is applicable when the wave is obliquely incident upon the canopy or when the horizontal-propagation path does not exceed a few rows. This result can be attributed to several reasons. First, the plant constituents at the various canopy heights are different, causing the wave not to go through identical environments in the different rows. Second,

the propagating wave travels through a very limited number of rows and, as a result, row periodicity does not affect the propagating wave. Based on these observation, a random-medium propagation model was developed. This propagation model, which is applicable to man-made vegetation canopies at oblique incidence and natural vegetation canopies at both oblique incidence and horizontal propagation, makes no assumption on the individual shapes of the scatterers and takes both absorption and scattering losses of the canopy constituents into account.

The experimental study of this research was performed on a corn field. A corn plant consists of a stalk surrounded by leaves (Figure 1.1). At very low frequencies, where plant constituent dimensions are much smaller than a wavelength, both stalks and leaves are weak scatterers and quasi-static models can be used to model the vegetation canopy [Allen and Ulaby, 1984; Ulaby and Wilson, 1984]. As the frequency of operation increases, the stalks' dimensions become comparable to the wavelength and behave as strong scatterers and quasi-static models are no longer applicable [Ulaby *et al.*, 1987]. At still higher frequencies, leaf dimensions also become comparable to the wavelength and scattering by leaves must also be taken into consideration. In this study, it was concluded that at the L-band, C-band, and X-band frequency ranges, corn stalks are always strong scatterers and quasi-static approaches are not applicable to them. Corn leaves on the other hand, exhibit quasi-static behavior at L-band (1.62 GHz), but not at C- and X-bands (4.75 and 10.2 GHz, respectively). Therefore, in the model stalks are represented as infinite dielectric cylinders, but leaves as randomly oriented dielectric disks in the Rayleigh region and randomly oriented resistive sheets of arbitrary shapes in the X-band region. Neither representation is appropriate for leaves at C-band, since the leaf dimensions are comparable to the wavelength.

The experimental measurements are presented in section 2.2. They include simultaneous coverage of wavelength, incidence angle, and polarization. Section 2.3 contains the general development of the propagation model. Section 2.4 presents the

application of the model to the defoliated canopy (stalks only) and sections 2.5 and 2.6 discuss the inclusion of the leaves in the model at L-band and X-band, respectively.

2.2 The experiment

Measurements of the transmission loss through a corn canopy were made at incidence angles of 20°, 40°, 60°, and 90° for both vertical and horizontal polarizations where the 90°-case represents horizontal propagation through the canopy. In addition, the phase difference between the vertically and the horizontally polarized waves transmitted simultaneously through the canopy was measured. The configurations used are illustrated in Figure 2.1. The transmitters for the 20°, 40°, and 60° measurements were placed on a truck-mounted platform at a height of 11.5 m above the ground surface and the receivers were placed underneath the canopy. For the 90° measurement, the transmitter platform was placed on the truck bed and the receiver was placed on a wooden platform whose height above the ground was the same as that of the transmitter. Because a vegetation canopy is an inhomogeneous medium at microwave frequencies, its coherent attenuation coefficient should be treated as a random variable. Consequently, to measure the mean attenuation with a reasonable degree of precision, it is necessary that the estimate be an average over a large number of statistically independent samples. Therefore, the arrangement shown in Fig. 2.2 was used to get statistically independent samples. The receiving platform was placed on a rail system on which it slid in synchronism with the motion of the truck as it was pulled by a rope connected to the truck through a pulley system.

The transmitters used three dual-polarized dish antennas with center frequencies of 1.62 (L-band), 4.75 (C-band), and 10.2 GHz (X-band). Table 2.1 presents a summary of the overall system specifications, including antenna sizes, beamwidths, and canopy parameters, and Fig. 2.3 is a block diagram of the receiver configurations used for power (amplitude) and phase measurements.

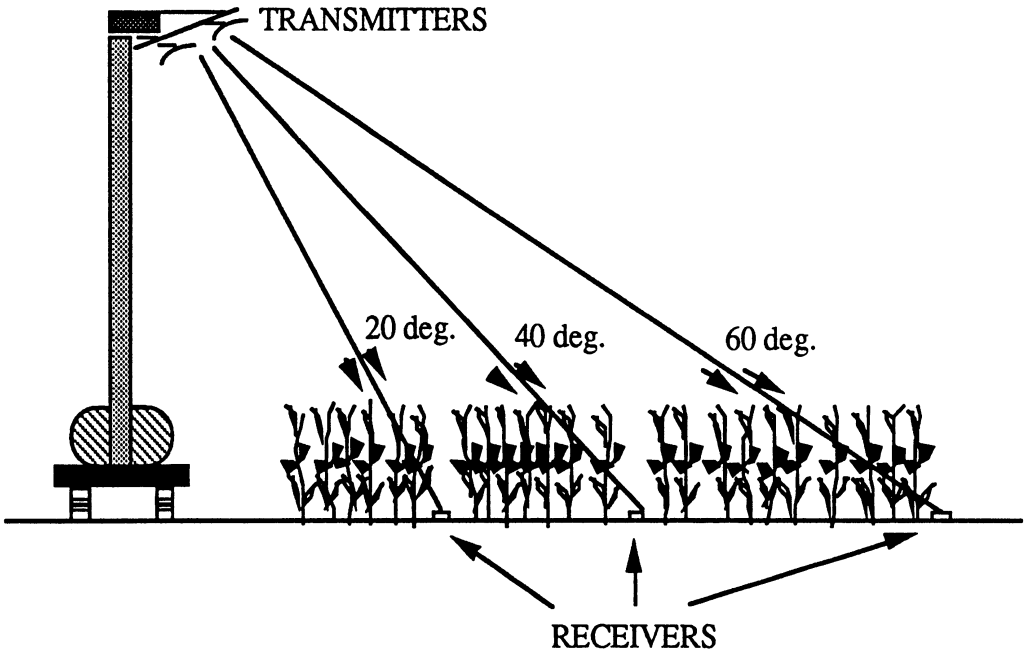

(a)

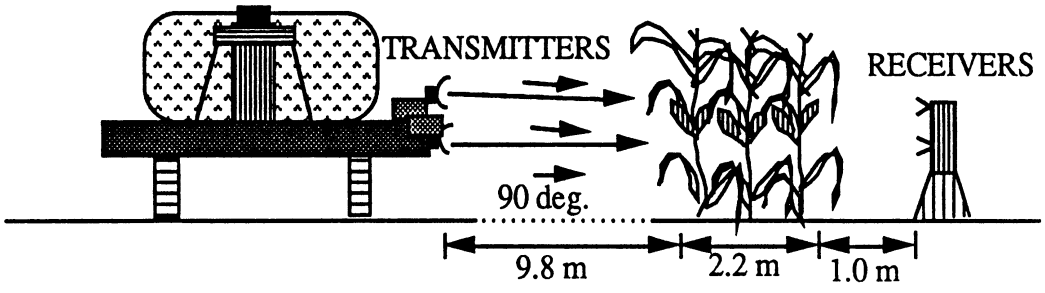

(b)

Figure 2.1 Configuration used for the transmission measurements at (a) 20°,40°, 60°, and (b) 90°

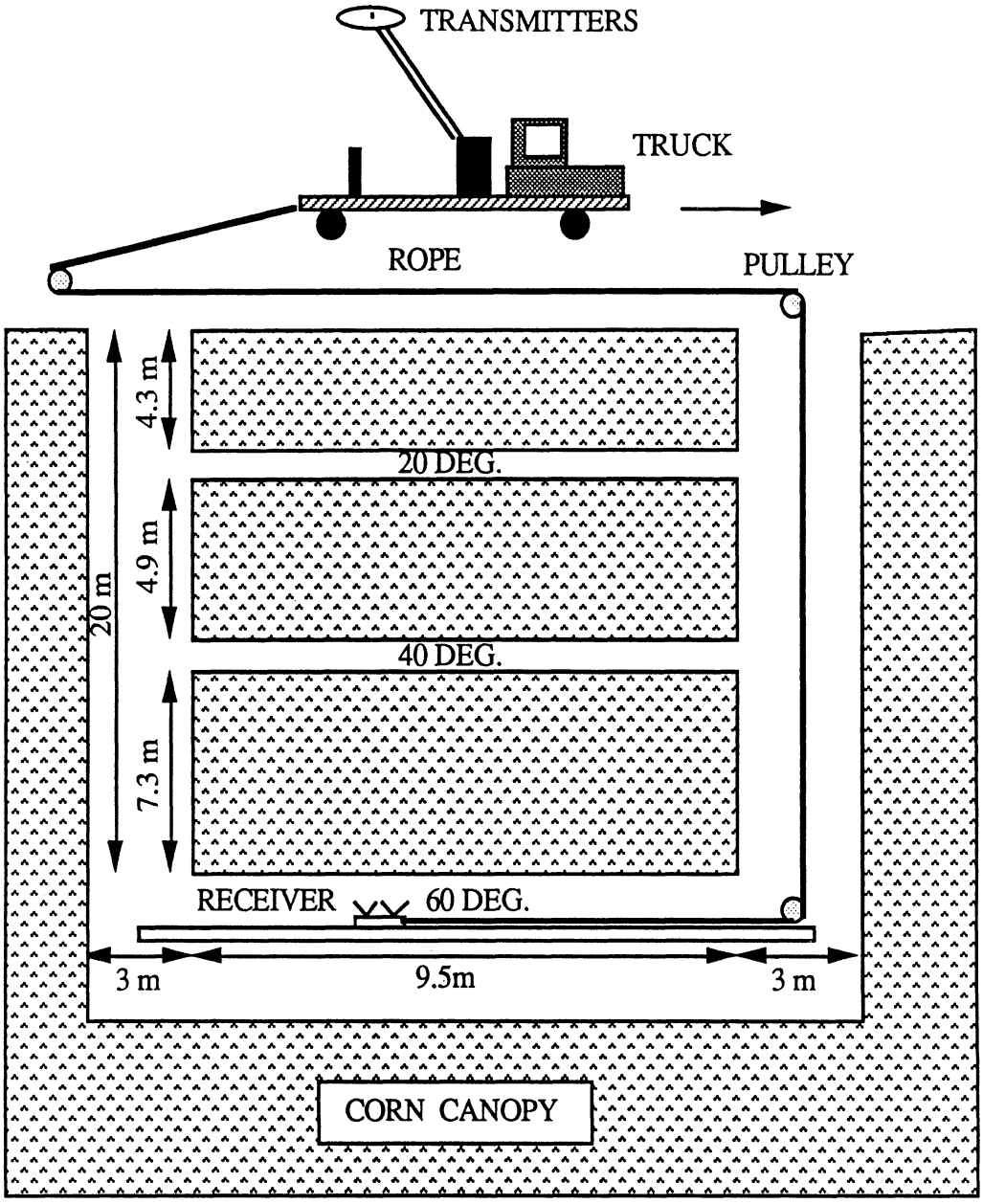

Figure 2.2 The pulley system was used so that as the truck moved forward, the transmit and receive antennas moved in space at exactly the same speed, thereby maintaining line of sight.

Antenna beamwidths

	L-Band	C-Band	X-Band
Transmitter	7.8°	4.6°	4.7°
Receiver	90.2°	53.1°	24.7°

Incidence Angle Information

Distance between	20°	40°	60°	90°
Transmitter and Receiver	11.7 m	14.3 m	22.0 m	13.0 m
Transmitter Height	11.5 m	11.5 m	11.5 m	1.2 m
Receiver Height	0.3 m	0.3 m	0.3 m	0.3 m
Slant path in canopy	2.6 m	3.2 m	4.8 m	2.2 m

Canopy Parameters

Average row spacing: 0.76 m
Average plant spacing: 0.20 m
No. of plant per unit area : 6.6
Stalk diameter: 2.8 cm at base
1.8 cm at 1.2 m
0.6 cm at top

Stalk gravimetric moisture: 0.77
Leaf gravimetric moisture : 0.72
Stalk volume fraction = 0.0035
Leaf volume fraction = 0.00058
Leaf area per unit volume : 0.78
Average leaf thickness: 0.27 mm

Table 2.1 Characteristics of the measurement system and the canopy parameters

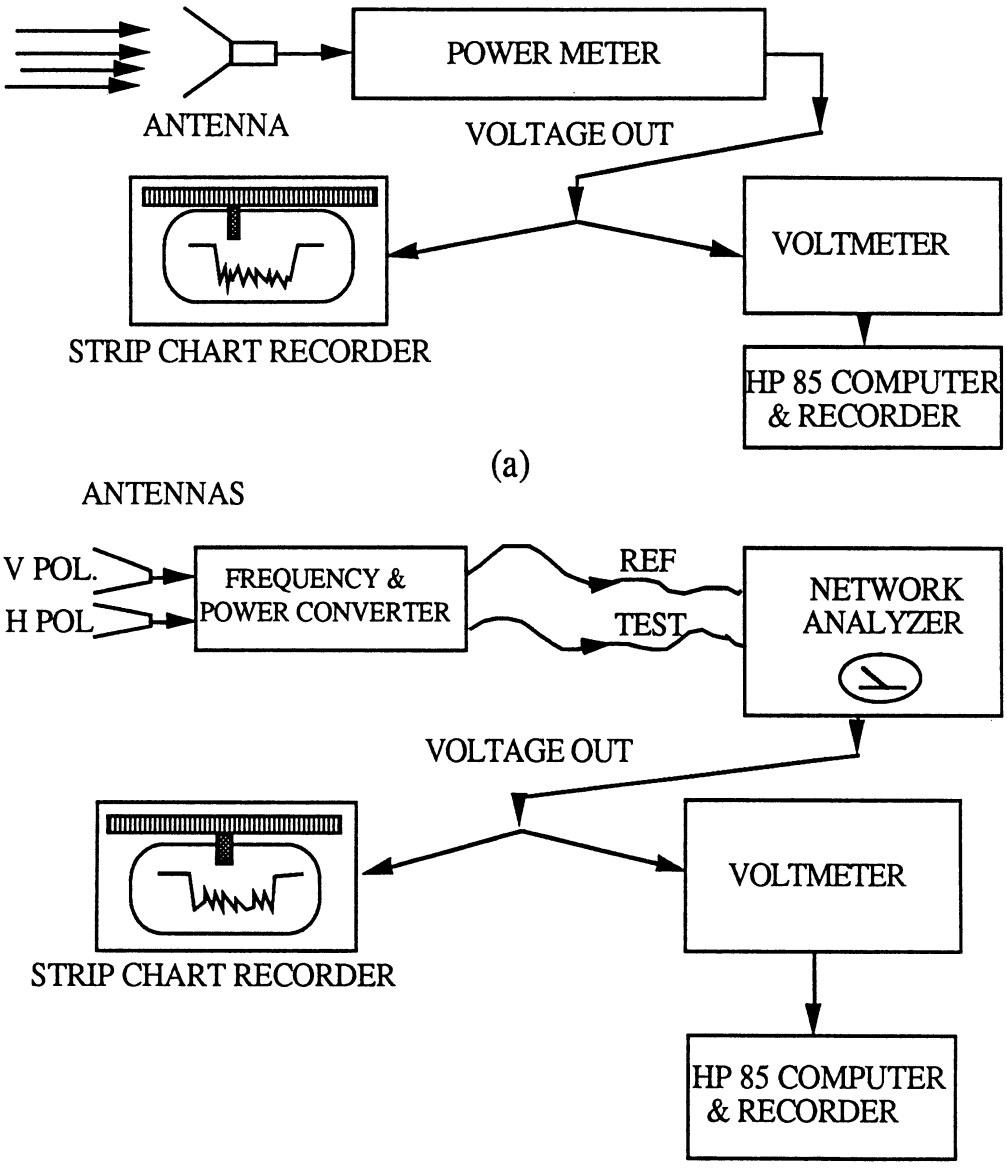

Figure 2.3 Block diagrams of the receivers used to measure (a) the amplitude of the received signal and (b) the phase difference between the V-polarized and H-polarized signals

The amplitude receiver consisted of microstrip patch antennas at L-band and dual-polarized horn antennas at C-band and X-band connected to a microwave detector, which in turn, was connected to a power meter through a 50-m coaxial cable. The output of the power meter was recorded on a strip-chart recorder for immediate display in the field as well as on a digital cassette recorder (using an HP 85 computer) for later analysis. The canopy loss factor L is defined in dB as

$$L = 10 \log \left(\frac{P_0}{P_r}\right) \tag{2.1}$$

where P_r is the power received when the canopy is present and P_0 is the free-space level received under identical conditions (antenna pointing, range between transmitter and receiver, etc.) but without an intervening canopy between the transmitter and the receiver.

The phase measurement refers to the phase difference $\Delta\phi$ between the vertically polarized (V) and horizontally polarized (H) waves transmitted through the canopy. On the transmitting side, H- and V-polarized waves were transmitted simultaneously by the dual-polarized antennas. At the receiver, the outputs of the antenna H- and V-polarization ports were down-converted in frequency to 20 MHz and then relayed to a network analyzer through a pair of 50 -m coaxial cables (Fig. 2.3). The phase difference measured by the network analyzer was recorded on a strip-chart recorder and on a digital recorder.

By cutting and removing the corn plants from an approximately 3-m wide strip on both ends of the canopy area (Fig. 2.2), it was possible to establish a free-space reference signal for both the amplitude and the phase measurements. Furthermore the stability of the signal across each of the 3-m wide strips provided an indication of the presence (or absence) of multiple ground reflections. As an additional test, the entire corn canopy was cut and removed at the conclusion of the experiments and direct free-space transmission measurements were made across the entire 10-m wide test area. The variability in the reference signal was found to be within $\pm$ 0.3 dB for amplitude and$\pm$ 4° for phase.

Measurements were conducted for a full canopy of stalks and leaves and then, the plants were defoliated and the measurements were repeated for the stalk canopy. Amplitude measurements were performed at all three frequency channels, four incident directions, and both polarizations. The polarization phase-difference measurements were made at L-band and C-band only, and the incidence angles were limited to 20°, 40°, and 90°.

Field measurements were performed to determine the density of plants, leaves, and stalks, row spacing, and the geometric sizes of stalks and leaves. In addition, samples were processed in the laboratory to determine their moisture contents. Figure 2.4 shows spectral plots of the relative dielectric constant of corn leaves and stalks at the moisture contents given in Table 2.1 based on the formula reported by [Ulaby and El-Rayes, 1987]:

$$\varepsilon' = (0.429 + 0.074\,f) + (14.62 - 0.834\,f)\,m_g + (39.396 - 0.616\,f)\,m_g^2$$

$$\varepsilon'' = (0.59 - \frac{0.977}{f} - 0.599\,f)\,m_g + (0.463 + \frac{9.368}{f} + 1.617\,f)\,m_g^2 \qquad (2.2)$$

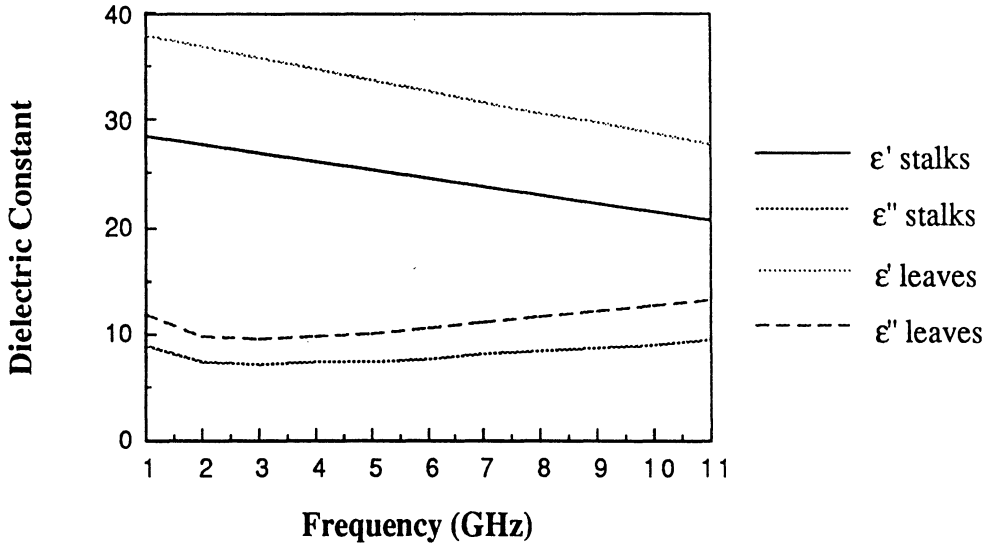

Figure 2.4 Dielectric constant of the corn leaves and stalks as a function of frequency. The moisture contents were m_g=0.82 for the stalks and m_g=0.71 for the leaves.

where f is the frequency in GHz and m_g is the gravimetric moisture content of the stalks or leaves.

As examples of the measured power of canopies containing both stalks and leaves, Figs. 2.5, 2.6, and 2.7 display the power level recorded by the digital tape recorded at L-band, C-band, and X-band at 60° incidence angle and their corresponding histograms. Each figure contains records for both H and V polarizations. The relatively flat levels at the ends of each record represents the free-space reference level of the received signal. The canopy transmission loss is measured in decibels relative to this reference level. It can be seen that as frequency of the operation increases the fluctuations in the received signal also increases. Figure 2.8 illustrates the received power when only stalks are present at X-band and 60° incidence angle. Close inspection of the recorded data reveals that at L-band stalk's contributions to the loss is much higher for V-polarization than H-polarization, but this difference reduces as frequency increases. Leaves are the main cause of the loss in the entire measurement frequency spectrum and they almost display the same level of loss at both polarizations. Another observation is that in the absence of leaves, the record of $L_V(x)$ contains more high-frequency fluctuations than the record of $L_H(x)$ does, which indicates that the coupling between the propagating wave and the stalks is strongly dependent on the stalk's orientation relative to the direction of the wave's electric field. When leaves are present, diffuse scattering increases, thereby reducing the sensitivity of L(x) to the polarization of the propagating wave.

Figure 2.9 is an example of the phase measurements and their histograms when only stalks are present at 90° incidence angle at (a) L-band and (b) C-band. Observations suggest that at L-band the vertically polarized wave leads the horizontally polarized wave, while at C-band the vertically polarized wave lags the horizontally polarized wave. The frequency of fluctuations at C-band is also higher than at L-band.

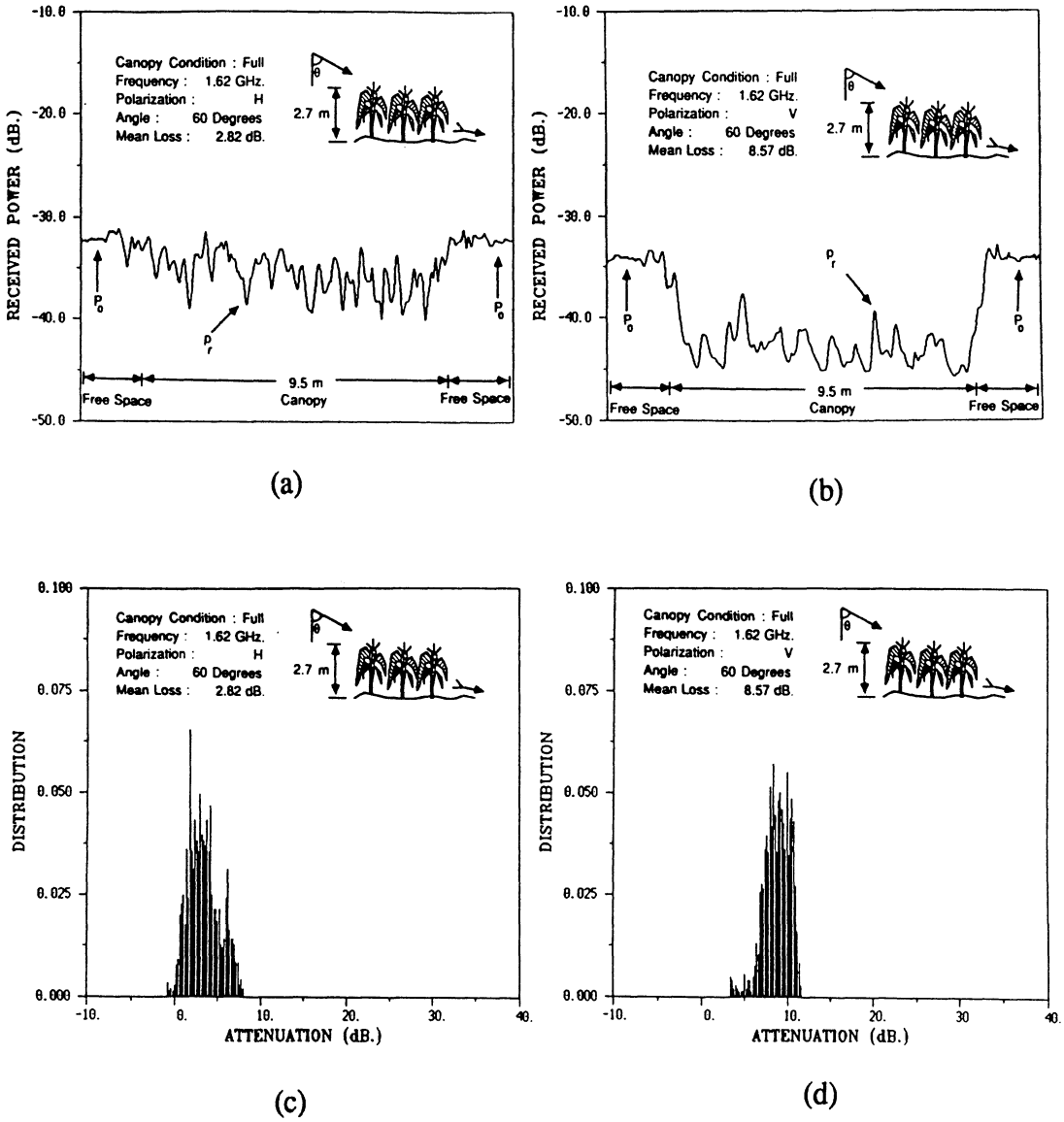

Figure 2.5 Received power at L-band as a function of spatial position, measured for a full corn canopy with (a) H-polarization, (b) V-polarization and corresponding histograms (c) H-polarization, and (d) V-polarization.

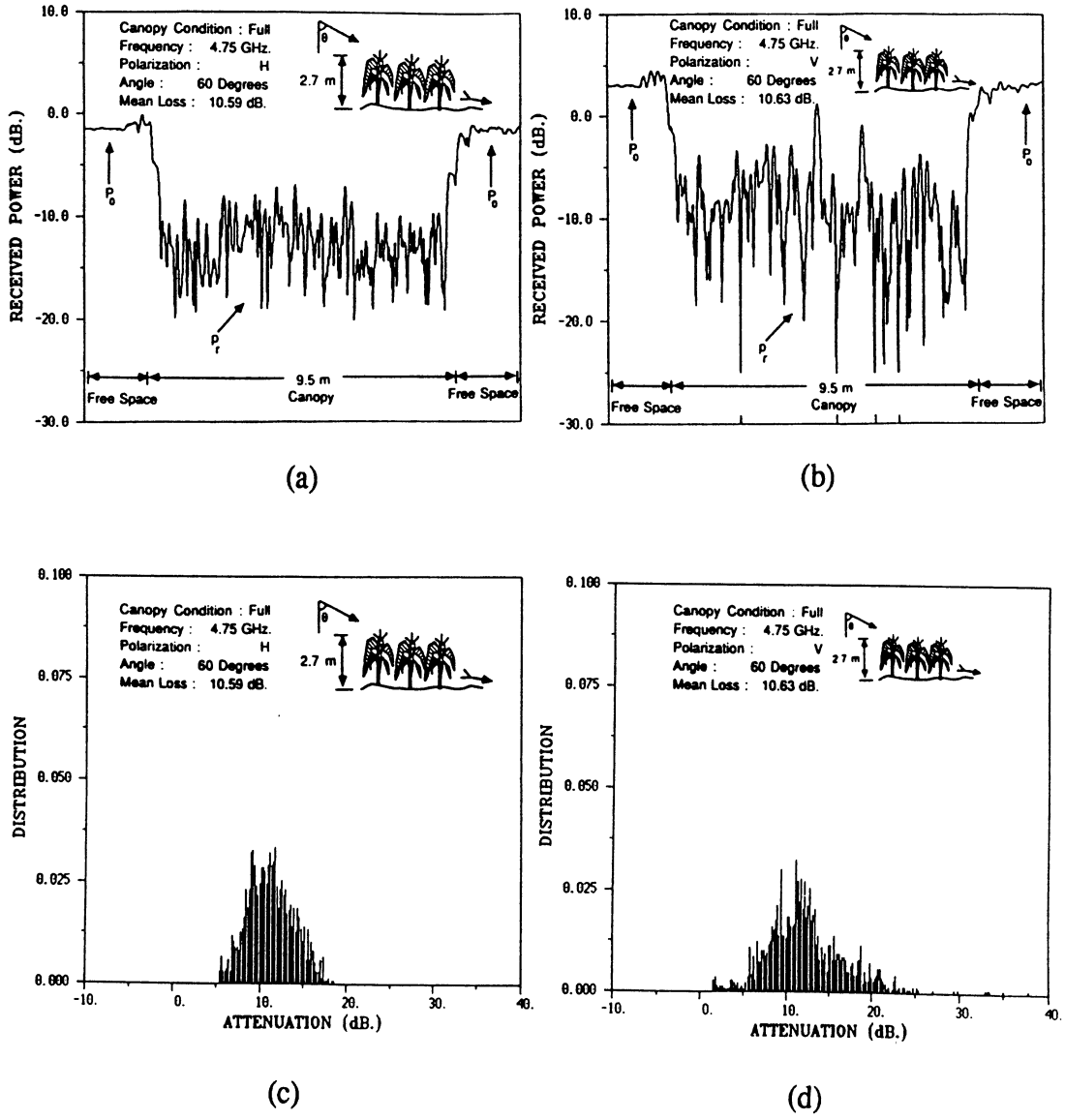

Figure 2.6 Received power at C-band as a function of spatial position, measured for a full corn canopy with (a) H-polarization, (b) V-polarization and corresponding histograms (c) H-polarization, and (d) V-polarization.

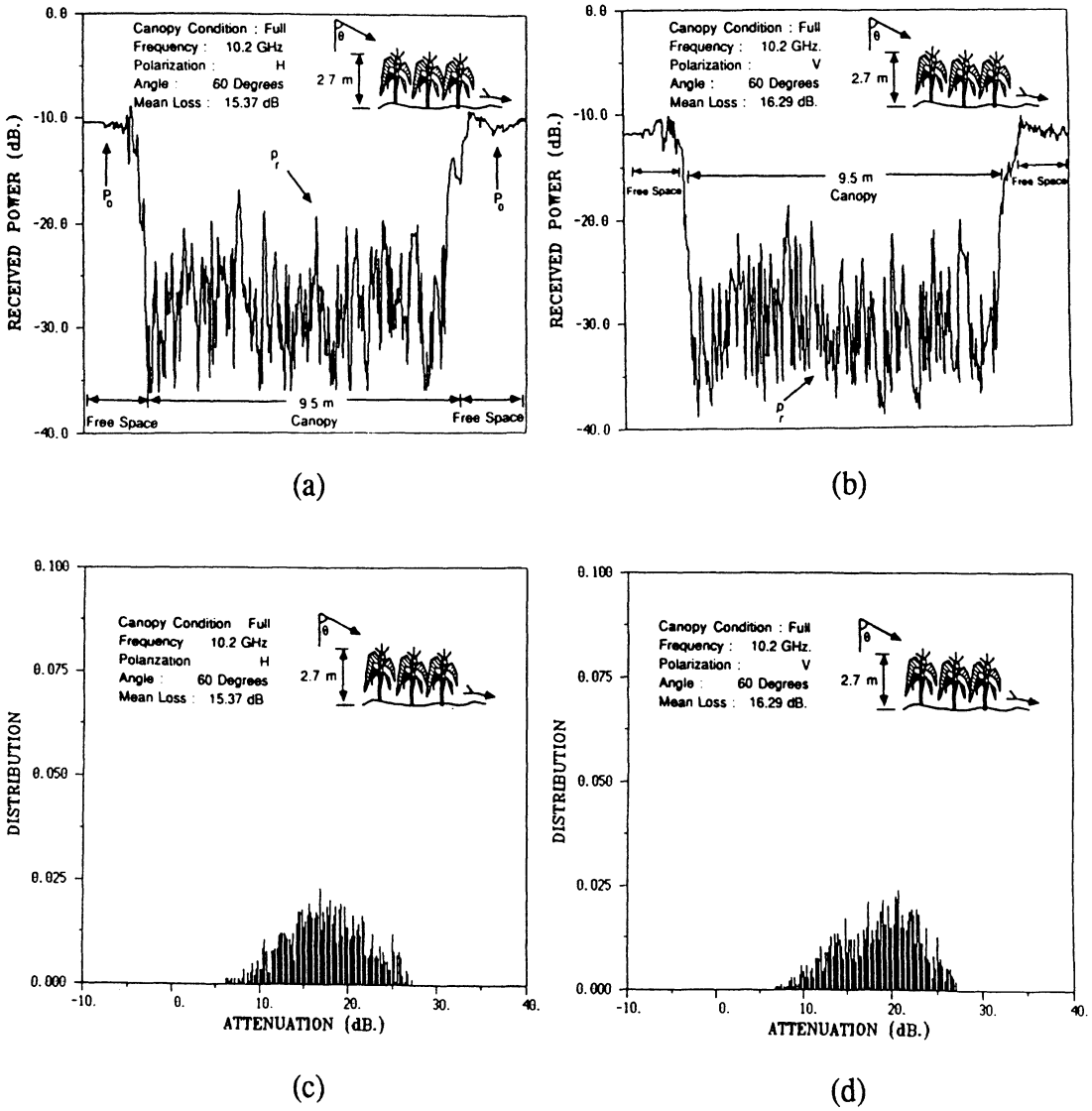

Figure 2.7 Received power at X-band as a function of spatial position, measured for a full corn canopy with (a) H-polarization, (b) V-polarization and corresponding histograms (c) H-polarization, and (d) V-polarization.

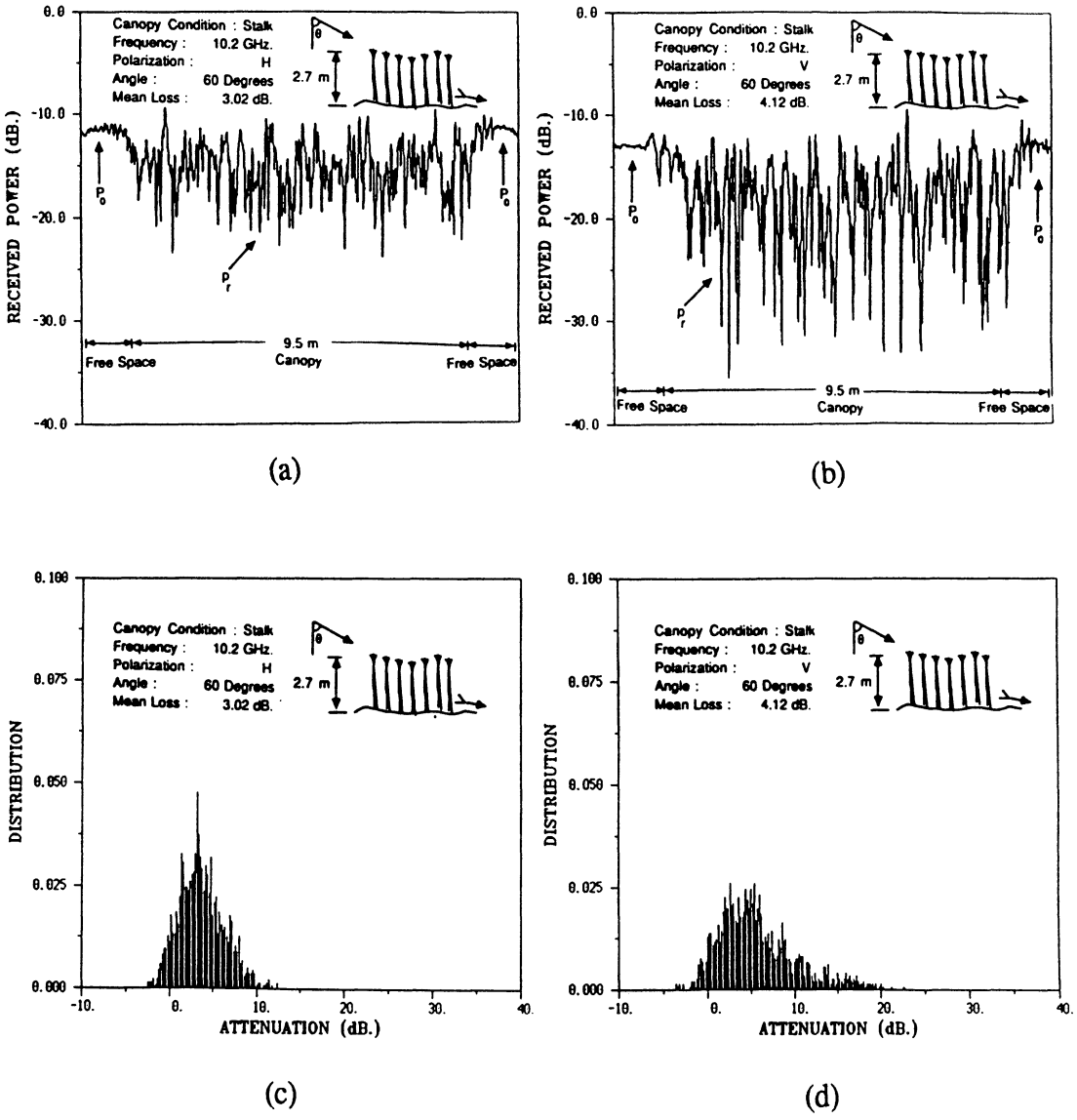

Figure 2.8 Received power at X-band as a function of spatial position, measured for a defoliated corn canopy with (a) H-polarization, (b) V-polarization and corresponding histograms (c) H-polarization, and (d) V-polarization.

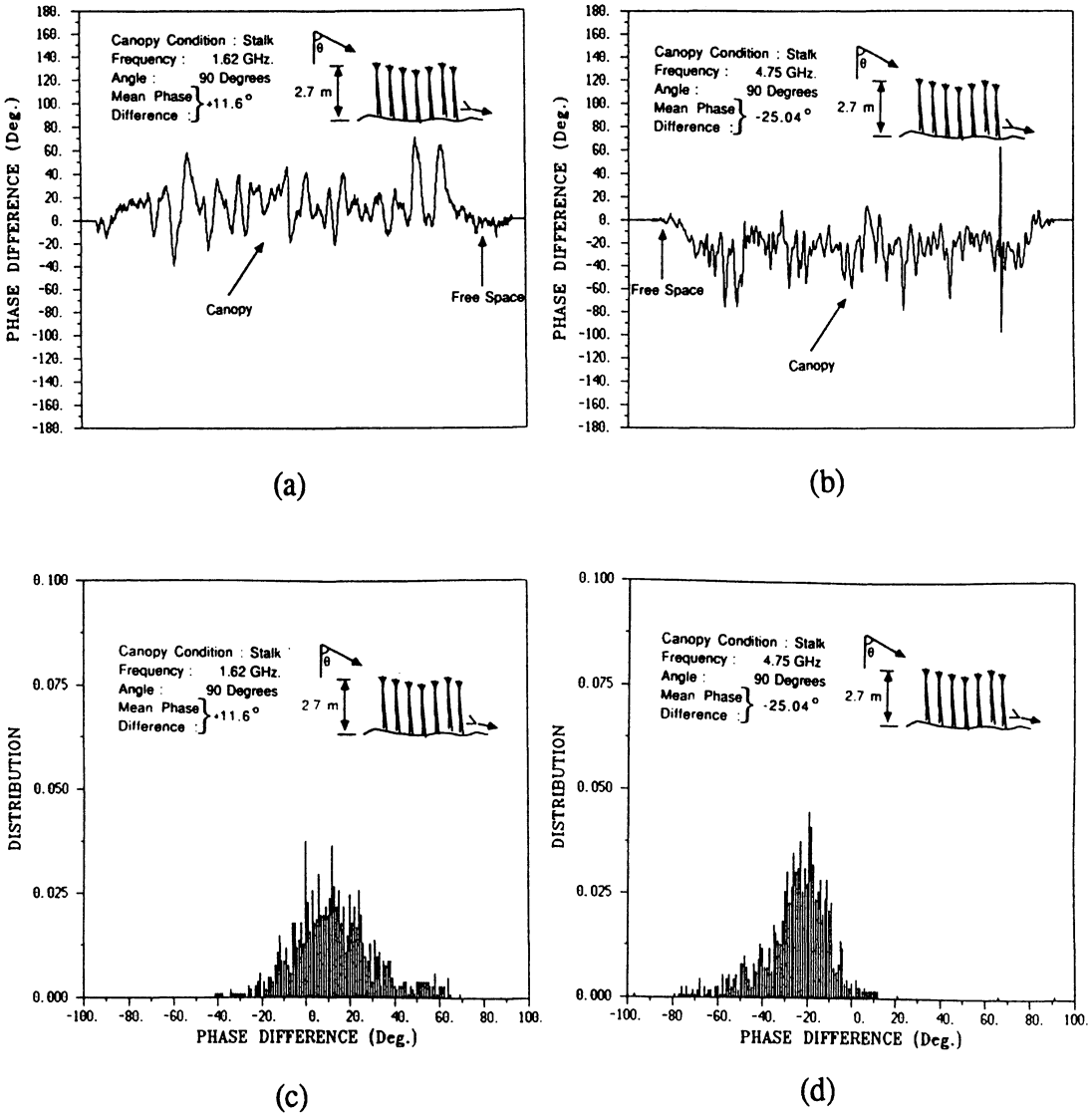

Figure 2.9 Measured propagation phase difference between the vertically polarized and horizontally polarized waves as a function of spatial position for a defoliated corn canopy at (a) L-band, (b) C-band and corresponding histograms (c) L-band, and (d) C-band.

2.3 Theoretical Model

The following theoretical development pertains to a general medium comprised of two-dimensional and three dimensional scatterers. The canopy is modeled as a slab-like region containing both two-dimensional and three-dimensional scatterers. Then, the equivalent dielectric constant of the medium based on the scattering properties of the scatterers in the medium are derived. Later, the stalks are modeled as infinitely long dielectric cylinders pointing in the z-direction (two-dimensional scatterers) ; and the leaves are modeled as thin (compared to the wavelength) dielectric disks or sheets (three-dimensional scatterers). We seek an expression for the propagation constant γ of an equivalent dielectric medium such that it is applicable at any incidence angle θ relative to the z-direction for both H- and V-polarization configurations. The slab contains two-dimensional scatterers (cylinders, stalks) with identical dielectric properties but not necessarily identical diameters, and statistically similar three-dimensional scatterers (leaves) with prescribed orientation and size distributions. Figure 2.10 represents a narrow layer of the canopy. It is assumed that the scatterers are sparse and interaction between them is negligible. The incident field travels in the x-direction and can be represented as

$$\vec{U}^{inc} = \hat{p} e^{i k_0 x} \tag{2.3}$$

where $e^{-i\omega t}$ is assumed and suppressed and $\hat{p}$ is a unit vector representing the wave polarization. The total field at the observation point $P(x_0,0,0)$ is composed of three parts: (1) the direct incident field at P, (2) the field due to scattering by the three dimensional scatterers (leaves), and (3) the field scattered by the two-dimensional scatterers (stalks). The fields corresponding to terms (2) and (3) will each be derived separately and then will be added to the incident field at point P.

For a sparse medium, the incident field on the n^{th} leaf located at (x_n,y_n,z_n) is represented by:

$$\vec{U}_n = \hat{p}\, e^{ik_0 x_n} \tag{2.4}$$

Assuming the observation point is far away from the slab, the scattered field due to this leaf observed at $P(x_0,0,0)$ is given by

$$\vec{U}_n^1 = e^{ik_0 x_n} \frac{e^{ik_0 r_n}}{k_0 r_n} \vec{S}_n(\hat{r}_n) \tag{2.5}$$

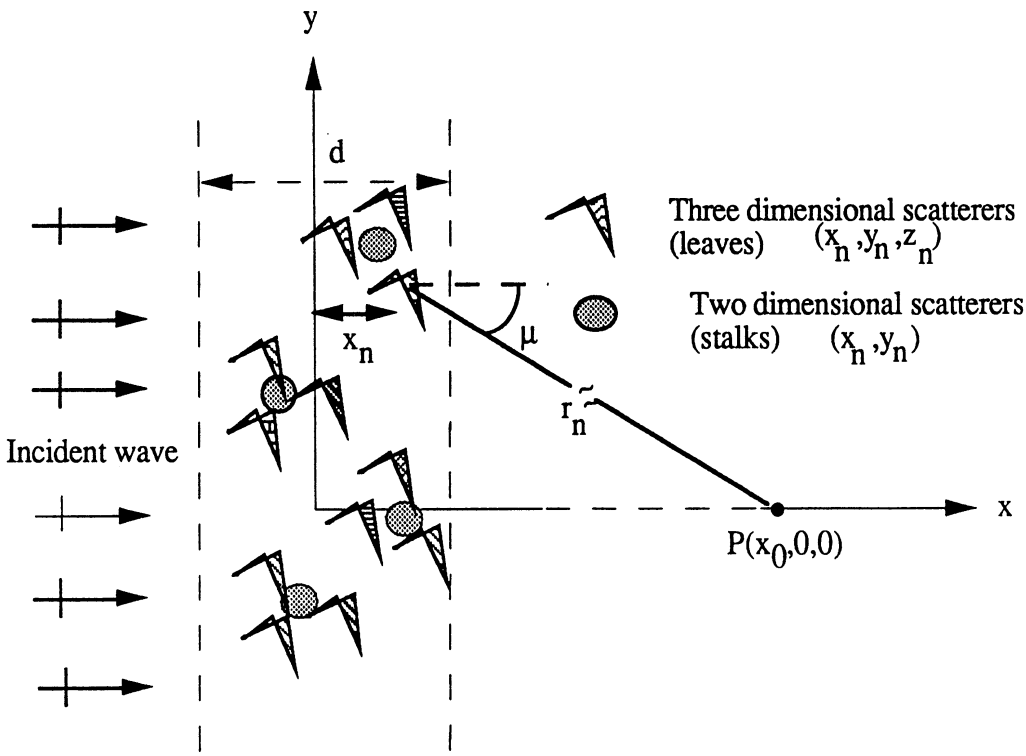

Figure 2.10 Geometry of a narrow slab containing leaves and stalks and the observation point P

where r_n is the distance between the n^{th} leaf and the observation point and $\vec{S}_n(\hat{r}_n)$ is the scattering amplitude of the leaf for scattering in direction $\hat{r}_n$ (Fig. 2.10). Since the medium is sparsely populated (vegetation volume fraction in a canopy is typically less than 1%), multiple scattering between the leaves may be ignored. Thus the total scattered field at the observation point is the superposition of contributions of all individual leaves in the slab, i.e.

$$\vec{U}^l = \sum_n e^{ik_0 x_n} \frac{e^{ik_0 r_n}}{k_0 r_n} \vec{S}_n(\hat{r}_n) \tag{2.6}$$

If N, the number of leaves per unit volume in the medium, is large, then the summation in (2.6) can be approximated by

$$\vec{U}^l = N \iiint e^{ik_0 x'} \frac{e^{ik_0 r'}}{k_0 r'} \langle \vec{S}(x_0; x', y', z') \rangle dx'dy'dz' \tag{2.7}$$

where $\langle \vec{S}(x_0; x', y', z') \rangle$ is the scattering amplitude averaged over the prescribed size and orientation distributions. To evaluate (2.7), two changes of variables are in order. First, the integration in y'-z' plane can be performed by cylindrical variables ρ' and ϕ', therefore,

$$\vec{U}^l = N \iiint e^{ik_0 x'} \frac{e^{ik_0 r'}}{k_0 r'} \langle \vec{S}(x_0; x', \rho', \phi' \rangle \rho \, d\rho' \, d\phi' \, dx' \tag{2.8}$$

where $r'=\sqrt{\rho'^2+(x_0-x')^2}$.

Second, the integration with respect to ρ' and x' can be performed by changing to variables ν and μ defined by:

$$\nu = x'$$
$$\mu = \tan^{-1} \frac{\rho'}{x_0 - x'} \tag{2.9}$$

In (2.9), μ is the angle between forward scattering direction (x-axis) and the observation point P (Fig. 2.10). Thus (2.8) becomes

$$\vec{U}^1 = N \int_0^{2\pi} \int_{-d/2}^{d/2} e^{ik_0 \nu} \left[\int_0^{\frac{\pi}{2}} < \vec{S}(\pi - \mu) > \frac{e^{ik_0 \frac{x_0 - \nu}{\cos \mu}}}{k_0 \cos \mu} (x_0 - \nu) \tan \mu \, d\mu \right] d\nu \, d\phi' \tag{2.10}$$

If the observation point is far away from the slab, that is $k_0 x_0 >> 1$, then the integrand of (2.10) rapidly changes with small changes in μ for values of μ away from zero (μ=0 is the stationary phase point). Therefore, the integral is dominated by the contribution of the integrand around the stationary phase point where the integrand can be approximated by its Taylor series expansion, i.e.,

$$\vec{U}^1 \cong N \int_0^{2\pi} \int_{-d/2}^{d/2} e^{ik_0 \nu} \left[\int_0 < \vec{S}(\pi) > \frac{e^{ik_0 (x_0 - \nu)(1 + \frac{\mu^2}{2})}}{k_0} (x_0 - \nu) \, \mu \, d\mu \right] d\nu \, d\phi' \tag{2.11}$$

Direct evaluation of (2.11) leads to

$$\vec{U}^{I} \cong e^{ik_0 x_0} \frac{i2\pi N d}{k_0^2} < \vec{S}(\pi) > \tag{2.12}$$

Following a similar approach, we can derive an expression for the total field due to scattering by the stalks. The field incident on the m^{th} stalk located at (x_0,y_0) is given by

$$\vec{U}_m = \hat{p} e^{ik_0 x_m} \tag{2.13}$$

which gives rise to a scattered field at point $P(x_0,0,0)$ given by [Stratton, 1941]

$$\vec{U}_m^{s} = e^{ik_0 x_m} \sqrt{\frac{2}{\pi k_0 \rho_m}} e^{i(k_0 \rho_m - \frac{\pi}{4})} \vec{T}_m(\vec{\rho}_m) \tag{2.14}$$

where $\vec{T}_m(\vec{\rho}_m)$ is the scattering amplitude of the stalk for scattering in direction $\vec{\rho}_m$ and ρ_m is the distance between the stalk and the observation point. The total scattered field at point P due to the contribution of all the stalks in the slab is

$$\vec{U}^{s} = \sum_m e^{ik_0 x_m} \sqrt{\frac{2}{\pi k_0 \rho_m}} e^{i(k_0 \rho_m - \frac{\pi}{4})} \vec{T}_m(\vec{\rho}_m) \tag{2.15}$$

If M, the number of stalks per unit area of the medium, is large, then the summation (2.15) can be approximated by

$$\vec{U}^s = M\sqrt{\frac{2}{\pi k_0}}\, e^{-i\frac{\pi}{4}} \iint e^{ik_0 x'} \frac{e^{ik_0\rho'}}{\sqrt{\rho'}} < \vec{T}_m(x_0; x', y') > dx'dy' \qquad (2.16)$$

where $< \vec{T}_m(x_0; x', y') >$ is the scattering amplitude averaged over the prescribed cylinder diameters. The total scattered field at P due to the two dimensional scatterers, derived in a manner similar to that used previously for the three dimensional scatterers, is

$$\vec{U}^s \cong e^{ik_0 x_0} \frac{2Md}{k_0} < \vec{T}(\pi) > \qquad (2.17)$$

where $< \vec{T}(\pi) >$ is the forward scattering amplitude of the stalks, averaged over the specified diameter distribution.

The total field at the observation point P is

$$\vec{U}^t = \vec{U}^i + \vec{U}^l + \vec{U}^s$$

$$\vec{U}^t = e^{ik_0 x_0}\left[\hat{p} + \frac{2Md}{k_0} < \vec{T}(\pi) > + \frac{i2\pi Nd}{k_0^2} < \vec{S}(\pi) >\right] \qquad (2.18)$$

Now, if we represent the thin layer of scatterers by an equivalent homogeneous dielectric slab with the index of refraction n, the total field at P would be

$$\vec{U}^t = \hat{p}\, e^{ik_0 x_0} e^{i(n-1)k_0 d}$$

$$\cong \hat{p}\, e^{ik_0 x_0}[1 + i(n-1)k_0 d] \qquad (2.19)$$

The Taylor series expansion used in the above approximation is justified by the fact that d is small, $n' = \mathrm{Re}[n] \cong 1$ and $n''=\mathrm{Im}[n] \ll 1$. Upon equating (2.18) and (2.19), we obtain the following expression for the index of refraction of the equivalent medium

$$\begin{aligned} n &= n' + n'' \\ n_p &= 1 - \frac{i2M}{k_0^2} < T_p(\pi) > + \frac{2\pi N}{k_0^3} < S_p(\pi) > \end{aligned} \tag{2.20}$$

where $S_p(\pi) = \vec{S}_p(\pi) . \hat{p}$ and $T_p(\pi) = \vec{T}_p(\pi) . \hat{p}$. The subscript p is used with n_p to emphasize its dependence on the wave polarization vector $\hat{p}$. The propagation constant of the equivalent medium γ_p is related to n_p by

$$\gamma_p = k_0 n_p = k_0 (n'_p + i n''_p) \tag{2.21}$$

and since $i\gamma_p = -\alpha_p + i\beta_p$, the attenuation constant α_p and phase constant β_p are given by

$$\begin{aligned} \alpha_p &= k_0 n''_p, \qquad p = \mathrm{V \text{ or } H} \\ \beta_p &= k_0 n'_p, \qquad p = \mathrm{V \text{ or } H} \end{aligned} \tag{2.22}$$

The power extinction coefficient κ_p is associated with propagation of the mean field through the layer and incorporates losses due to both scattering and absorption by the scatterers. The loss factor L corresponding to propagation over a distance d is given by

$$L = 4.343\ \kappa_p\ d = 8.686\ k_0\ n_p''\ d, \quad \text{dB}. \tag{2.23}$$

The polarization phase difference for one-way propagation is defined by

$$\Delta\phi = (\beta_H - \beta_V)\, d = k_0 d\, (n'_H - n'_V). \tag{2.24}$$

In the above derivation no assumption on particular shape and sizes of the scatterers are made. By selection of appropriate models for single scatterers, the model can predict the average power and phase properties of the propagating wave.

2.4 The Defoliated Canopy

As mentioned before, stalks can be modeled as infinitely long cylinders oriented vertically in the z-direction. For a defoliated canopy the contribution of the three-dimensional scatterers (leaves) in equation (2.18) must be ignored. Hence, the equivalent index of refraction of the defoliated canopy is given by

$$n_p = 1 - \frac{i2M}{k_0^2} < T_p(\pi) > \tag{2.25}$$

Because the wave is obliquely incident on the cylinders, the scattering amplitude T_p will be a function of the incidence angle θ. Also, M, the number of cylinders per unit area in the plane of propagation (defined as the plane containing the direction of the propagation and the y-axis) is related to the number of plants per unit area on the ground, M_g by

$$M = M_g \sin\ \theta \tag{2.26}$$

The V- and H-polarized forward scattering amplitudes of the cylinders are given by [Ruck, *et al.*, 1970]

$$T_V(\theta, \pi) = \frac{1}{\sin\theta} \sum_{n=-\infty}^{\infty} C_n^{TM}(\theta)$$
$$T_H(\theta, \pi) = \frac{1}{\sin\theta} \sum_{n=-\infty}^{\infty} C_n^{TE}(\theta) \qquad (2.27)$$

where the functions $C_n^{TM}(\theta)$ and $C_n^{TE}(\theta)$ for cylinders with diameter a_0 and relative permittivity ε_r are given by :

$$C_n^{TM} = -\frac{V_n P_n - q_n^2 J_n(x_0) H_n^{(1)}(x_0) J_n^2(x_1)}{P_n N_n - [q_n H_n^{(1)}(x_0) J_n(x_1)]^2} \qquad (2.28)$$

$$C_n^{TE} = -\frac{M_n N_n - q_n^2 J_n(x_0) H_n^{(1)}(x_0) J_n^2(x_1)}{P_n N_n - [q_n H_n^{(1)}(x_0) J_n(x_1)]^2} \qquad (2.29)$$

where J_n and $H_n^{(1)}$ are Bessel and Hankel functions of the first kind of order n, and

$$x_0 = k_0 a_0 \sin\theta \qquad (2.30)$$

$$x_1 = k_0 a_0 \sqrt{\varepsilon_r - \cos^2\theta} \qquad (2.31)$$

$$q_n = \frac{n\cos\theta}{k_0 a_0}\left(\frac{1}{\varepsilon_r - \cos^2\theta} - \frac{1}{\sin^2\theta}\right) \qquad (2.32)$$

$$V_n = s_1 J_n(x_0) J'_n(x_1) - s_0 J'_n(x_0) J_n(x_1) \qquad (2.33)$$

$$P_n = r_1 H_n^{(1)}(x_0) J'_n(x_1) - s_0 H_n^{(1)'}(x_0) J_n(x_1) \tag{2.34}$$

$$N_n = s_1 H_n^{(1)}(x_0) J'_n(x_1) - s_0 H_n^{(1)'}(x_0) J_n(x_1) \tag{2.35}$$

$$M_n = r_1 J_n(x_0) J'_n(x_1) - s_0 J'_n(x_0) J_n(x_1) \tag{2.36}$$

and

$$s_0 = \frac{1}{\sin\theta}, \qquad s_1 = \frac{\varepsilon_r}{\sqrt{\varepsilon_r - \cos^2\theta}}, \qquad r_1 = \frac{1}{\sqrt{\varepsilon_r - \cos^2\theta}} \tag{2.37}$$

In the above formulas, prime denotes derivative with respect to the argument.

Figure 2.11 provides the angular variation of the extinction coefficient $\kappa_p(\theta)$ at (a) L-band, (b) C-band, and (c) X-band for a canopy of stalks using the dielectric function given in Fig. 2.4. Also included are the data obtained at 20°, 40°, 60°, and 90°, presented in the form of the mean value of the measured loss and the associated standard deviation. Overall, excellent agreement is observed between the measured data and the theoretical curves for vertical polarization. Since stalks are not completely vertical and the horizontally polarized wave suffers some vertical attenuation the calculated data underestimates the propagation loss for horizontal polarization.

The variation of the polarization phase-difference with frequency was calculated using (2.22) and is compared with the measured data in Fig. 2.12 at (a) 20°, (b) 40°, and (c) 90°. The calculation reconfirms that the vertically polarized wave leads the horizontally polarized wave at L-band, but the lead diminishes as frequency increases and eventually the V-polarization lags the H-polarization at C-band. Good overall qualitative agreement exists between the theory and the experimental observations.

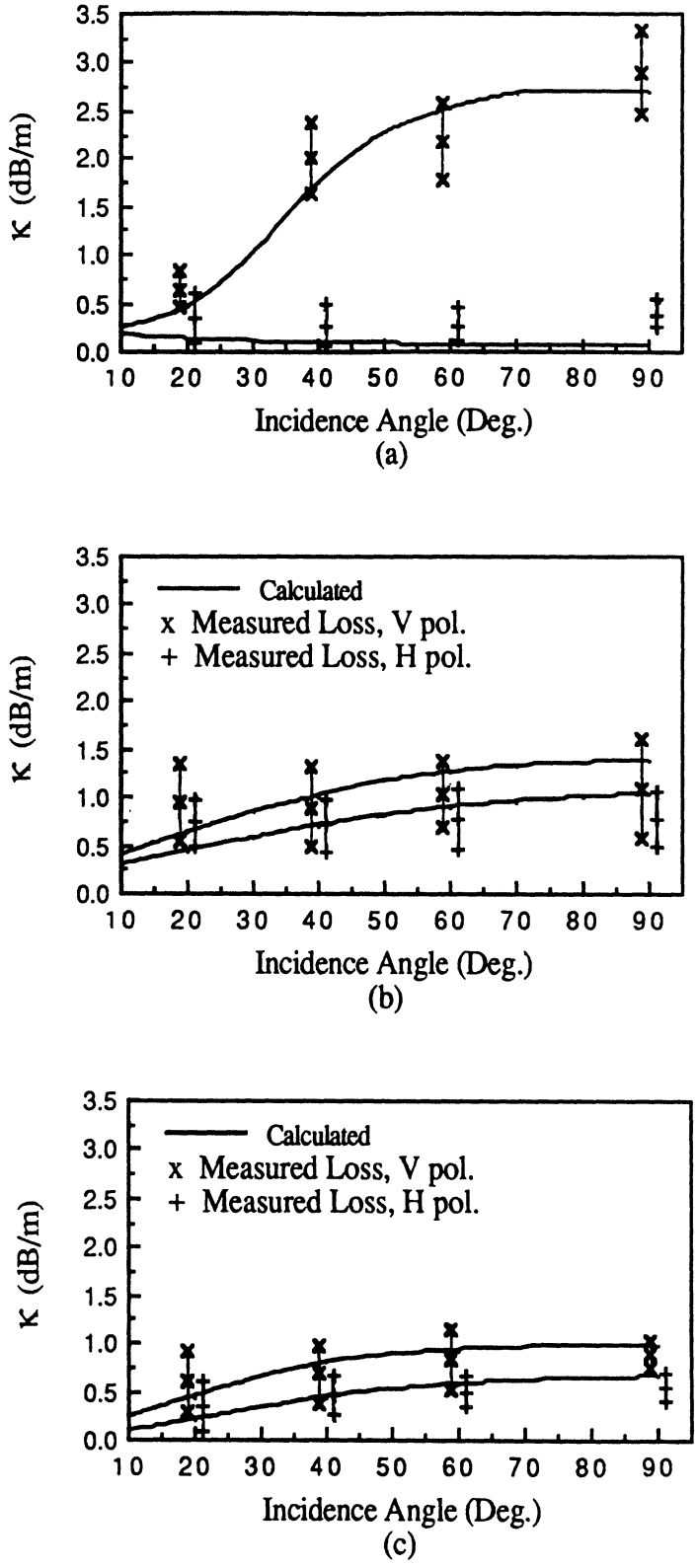

Figure 2.11 Comparison of calculated extinction coefficient for stalks with measured values at (a) L-band, (b) C-band, and (c) X-band.

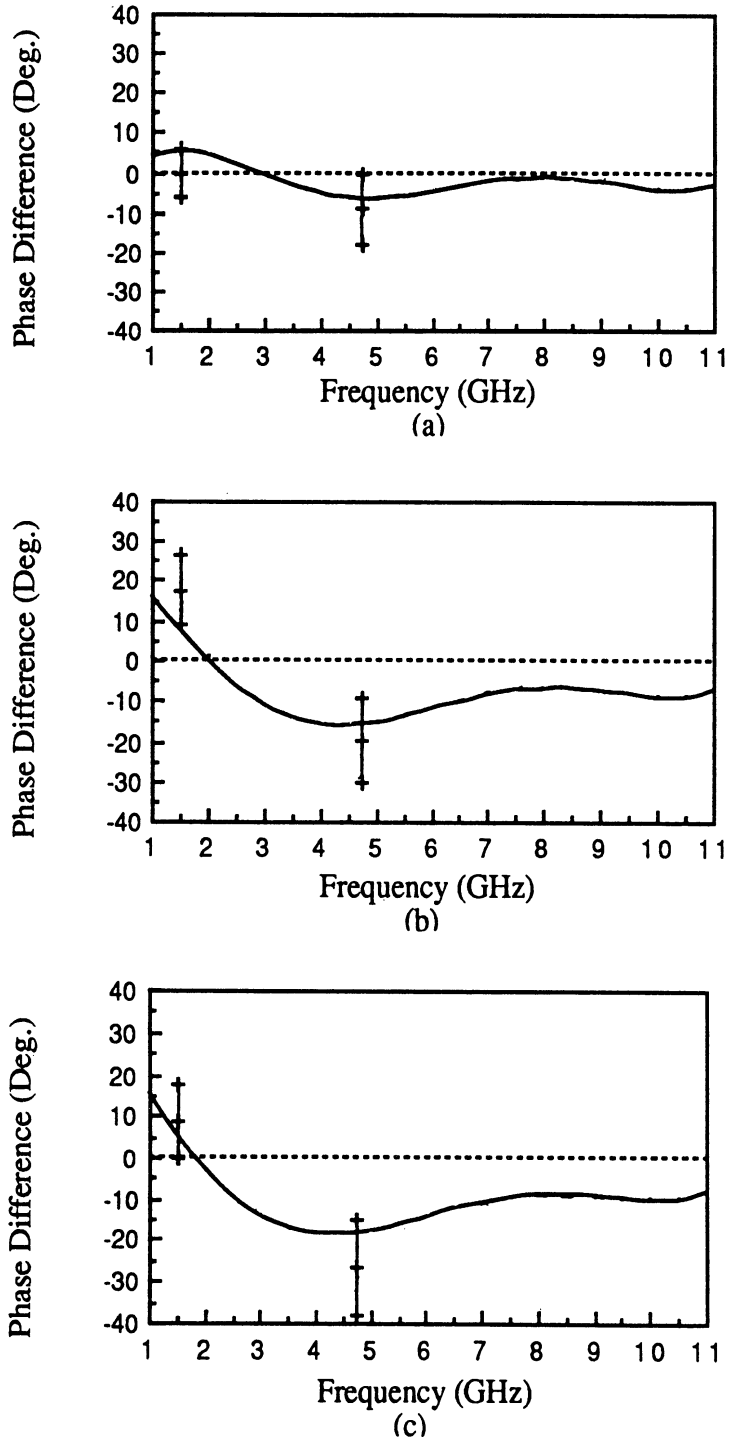

Figure 2.12 Comparison of calculated phase difference $\Delta\phi$ with measured data at incidence angles of (a) 20°, (b) 40°, and (c) 90°.

2.5 Full Canopy at Low Frequencies (Leaf Dimensions << λ)

At low frequencies, when leaf dimensions are small compared to the waveler leaves behave as weak scatterers, which allows the use of the quasi-static approximation to represent scattering by the leaves. If we consider leaves to be thin circular discs, small in size relative to λ, and randomly oriented, we can use a dielectric mixing formula [de Loor, 1968; Ulaby, *et al.*, 1986] to relate the relative dielectric constant of the leaf material ε_l to that of a medium with equivalent propagation properties for the mean field. The equivalent medium, which is comprised of a background dielectric constant ε, representing the stalks in air derived in section 2.4, and inclusions (the leaves) of dielectric constant ε_l and volume fraction v_l, has a relative dielectric constant ε_c given by

$$\varepsilon_c = \varepsilon + \frac{v_l}{3}(\varepsilon_l - \varepsilon)\left(2 + \frac{\varepsilon}{\varepsilon_l}\right) \tag{2.38}$$

ıckground dielectric $\varepsilon = \varepsilon_p(\theta)$ is a function of both the incidence angle θ and the polarization p, so is the canopy dielectric constant ε_c. The background dielectric constant is related to the index of refraction defined by (2.23) through $\varepsilon = \varepsilon_p(\theta) = n_p^2(\theta)$. Using the preceding formulation, κ_c was computed for V and H polarizations at L-band and C-band and the results are presented in Figure 2.13. Comparison of the theoretical results with the measured data indicates very good agreement at L-band, but under-estimates the propagation loss at C-band. This result can be attributed to the fact that at C-band the geometrical sizes of the leaves are comparable to the wavelength and scattering loss is not negligible, which is an inherent assumption of the model leading to (2.38).

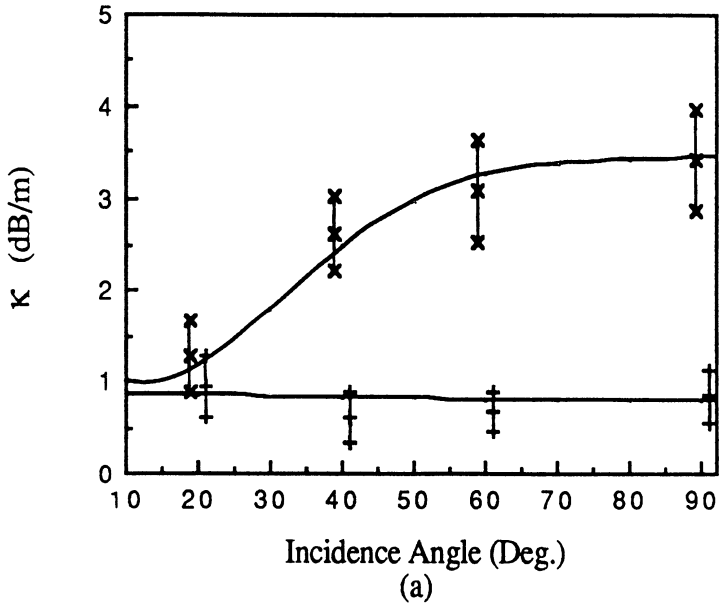

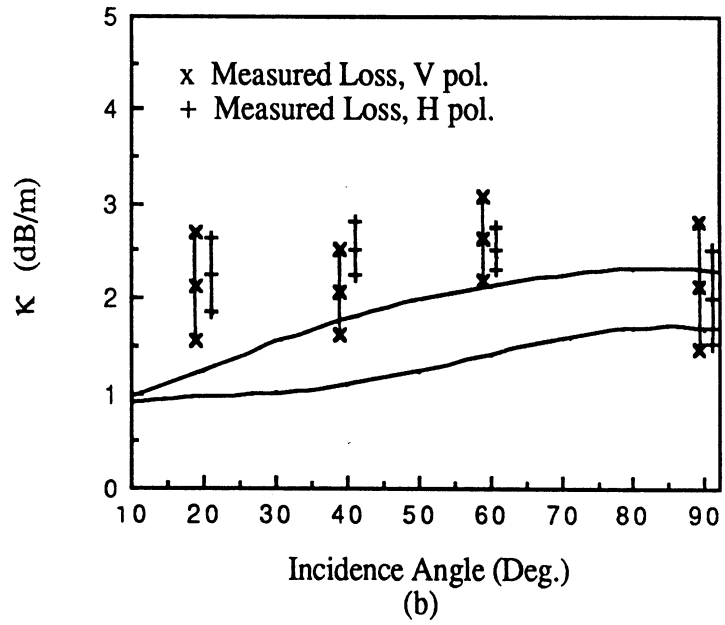

Figure 2.13 Comparison of calculated extinction coefficient with measured values for a full corn canopy at (a) L-band, (b) C-band.

2.6 Full Canopy at High Frequencies (Leaf Surface Dimensions >> λ)

When the leaf surface dimensions are much larger than the wavelength, the scattering loss is comparable to the absorption loss of the leaves. Therefore, the scattering amplitude and orientation distribution of the leaves must be taken into consideration. Here,we will model the leaves as randomly oriented thin dielectric sheets of arbitrary shapes and surface dimensions that are much larger than a wavelength. A leaf can be considered as a thin layer (of thickness τ) of a non-magnetic dielectric material with permittivity ε. Then it can be represented by a resistive sheet whose resistivity R in ohms per unit area is given by [Harrington and Mautz, 1975; Sarabandi, 1989]

$$R = \frac{iZ_0}{k_0\tau(\varepsilon - 1)} \tag{2.39}$$

where Z_0 is the free space impedance. When R = 0 the sheet appears perfectly conducting and when R = ∞ it ceases to exists. The sheet is an electric current sheet whose strength is proportional to the tangential electric field and is related to R. If $\hat{n}$ is the unit vector normal drawn outward to the upper (positive) side of the sheet and $[\ ]_-^+$ denotes the discontinuity across the sheet, the boundary conditions for the resistive sheet are

$$\begin{aligned} [\hat{n} \times \vec{E}]_-^+ &= 0 \\ \hat{n} \times (\hat{n} \times \vec{E}) &= -R\vec{J} \end{aligned} \tag{2.40}$$

where

$$\vec{J} = [\hat{n} \times \vec{H}]^{+}_{-} \tag{2.41}$$

is the total electric current supported by the sheet. The scattering properties of a leaf with large surface dimensions compared to λ can be derived by using the physical optics approximation for a finite size sheet in conjunction with the electric current supported by an infinite resistive sheet. The reflection coefficients of an infinite resistive sheet for V- and H-polarizations are:

$$\Gamma_V = \left(1 + \frac{2R\cos\psi}{Z_0}\right)^{-1}$$
$$\Gamma_H = \left(1 + \frac{2R\sec\psi}{Z_0}\right)^{-1} \tag{2.42}$$

where ψ is the incidence angle with respect to the normal to the sheet surface. For a plane wave traveling in the x-direction and a leaf whose normal $\hat{n}$ to the surface is defined by the angles ψ and ξ (Fig. 2.14), the forward scattering amplitudes are given by [Sarabandi, 1989]

$$S_V(\pi) = -\frac{iAk_0^2}{2\pi}\cos\psi\left[\Gamma_V\cos^2\xi + \Gamma_H\sin^2\xi\right]$$
$$S_H(\pi) = -\frac{iAk_0^2}{2\pi}\cos\psi\left[\Gamma_V\sin^2\xi + \Gamma_H\cos^2\xi\right] \tag{2.43}$$

where A is the leaf area and Γ_V and Γ_H are as defined in (2.42). In the propagation model, we need an ensemble average of the forward scattering amplitude of the leaves. The

average forward scattering amplitude for randomly oriented leaves can be obtained by averaging $S(\pi)$ over all possible orientation angles; thus,

$$< S_{V,H}(\pi) > = < S(\pi) > = \frac{1}{4\pi} \int_0^{2\pi} d\xi \int_0^{\pi} S_{V,H}(\pi) \sin \psi \, d\psi \tag{2.44}$$

Γ_V and Γ_H are independent of the angle ξ, therefore, the integration over ξ can be easily performed to give:

$$< S(\pi) > = - \frac{i A k_0^2}{8\pi} \int_0^{\pi} (\Gamma_V + \Gamma_H) \cos \psi \sin \psi \, d\psi \tag{2.45}$$

Upon substitution of the values of Γ_V and Γ_H in (2.45), the following relation is obtained:

$$< S(\pi) > = - \frac{i A k_0^2}{8\pi} \{ \int_0^{\pi} (1 + \frac{2 R \cos \psi}{Z_0})^{-1} \cos \psi \sin \psi d\xi\psi + \int_0^{\pi} (1 + \frac{2 R}{Z_0 \cos \psi})^{-1} \cos \psi \sin \psi d\psi \} \tag{2.46}$$

Through the change of variable $\alpha = \cos \psi$, $<S(\pi)>$ assumes the following form

$$< S(\pi) > = - \frac{i A k_0^2}{8\pi} \{ \int_{-1}^{1} \frac{\alpha}{1 + \frac{2R}{Z_0} \alpha} d\alpha + \int_{-1}^{1} \frac{\alpha^2}{\alpha + \frac{2R}{Z_0}} d\alpha \} \tag{2.47}$$

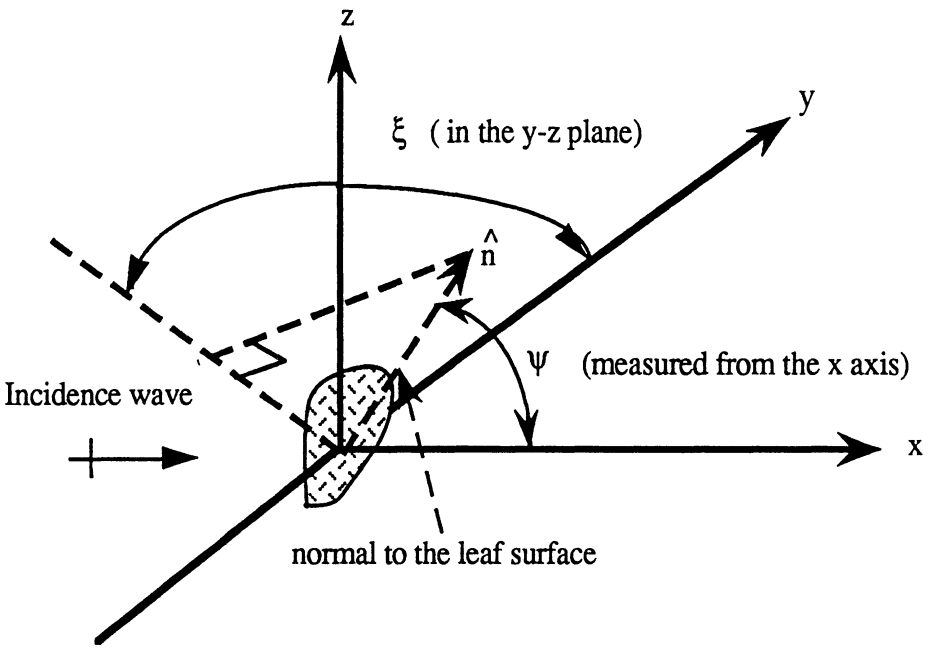

Figure 2.14 Scattering geometry for an arbitrary shaped thin dielectric leaf

which leads to the result

$$< S(\pi) > = - \frac{i A k_0^2}{8\pi} \left\{ \frac{Z_0}{R} - \frac{4R}{Z_0} + i 4\pi \frac{R^2}{Z_0^2} + \left[\frac{4R^2}{Z_0^2} - \frac{Z_0^2}{4R^2} \right] \ln \left(\frac{Z_0 + 2R}{Z_0 - 2R} \right) \right\} \tag{2.48}$$

Because the physical-optics approximation is used in the derivation of $<S(\pi)>$, equation (2.48) is valid for leaves with surface dimensions larger than a wavelength. Upon substituting (2.27) and (2.48) in (2.20), we obtain the following expressions for the equivalent dielectric constant of the canopy:

$$n^{V,H} = 1 - \frac{i\,2M_g}{k_0^2} \sum_{n=-\infty}^{\infty} C_n^{TE,TM}(\theta) - \frac{i\zeta}{4k_0}\left\{\frac{Z_0}{R} - \frac{4R}{Z_0} + i4\pi\frac{R^2}{Z_0^2} + \left[\frac{4R^2}{Z_0^2} - \frac{Z_0^2}{4R^2}\right]\ln\left(\frac{Z_0+2R}{Z_0-2R}\right)\right\} \quad (2.49)$$

where ζ is the leaf area per unit volume. It can be seen that as long as the leaves are large compared with λ, the exact sizes and numbers of leaves are not needed in the computations, and only the knowledge of ζ suffices.

Figure 2.15 depicts the contributions of the stalks and leaves to the total extinction coefficient $\kappa_p(\theta)$ according to (2.49) and the data given in Table 2.1 at X-band. The simulation reconfirms the experimental observation that the attenuation loss in the medium is dominated by the leaves at X-band. Since the leaves are assumed to have uniform orientation distributions, the dependence of the extinction coefficient on the incidence angle is only caused by the stalks. Figure 2.16 shows the calculated angular variation of the extinction coefficient including the data measured at 20°, 40°, 60°, and 90°, presented in the form of the mean value of the measured extinction coefficient and the associated standard deviation. Overall, good agreement is observed between the measured data and the theoretical curves for both polarizations at X-band.

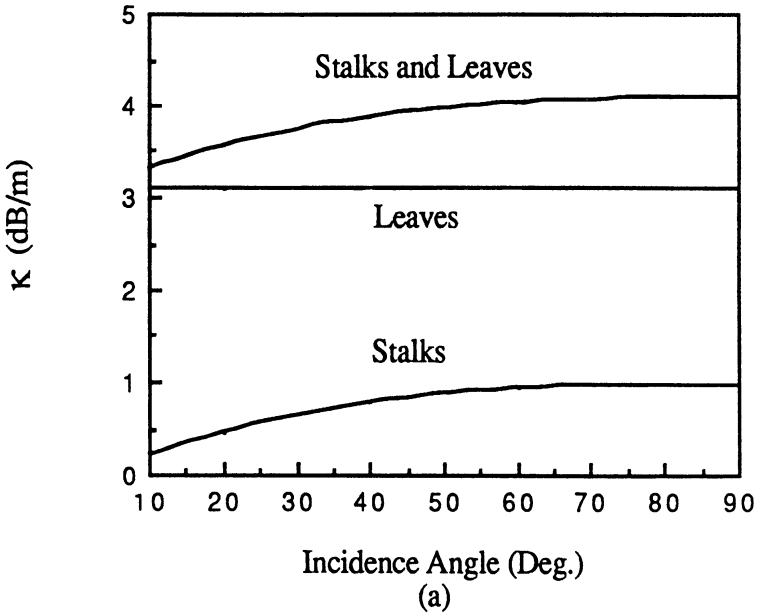

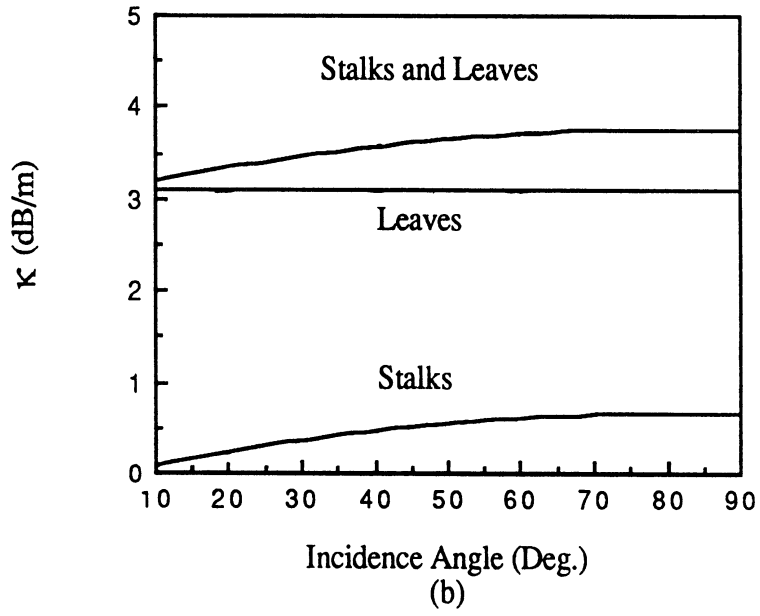

Figure 2.15 Comparison between the contributions of the stalks and leaves to the extinction coefficient at X-band for (a) V-polarization, (b) H-polarization.

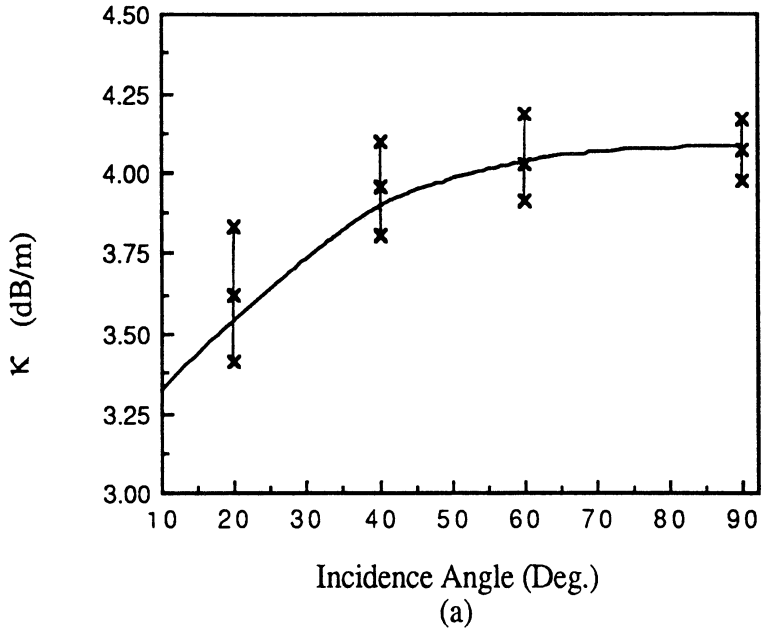

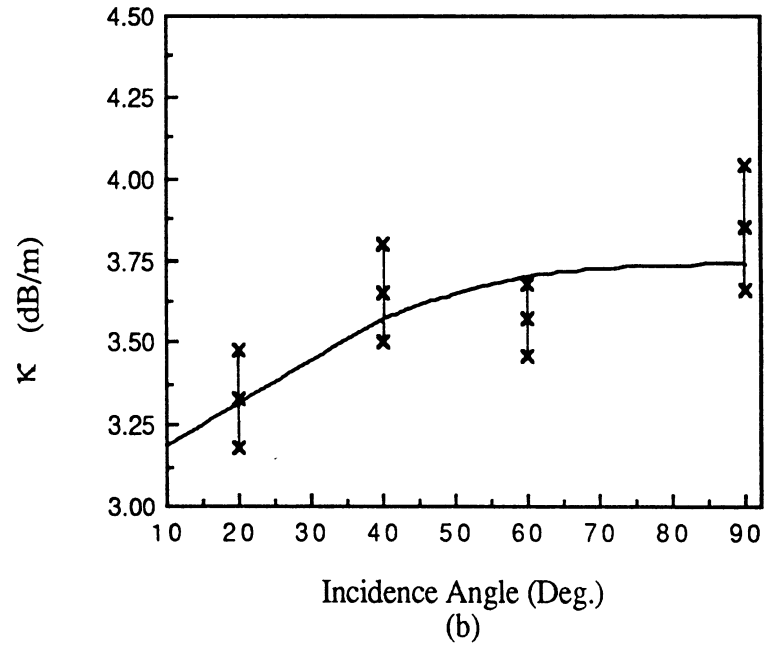

Figure 2.16 Comparison between the calculated extinction coefficient and the measured data for a full corn canopy at X-band for (a) V-polarization, (b) H-polarization.

Similar calculations were performed at C-band and the calculated values of $\kappa_p(\theta)$ exceeded the measured values considerably (Fig. 2.17). This result is due to the fact that at C-band the corn leaf dimensions are smaller than or comparable to the wavelength and, as a result, the physical-optics approximation fails to predict the correct leaf scattering amplitude.

2.7 Conclusion

The propagation model developed in this chapter can account for both scattering and absorption by the canopy scatterers. The model can also characterize the phase information associated with the propagation of the mean field. Representation of the stalks by infinitely long cylinders produced results in good agreement with the measured data. A simple representation of the leaves that could produce satisfactory results at all frequencies was not attained. At low frequencies, where leaf dimensions are small compared to λ, scattering loss is negligible and the dielectric mixing formula for randomly oriented dielectric discs was successfully used to represent the leaves. When surface dimensions of the leaves are much larger than λ, the physical-optics approximation along with the resistive sheet representation of thin dielectric sheets was used to represent the leaves. Both absorption and scattering losses of leaves are accounted for in this representation and successful results were obtained at 10.2 GHz. In the intermediate frequency range where leaf dimensions are comparable to the wavelength, a different model for leaves is needed.

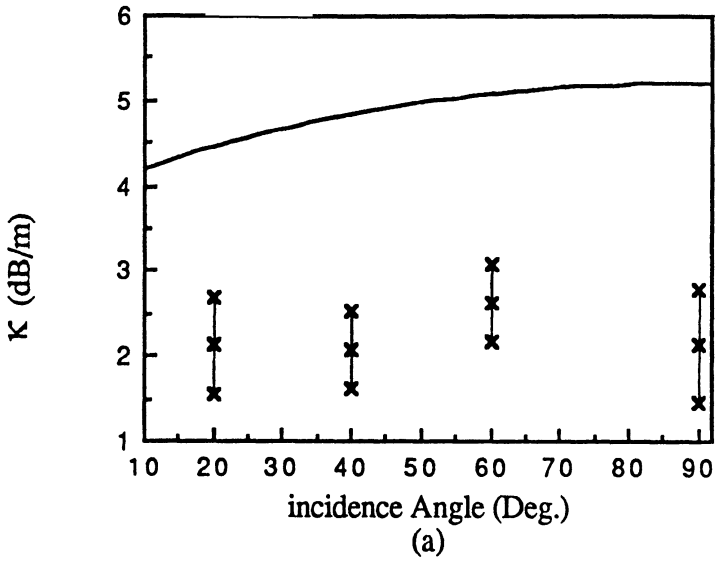

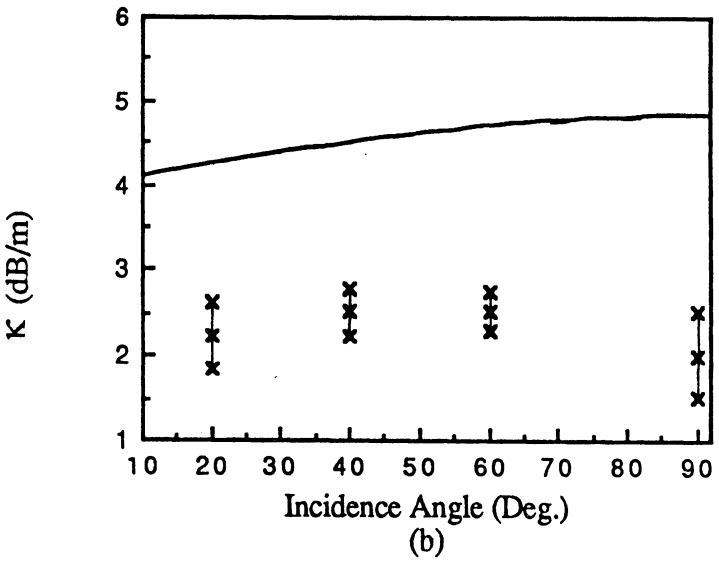

Figure 2.17 Comparison between the calculated extinction coefficient and the measured data for a full corn canopy at C-band for (a) V-polarization, (b) H-polarization.

CHAPTER III

COHERENT WAVE PROPAGATION THROUGH MAN-MADE VEGETATION CANOPIES

.1 Introduction

In many man-made vegetation canopies such as agricultural fields, orchards, artificial forests, and plantations, the position of each plant within each row and the separation between rows are deterministic quantities (Fig. 3.1). In other words, the distance between plants in each row and the row spacing are kept constant within some small fluctuations. In certain wavelength ranges depending on row spacing and plant spacing, horizontal wave propagation through the canopy becomes a coherent process and a field approach is needed to characterize wave-vegetation interactions.

The goal of this chapter is to formulate a model that can adequately characterize coherent horizontal wave propagation in a medium comprised of a one-dimensional periodic row structure with known row periodicity, and known within-row plant periodicity. A two-dimensional semi-deterministic model has been developed for media containing vertical cylinders, representing the stalks, and randomly oriented disks, representing the leaves. The vegetation canopy is divided into slabs (rows) that statistically exhibit similar electromagnetic properties. For a given incident direction, transmission through and reflection by an individual slab occurs at only a specific set of directions determined according to diffraction Bragg theory. After deriving the transmission and

reflection coefficient matrices corresponding to the Bragg-modes for a single slab, network theory is applied to derive the overall transmission and reflection coefficient matrices of the entire canopy (cascaded slabs). The overall transmitted field due to the cylindrical incident wave is then calculated by taking the inverse Fourier transform of the product of the total transmission coefficient spectrum of the medium and the angular spectrum of the incident field.

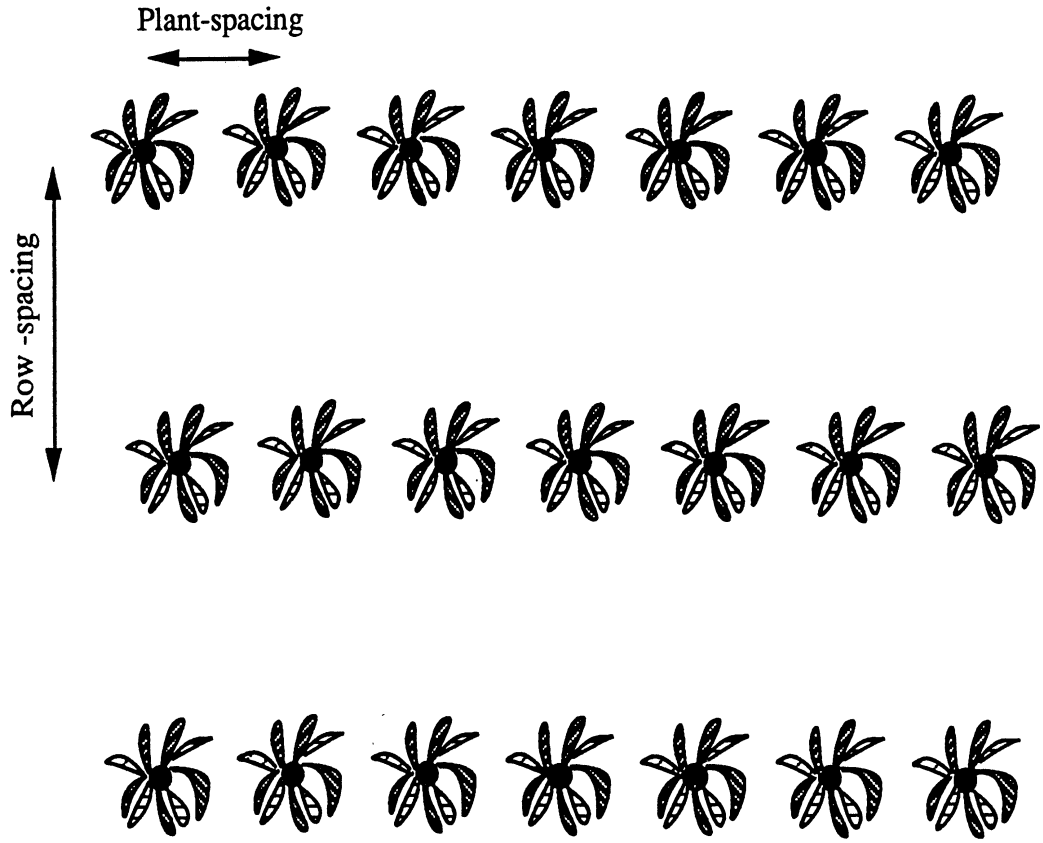

Figure 3.1 Top view of three rows of an agricultural field depicting the row and plant spacings.

A set of measurements were conducted, first, to investigate experimentally the effect of look direction on the wave propagation behavior, and second, to help the development of a model that can explain wave propagation in such media. Details of the measurement procedure and the experimental results are given in section 3.2. Sections 3.3 through 3.6 contain the development of the coherent propagation model. Comparison between the theoretical model and the experimental results for a defoliated canopy are made in sections 3.7 and 3.8. Section 3.9 discusses inclusion of leaves in the theoretical model when the leaf surface dimensions are much smaller than the wavelength and provides comparison with the experimental data.

3.2 Description of the Experiment

Experiments were conducted to examine the role of row direction and azimuth angle on a wave propagating horizontally in a semi-deterministic medium. Measurements of the magnitude and phase of waves transmitted horizontally through a corn canopy were made at 1.50 (L-band) and 4.75 (C-band) GHz for both vertical and horizontal polarizations, using the two configurations shown in Figure 3.2. The receivers on the truck were stationary and the transmitters were made to glide along a rail system at the same height above the ground (1.2 m) as the transmitters. Vertical and horizontal polarizations were transmitted simultaneously and the detected power and phase of the received fields were recorded using an HP-8510 network analyzer. The reference field for the network analyzer was supplied through a cable from the transmitter. At L-band the transmitter used microstrip patch antennas with a beamwidth of 90.2° each and the receiver used a dual-polarized dish antenna with a beamwidth of 7.8°. At C-band the transmitter used a dual-polarized quadridge horn antenna with a beamwidth of 53.1° and the receiver used a dual-polarized dish antenna with a beamwidth of 4.6°. Each measurement was repeated several

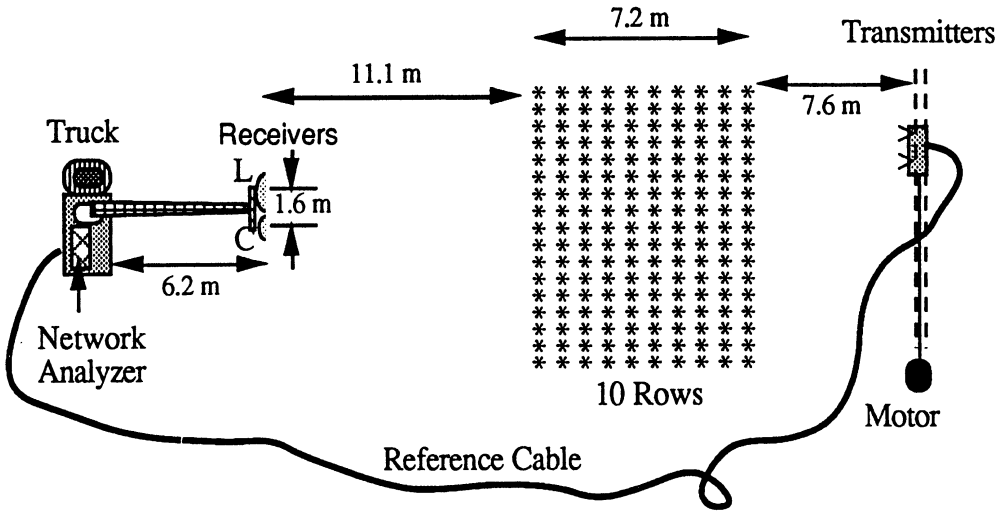

(a)

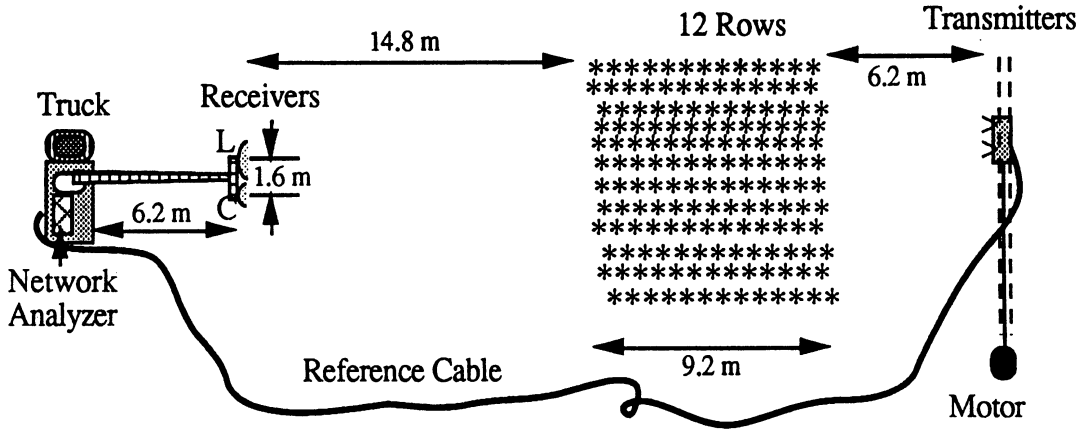

(b)

Figure 3.2 Measurement configuration showing the transmitter and receiver sections, both at the same height at 1.2 m above the ground level for (a) perpendicular to rows configuration and (b) parallel to rows configuration. The transmitter platform was made to glide on a rail under motor control.

times to check repeatability. The observations show that the data is quite consistent, with the received power and phase patterns being repeatable within 2 dB for power and 20° for phase.This variation is attributed to wind-induced movements of corn plants and movements of the reference cable. Propagation measurements were conducted for look directions parallel to the rows and perpendicular to the rows. For both configurations, the measurements were performed for various canopy path lengths. Measurements with and without cobs and leaves were performed to study the effects of individual crop constituents. Then, the density of the remaining stalks was reduced to one half by cutting and removing every other plant in each row, and the measurements were performed again. At the end of the experiment, the corn plants were cut and removed and then direct line-of-sight measurements were conducted for calibration purposes and to check that ground reflections were not present.

The moisture content, sizes, and densities of each constituent of the canopy were measured for incorporation in the theoretical calculations. Figures 3.3 and 3.4 show examples of the data. Figure 3.3 shows a comparison of the received and reference (without vegetation) powers at L band for stalks with no leaves. Figure 3.4 depicts the received power at C band when both stalks and leaves were present. Note that a "beam widening" effect occurs when the vegetation is present and the received power pattern does not follow the reference power pattern.

Figures 3.5 and 3.6 present estimates of the transmission loss measured over the central part of the beam for perpendicular and parallel row orientations. The number next to each data point is a measure of the variation in power level observed over the central part of the beam, relative to the mean value. The following observations can be made about the data:

1- Row direction affects the beam pattern of the transmitted wave and a propagation model that takes the effect of rows into consideration is needed to explain wave propagation in the canopy.

2- At 1.5 GHz, for H polarization, leaves are the dominant contributors to the loss suffered by the wave, but for V polarization, the stalks are the major attenuators of the electromagnetic wave.

3- At 4.75 GHz, leaves are the major contributors to the loss at both polarizations.

4- Power loss is higher when the electromagnetic wave travels perpendicular to the rows than when it travels parallel to the rows.

5- Leaf distribution is not azimuthally symmetric because the leaves tend to hang out more in between rows than in between plants. The horizontally polarized wave suffers more loss when travelling parallel to the rows than the vertically polarized wave. The reverse is true when the microwave energy is transmitted perpendicular to the rows.

6- Frequency of variation of received power is higher when the transmitted wave travels normal to the rows than in a direction parallel to the rows.

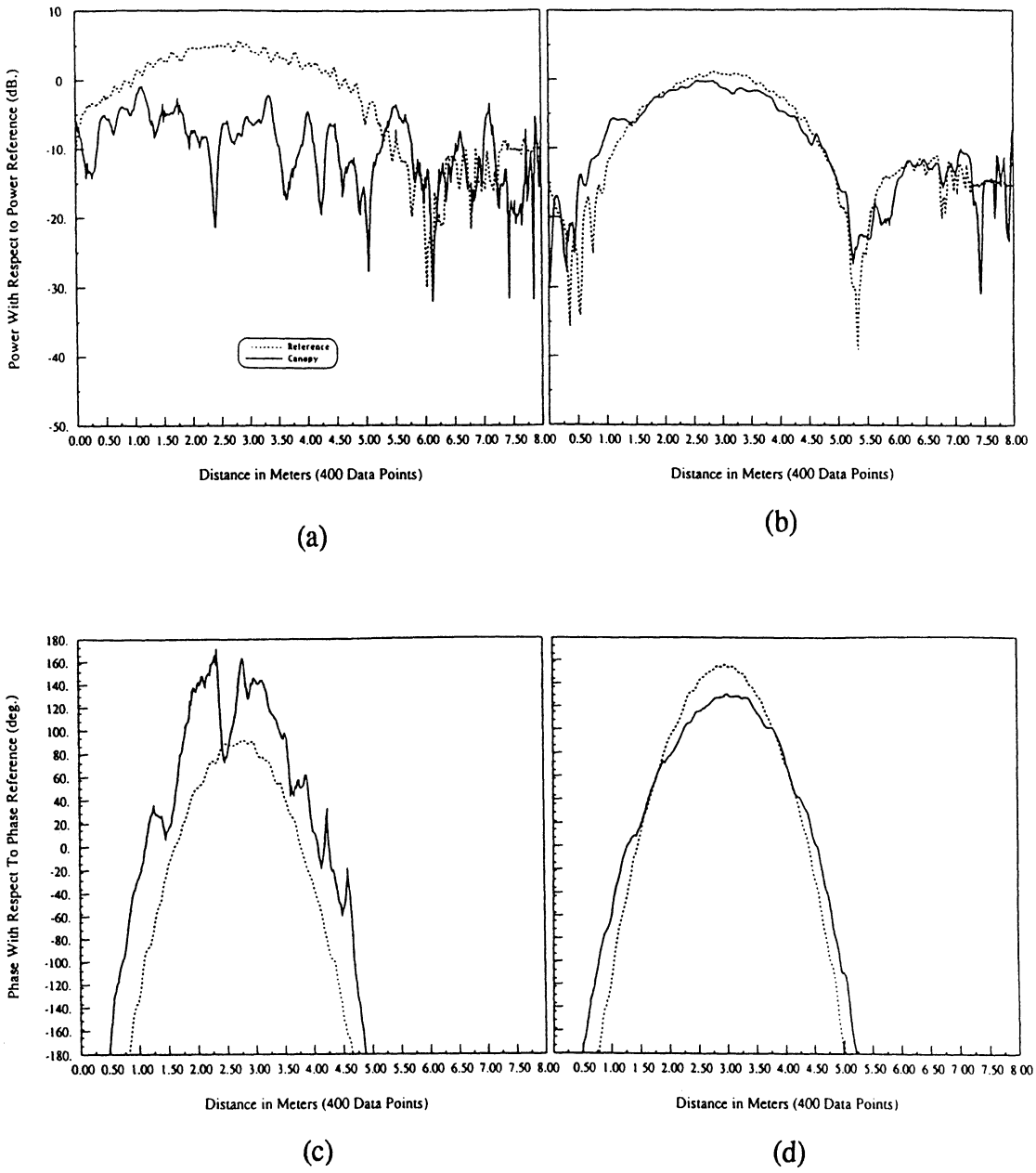

Figure 3.3 Comparison between canopy and reference measurements of amplitude patterns for (a) V-polarization, (b) H-polarization and phase patterns for (c) V-polarization, and (d) H-polarization. The wave was transmitted through seven rows of stalks at L-band.

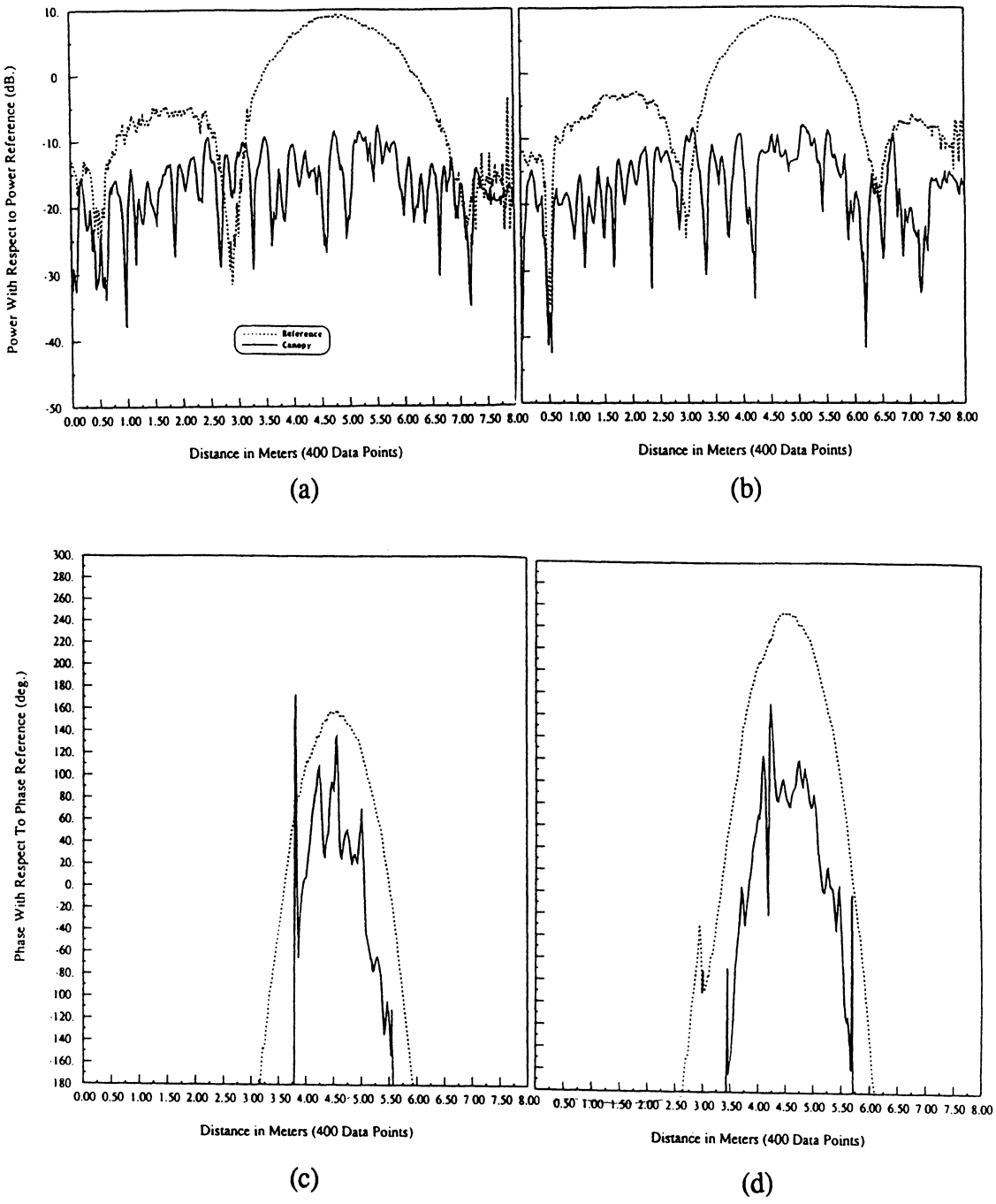

Figure 3.4 Comparison between canopy and reference measurements of amplitude patterns for (a) V-polarization, (b) H-polarization and phase patterns for (c) V-polarization, and (d) H-polarization. The wave was transmitted through seven rows of stalks and leaves at C-band.

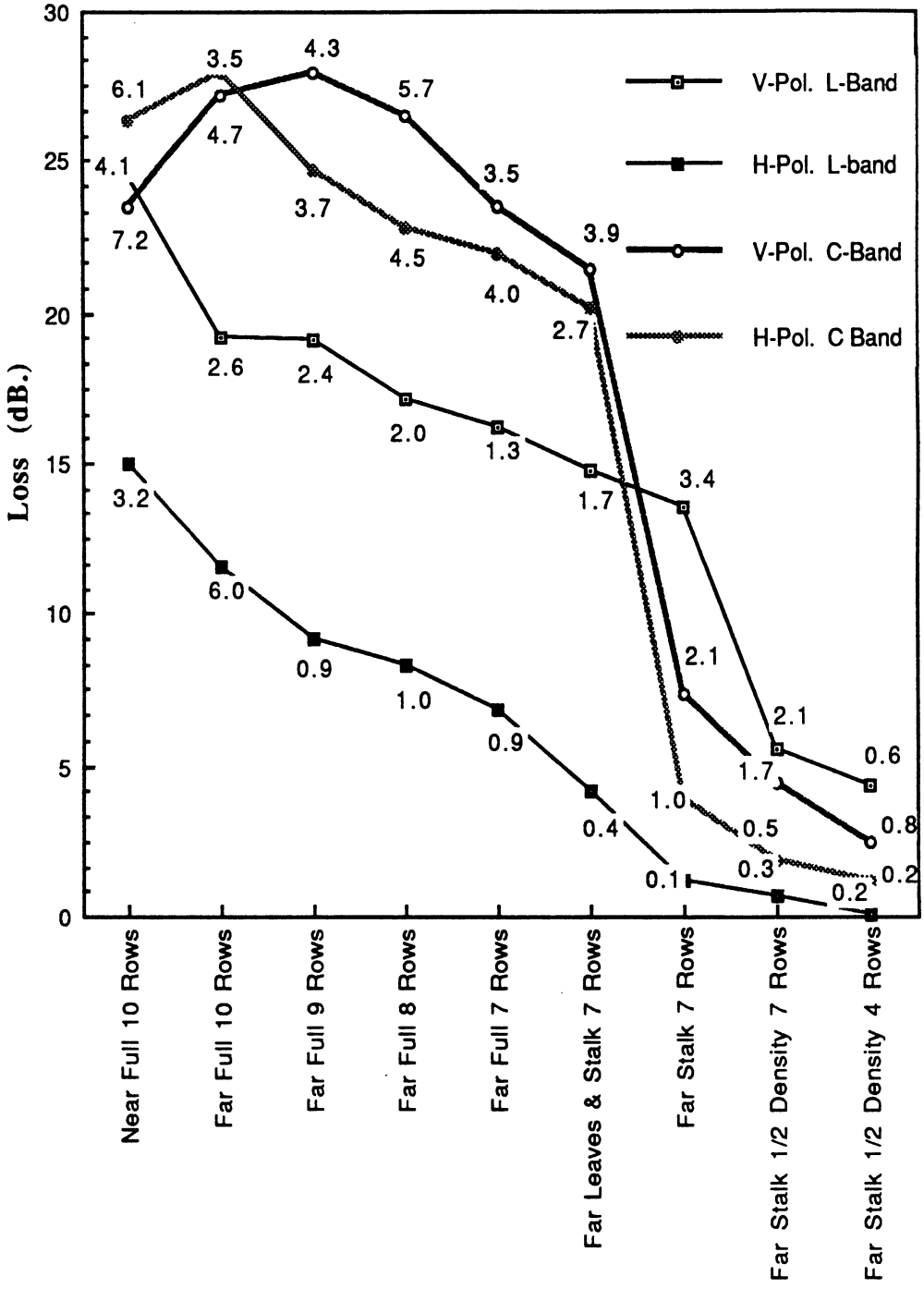

Figure 3.5 Loss estimates for perpendicular-to-rows configuration. The number next to each data point is a measure of the variation in power level observed over the central part of the beam, relative to the mean value.

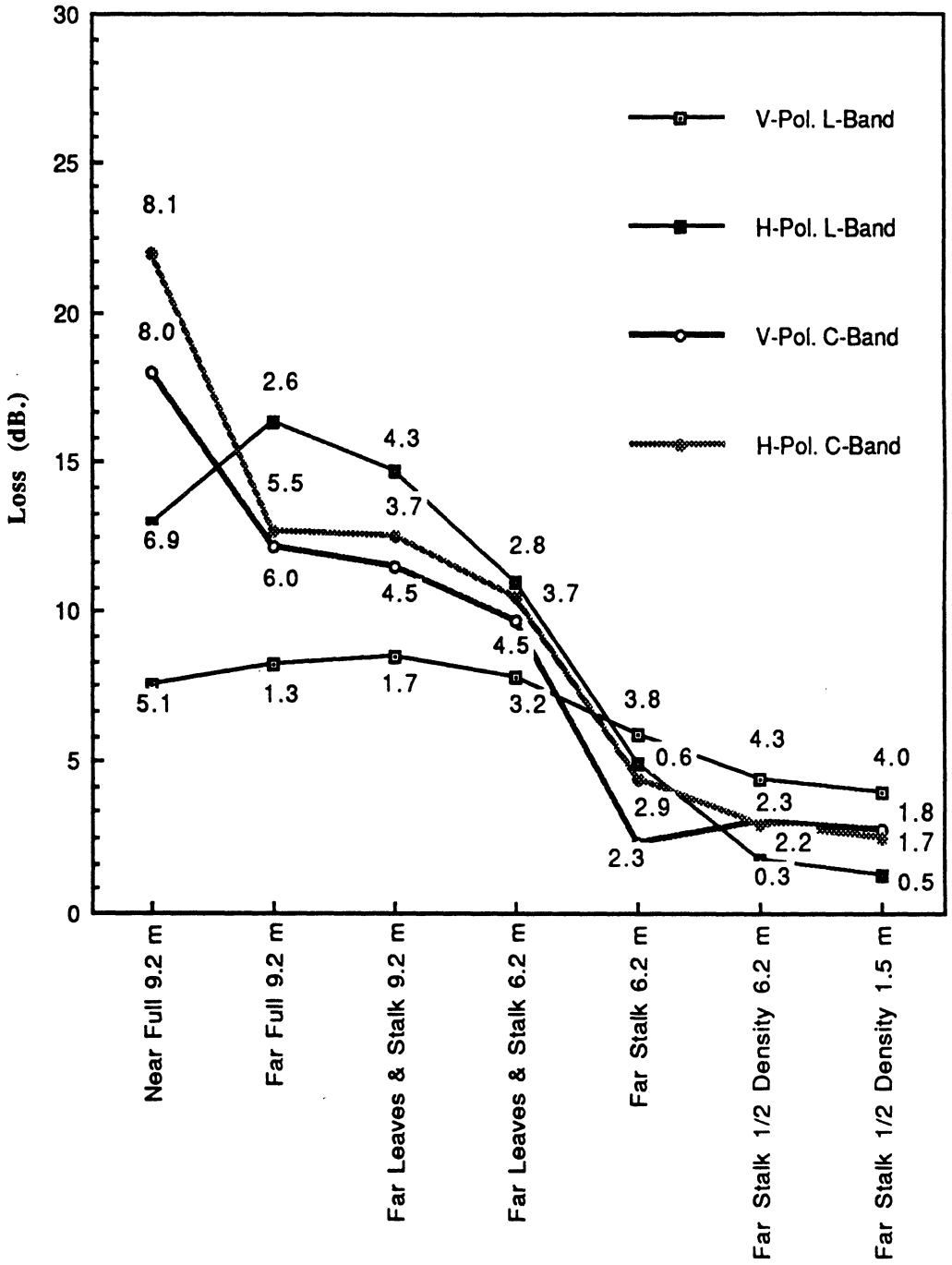

Figure 3.6 Loss estimates for parallel-to-rows configuration. The number next to each data point is a measure of the variation in power level observed over the central part of the beam, relative to the mean value.

3.3 Theoretical Approach

Based on the experimental observations, it was decided to develop a propagation model for a non-random scattering medium. The purpose of the model is to produce wave patterns similar to those observed experimentally. During the course of model development, it was concluded that the propagation mode is primarily coherent in nature when only stalks are present. Therefore, the following treatment pertains to a row-crop vegetation canopy comprised of vertically oriented stalks or any medium with similar structure. Each row is modelled as a slab-like region composed of an infinite number of infinitely long cylinders located periodically with spacing L between adjacent cylinders. Guided by the experimental observations noted in the preceding section, a wave structure propagation model (WSPM) was developed, consisting of three major steps:

(1) Using wave theory, expressions were derived for the effective reflection and transmission coefficient matrices $[R_S]$ and $[T_S]$ of an individual row of vegetation (slab).

(2) Then, using the above matrices for a single row, the total transmission matrix of the multi-row structure was derived for any specified number of rows .

(3) Finally, using the resultant total transmission matrix of the canopy for plane wave incidence, the transmitted wave pattern through the medium was derived for a non-uniform incident wave. This is called a Wave Structure Propagation Model (WSPM).

3.4 A Single Slab of Periodically Distributed Cylinders

Figure 3.7 depicts a top view of an array of periodically distributed cylinders. Consider a plane wave illuminating the array at an angle ϕ_0. The scattering from such a

periodic structure can be formulated *via* an integral equation involving polarization currents whose domain is confined over a period L of the structure using the Floquet's theorem [Sarabandi, 1990]. For a vertically polarized incident wave, the polarization current, J_y, of the cylinders can be found from the following integral equation:

$$J_y(x, z) = -ik_0 Y_0(\varepsilon(x, z) - 1)\{e^{ik_0(\sin\phi_0 x + \cos\phi_0 z)} + \int\int J_y(x', z')\, G^p_{yy}(x, z; x', z')dx'\, dz'\} \tag{3.1}$$

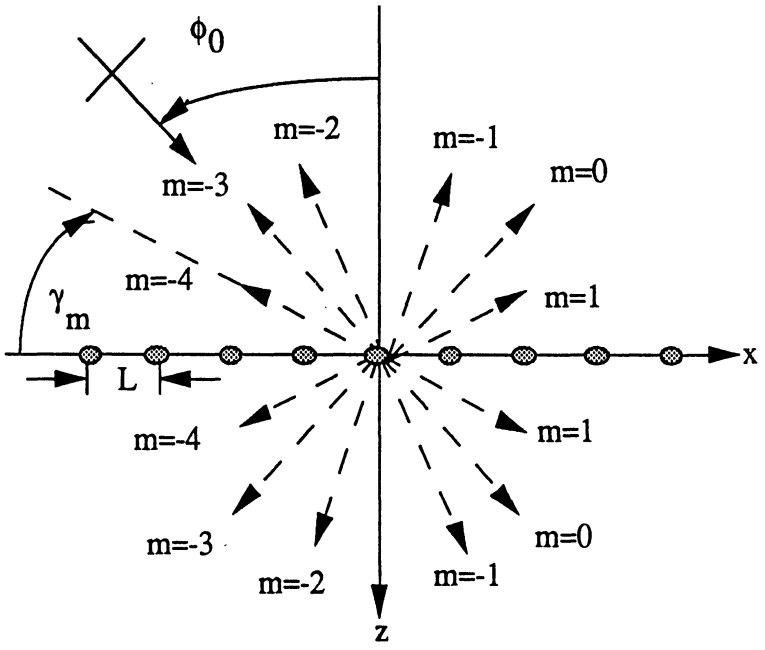

Figure 3.7 Top view of a row of periodically distributed cylinders. The arrows depict the directions of scattered Bragg modes.

where the integral is over the area of a cylinder, Y_0 is the free space admittance ($1/Z_0$), and ε (x,y) is the permittivity function of the cylinder. The quantity G^p_{yy} is the periodic Green's function and is given by:

$$G^p_{yy}(x, z; x', z') = -\frac{k_0 Z_0}{2L} \sum_{m=-\infty}^{+\infty} \frac{1}{k_{mz}} e^{i k_{mz}|z - z'| - i k_{mx}(x - x')} \tag{3.2}$$

where

$$k_{mx} = \frac{2\pi m}{L} - k_0 \sin \phi_0, \qquad k_{mz} = \sqrt{k_0^2 - k_{mx}^2} \tag{3.3}$$

For a horizontally polarized incident plane wave, the polarization currents, J_x and J_z, can be found from the following coupled integral equations:

$$J_x(x, z) = i k_0 Y_0 (\varepsilon(x, z) - 1) \{\cos \phi_0 e^{i k_0 (\sin \phi_0 x + \cos \phi_0 z)} + \iint [\, J_x(x', z')\, G^p_{xx}(x, z; x', z') + J_z(x', z')\, G^p_{xz}(x, z; x', z') \,] dx'\, dz'\} \tag{3.4}$$

$$J_z(x, z) = i k_0 Y_0 (\varepsilon(x, z) - 1) \{\sin \phi_0 e^{i k_0 (\sin \phi_0 x + \cos \phi_0 z)} + \iint [\, J_x(x', z')\, G^p_{zx}(x, z; x', z') + J_z(x', z')\, G^p_{zz}(x, z; x', z') \,] dx'\, dz'\} \tag{3.5}$$

where the corresponding periodic Green's functions are given by:

$$G^p_{xx}(x, z; x', z') = -\frac{k_0 Z_0}{2L} \left(1 + \frac{1}{k_0^2} \frac{\partial^2}{\partial x^2}\right) \sum_{m=-\infty}^{+\infty} \frac{1}{k_{mz}} e^{i k_{mz}|z - z'| - i k_{mx}(x - x')} \tag{3.6}$$

$$G^{p}_{xz}(x, z; x', z') = -\frac{Z_0}{2L k_0}\frac{\partial^2}{\partial x \partial z}\sum_{m=-\infty}^{+\infty}\frac{1}{k_{mz}} e^{i k_{mz}|z-z'| - i k_{mx}(x-x')} \tag{3.7}$$

$$G^{p}_{zx}(x, z; x', z') = G^{p}_{xz}(x, z; x', z') \tag{3.8}$$

$$G^{p}_{zz}(x, z; x', z') = -\frac{k_0 Z_0}{2L}\left(1+\frac{1}{k_0^2}\frac{\partial^2}{\partial z^2}\right) \sum_{m=-\infty}^{+\infty}\frac{1}{k_{mz}} e^{i k_{mz}|z-z'| - i k_{mx}(x-x')} \tag{3.9}$$

The solution of the integral equations can be obtained by numerical techniques, from which the scattered fields can be calculated. Far away from the scatterers (i.e. $z >> \lambda_0$), only the contributions of the terms corresponding to real values of k_{mz} in the summations of the periodic Green's functions are observable. The scattered plane waves associated with these terms are known as Bragg modes. For a plane wave incident at angle ϕ_0, the travelling direction of the m^{th} Bragg mode is defined by the angle γ_m such that:

$$\cos \gamma_m = \frac{m\lambda_0}{L} - \sin \phi_0 \tag{3.10}$$

where L is the period and λ_0 is the wavelength. The m^{th} mode is a propagating Bragg mode if

$$(-1 + \sin \phi_0)\frac{L}{\lambda_0} \le m \le (1 + \sin \phi_0)\frac{L}{\lambda_0} \tag{3.11}$$

Numerical techniques such as the method of moments can be used to solve the integral equations, as discussed by [Sarabandi, 1990]. However, such techniques are computationally inefficient when the size of the scatterers or the spatial period of the cylinders are large compared to the wavelength. For the purpose of reducing the computational time needed for the calculation, an approximate solution for the scattering problem of an array of periodic infinite dielectric cylinders is derived assuming that the separation between the cylinders is large enough so that the internal field of each cylinder is not affected by the fields of the other cylinders. In other words, the internal field of a cylinder in free space is assumed to hold true for each cylinder in the infinite array of cylinders. Refering to figure 3.7, scatterers in the array are infinitely long dielectric cylinders illuminated by a plane wave at an incidence angle ϕ_0. If the tangential electric and magnetic fields on the cylinders are known, then the scattered field can be calculated by employing the field equivalence principle [Harrington, 1961]. The equivalent electric and magnetic source functions in terms of the total surface fields are given by:

$$\vec{J}_e = \hat{n} \times \vec{H}_t \tag{3.12}$$

$$\vec{J}_m = -\hat{n} \times \vec{E}_t \tag{3.13}$$

where $\hat{n}$ is the unit normal to the cylinder surface.The Hertz vector potentials due to electric and magnetic sources are then given by:

$$\vec{\pi}_e = -\frac{z_0}{4k_0} \int_{\Sigma C_n} \vec{J}_e(x', z')\, H_0^{(1)}\left(k_0 \sqrt{(x-x')^2 + (z-z')^2}\right) dc' \tag{3.14}$$

$$\vec{\pi}_m = -\frac{Y_0}{4k_0} \int_{\sum C_n} \vec{J}_m(x', z')\, H_0^{(1)}(k_0\sqrt{(x-x')^2 + (z-z')^2})\, dc' \qquad (3.15)$$

where $\sum C_n$ represents the contours of all the cylinders in the array. Since the incident field is a plane wave and the cylinders are identical, it can be concluded that the equivalent surface currents on the cylinders are similar except for a progressive phase factor. Thus, the current on the n^{th} cylinder in terms of the currents of the zeroth cylinder is given by:

$$\vec{J}_{e,m}(x'_n, z'_n) = \vec{J}_{e,m}(x'_0, z'_0)\, e^{i k_0 \sin\phi_0 n L} \qquad (3.16)$$

where L is the period. Using (3.16) in (3.14) and (3.15), the Hertz vector potentials can be represented as:

$$\vec{\pi}_e = -\frac{z_0}{4k_0} \sum_{m=-\infty}^{+\infty} \int_{C_0} \vec{J}_e(x', z')\, e^{i k_0 \sin\phi_0 m L} H_0^{(1)}(k_0\sqrt{(x-x'-mL)^2 + (z-z')^2})\, dc' \qquad (3.17)$$

$$\vec{\pi}_m = -\frac{Y_0}{4k_0} \sum_{m=-\infty}^{+\infty} \int_{C_0} \vec{J}_m(x', z')\, e^{i k_0 \sin\phi_0 m L} H_0^{(1)}(k_0\sqrt{(x-x'-mL)^2 + (z-z')^2})\, dc' \qquad (3.18)$$

Using the following identity, the Hankel function can be represented in an integral form as:

$$H_0^{(1)}(k_0\sqrt{(x-x'-mL)^2+(z-z')^2}) = \frac{1}{\pi}\int_{-\infty}^{+\infty}\frac{e^{ik_z|z-z'|-ik_x(x-x'-mL)}}{k_z}dk_x \qquad (3.19)$$

where $k_z = \sqrt{k_0^2 - k_x^2}$. By employing the Poison's summation formula [Davis, 1985],

$$\sum_{m=-\infty}^{+\infty} e^{ik_0 \sin\phi_0 mL} = 2\pi \sum_{m=-\infty}^{+\infty} \delta(ik_0 \sin\phi_0 L + 2\pi m) \qquad (3.20)$$

and (3.19),the following relation can be derived:

$$\sum_{m=-\infty}^{+\infty} e^{ik_0 \sin\phi_0 mL} H_0^{(1)}(k_0\sqrt{(x-x'-mL)^2+(z-z')^2}) = \frac{2}{L}\sum_{m=-\infty}^{+\infty}\frac{e^{ik_{mz}|z-z'|-ik_{mx}(x-x')}}{k_{mz}} \qquad (3.21)$$

Where $k_{mx} = \frac{2\pi m}{L} - k_0 \sin\phi_0$ and $k_{mz} = \sqrt{k_0^2 - k_{mx}^2}$. The branch cut of the square root function is chosen such that $\sqrt{-1}$ = i. By changing the order of the summation and the integration in the (3.17) and (3.18) and applying (3.21), the Hertz vector potentials simplify to

$$\vec{\pi}_e = -\frac{Z_0}{2k_0 L}\sum_{m=-\infty}^{+\infty}\frac{1}{k_{mz}}\int_{C_0}\vec{J}_e(x', z')\, e^{i\,[k_{mz}|z-z'|-k_{mx}(x-x')]}dc' \quad (3.22)$$

$$\vec{\pi}_m = -\frac{Y_0}{2k_0 L}\sum_{n=-\infty}^{+\infty}\frac{1}{k_{mz}}\int_{C_0}\vec{J}_m(x', z')\, e^{i\,[k_{mz}|z-z'|-k_{mx}(x-x')]}dc' \quad (3.23)$$

Far away from the scatterers ($|z-z'| \gg \lambda$), only few terms of the summations contribute to the scattered field. These terms correspond to the Bragg-modes for which the k_{mz} is real, or equivalently $|k_{mx}| \leq k_0$. Thus m corresponds to a propagating Bragg mode if $m \in M$, where

$$M = \left\{ m:(-1+\sin\phi_0)\frac{L}{\lambda_0} \leq m \leq (1+\sin\phi_0)\frac{L}{\lambda_0} \right\} \quad (3.24)$$

By defining $k_{mx} = k_0 \cos\gamma_m$ and $k_{mz} = k_0 \sin\gamma_m$, the far field approximation of the Hertz vector potentials are derived as:

$$\vec{\pi}_e \cong -\frac{Z_0 r}{2L k_0}\sum_{m\in M}\frac{e^{i(\pm k_{mz}z - k_{mx}x)}}{k_{mz}}\int_0^{2\pi}\vec{J}_e(\phi')\, e^{-ik_0 r\cos(\phi'-\gamma_m)}d\phi' \quad (3.25)$$

$$\vec{\pi}_m \cong -\frac{Y_0 r}{2L k_0}\sum_{m\in M}\frac{e^{i(\pm k_{mz}z - k_{mx}x)}}{k_{mz}}\int_0^{2\pi}\vec{J}_m(\phi')\, e^{-ik_0 r\cos(\phi'-\gamma_m)}d\phi' \quad (3.26)$$

where r is the radius of the cylinders and the plus and minus signs correspond to the upper and lower half space.

In equations (3.25) and (3.26) $\vec{J}_e$ and $\vec{J}_m$ are the equivalent electric and magnetic current on the surface of the cylinders. Generally, presence of other cylinders affect the equivalent surface currents, but if the period is large compared to the wavelength, $\vec{J}_e$ and $\vec{J}_m$ can be approximated by their values when no other cylinder is present (i.e. an infinite cylinder in free space).

Consider the cylinder which is oriented vertically in the z direction, and is illuminated by a plane wave of the form (Figure 3.8)

$$E^i_y\,(H^i_y) = e^{\,i k_0 (\sin \phi_0 x - \cos \phi_0 z)} \tag{3.27}$$

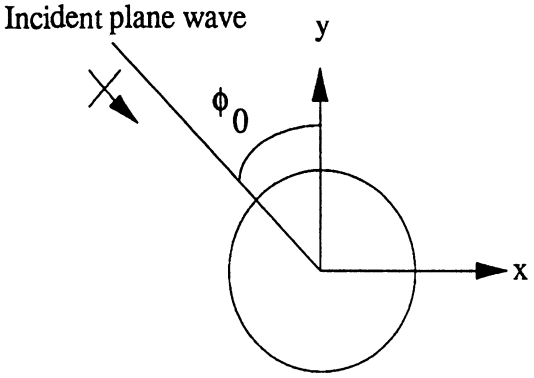

Figure 3.8 Scattering geometry for an infinitely long cylinder with axis perpendicular to the page.

The scattered field for V-polarization is given by [Ruck, *et al.*, 1970]:

$$E_y(\rho, \phi) = \sum_{\beta=-\infty}^{+\infty} (-e^{-i\phi_0})^{\beta} A_{\beta}^{E} H_{\beta}^{(1)}(k_0\rho)\, e^{i\beta\phi} \tag{3.28}$$

$$H_{\phi}(\rho, \phi) = \frac{i}{Z_0} \sum_{\beta=-\infty}^{+\infty} (-e^{-i\phi_0})^{\beta} A_{\beta}^{E} H_{\beta}^{(1)'}(k_0\rho)\, e^{i\beta\phi} \tag{3.29}$$

For H-polarization, the scattered wave is represented by:

$$H_y(\rho, \phi) = \sum_{\beta=-\infty}^{+\infty} (-e^{-i\phi_0})^{\beta} A_{\beta}^{H} H_{\beta}^{(1)}(k_0\rho)\, e^{i\beta\phi} \tag{3.30}$$

$$E_y(\rho, \phi) = \frac{-iZ_0}{k_0} \sum_{\beta=-\infty}^{+\infty} (-e^{-i\phi_0})^{\beta} A_{\beta}^{H} H_{\beta}^{(1)'}(k_0\rho)\, e^{i\beta\phi} \tag{3.31}$$

where coefficients A_{β}^{V} and A_{β}^{H} are given by:

$$A_{\beta}^{V} = \frac{n_c J_{\beta}(k_0 r)\, J'_{\beta}(n_c k_0 r) - n_a J'_{\beta}(k_0 r)\, J_{\beta}(n_c k_0 r)}{n_a H_{\beta}^{(1)}(k_0 r)\, J'_{\beta}(n_c k_0 r) - n_c H_{\beta}^{(1)'}(k_0 r)\, J_{\beta}(n_c k_0 r)} \tag{3.32}$$

$$A_{\beta}^{H} = \frac{n_a J_{\beta}(k_0 r)\, J'_{\beta}(n_c k_0 r) - n_c J'_{\beta}(k_0 r)\, J_{\beta}(n_c k_0 r)}{n_c H_{\beta}^{(1)}(k_0 r)\, J'_{\beta}(n_c k_0 r) - n_a H_{\beta}^{(1)'}(k_0 r)\, J_{\beta}(n_c k_0 r)} \tag{3.33}$$

n_c and n_a are the indices of refraction of the homogeneous cylinders and the surrounding homogeneous material (air), J_β and $H_\beta^{(1)}$ are Bessel and Hankel functions of the first kind of order β, and prime denotes derivative with respect to the argument.

The tangential fields on the surface of the array of cylinders may now be approximated by the tangential fields of a single cylinder in free space. Using (3.28) through (3.31) at $\rho = r$ in (3.12) and (3.13), the equivalent surface currents for V and H-polarizations are:

$$\vec{J}_e^{V}(\phi) = Y_0 \sum_{\beta=-\infty}^{+\infty} C_\beta^V e^{i\beta\phi}\,\hat{y} \tag{3.33}$$

$$\vec{J}_m^{V}(\phi) = \sum_{\beta=-\infty}^{+\infty} D_\beta^V e^{i\beta\phi}\,\hat{\phi} \tag{3.34}$$

$$\vec{J}_e^{H}(\phi) = \sum_{\beta=-\infty}^{+\infty} C_\beta^H e^{i\beta\phi}\,\hat{\phi} \tag{3.35}$$

$$\vec{J}_m^{H}(\phi) = Z_0 \sum_{\beta=-\infty}^{+\infty} D_\beta^H e^{i\beta\phi}\,\hat{y} \tag{3.36}$$

where coefficients $C_\beta^{V;H}$ and $D_\beta^{V;H}$ are given by:

$$C_\beta^V = i(-e^{-i\phi_0})^\beta [J'_\beta(k_0 r) + A_\beta^V H_\beta^{(1)'}(k_0 r)] \tag{3.37}$$

$$D_\beta^V = (-e^{-i\phi_0})^\beta [J_\beta(k_0 r) + A_\beta^V H_\beta^{(1)}(k_0 r)] \tag{3.38}$$

$$C_\beta^H = -(-e^{-i\phi_0})^\beta [J_\beta(k_0 r) + A_\beta^H H_\beta^{(1)}(k_0 r)] \tag{3.39}$$

$$D_\beta^H = i(-e^{-i\phi_0})^\beta [J'_\beta(k_0 r) + A_\beta^H H_\beta^{(1)'}(k_0 r)] \tag{3.40}$$

Upon inserting (3.33) through (3.36) in (3.25) and (3.26) the approximate Hertz vector potentials can be obtained. The scattered field in terms of Hertz vector potentials for an V-polarized incident wave is given by:

$$\begin{aligned} E_y^s &= k_0^2 \pi_{ey} + i k_0 Z_0 \left(\frac{\partial}{\partial x}\pi_{mz} - \frac{\partial}{\partial z}\pi_{mx}\right) \\ E_x^s &= E_z^s = 0 \end{aligned} \tag{3.41}$$

Similarly for an H-polarized wave the Hertz vector potentials are given by:

$$\begin{aligned} H_y^s &= k_0^2 \pi_{my} - i k_0 Y_0 \left(\frac{\partial}{\partial x}\pi_{ez} - \frac{\partial}{\partial z}\pi_{ex}\right) \\ H_x^s &= H_z^s = 0 \end{aligned} \tag{3.42}$$

Upon applying the following integral identities

$$\int_0^{2\pi} e^{i[\beta\phi' + k_0 r\cos(\phi' \pm \gamma_m)}\, d\phi' = 2\pi (-i)^\beta J_\beta(k_0 r) e^{\mp i\beta\gamma_m} \tag{3.43}$$

$$\int_0^{2\pi} e^{i[\beta\phi' - k_0 r\cos(\phi' \pm \gamma_m)}\,\hat{\phi}'\,d\phi' = -2\pi(-i)^{\beta} e^{\mp i\beta\gamma_m}$$

$$\{[\mp i\sin\gamma_m J'_m(k_0 r) - \cos\gamma_m \frac{\beta}{k_0 r} J_m(k_0 r)]\,\hat{x}$$

$$-[i\sin\gamma_m J'_m(k_0 r) \mp \sin\gamma_m \frac{\beta}{k_0 r} J_m(k_0 r)]\,\hat{z}\} \qquad (3.44)$$

in the scattered field expressions, the scattering amplitude of the m^{th} Bragg mode is found to be:

$$F_p^m = \frac{2}{L k_a \sin\gamma_m}\left\{A_0^p + 2\sum_{\beta=1}^{\infty}\cos\left[\beta(\phi_0 \pm \gamma_m + \frac{\pi}{2})\right]A_\beta^p\right\} \qquad (3.45)$$

where again ϕ_0 and γ_m are respectively the incidence and Bragg mode angles (Figure 3.7), L is the spatial period of the scatterers within the row, k_a is the wave number of the homogeneous material surrounding the cylinders, and p indicates the polarization.

The approximate representation of the far field scattering amplitude of an array of periodic cylinders becomes more accurate as the frequency or the spatial period of the cylinders increases. In order to investigate the accuracy of the approximate solution, a comparison is made with the exact solution, calculated by the method of moments, for the following set of canopy parameters:

Cylinder spacing, L = 25 cm,

Diameter of the cylinders, 2r = 1.75 cm,

Permittivity of the cylinders, $\varepsilon = 36 + i10$,

$\lambda = 20$ cm.

The scattering amplitudes of both the exact numerical solution and the approximate solution are given in Table 3.1. The amplitude of the approximation is in excellent agreement with the numerical solution and the phase difference is at the most 20° off from the exact value.

Incidence angle, $\phi_0 = 0°$

m	Exact (transmission)	Approximate (transmission)	Exact (reflection)	Approximate (reflection)
0	0.778∠ -0.97°	0.821∠ -5.47°	0.196∠ -166°	0.196∠ -146°
± 1	0.329∠ -174°	0.347∠ -154°	0.331∠ -168°	0.326∠ -148°

Incidence angle, $\phi_0 = \pm 53.08°$

m	Exact (transmission)	Approximate (transmission)	Exact (reflection)	Approximate (reflection)
0	0.649∠ -2.1°	0.707∠ -10.6°	0.340∠ -172°	0.328∠ -152°
1	0.208∠ -174°	0.197∠ -154°	0.199∠ -168°	0.196∠ -148°
2	0.337∠ -170°	0.327∠ -150°	0.328∠ -167°	0.326∠ -146°

Table 3.1 Exact *versus* approximate solutions of the scattering amplitude

3.5 Transmission and Reflection Coefficients of Cascaded Slabs of Periodically Distributed Scatterers

Expressions for the Bragg-mode scattering amplitudes of a single row were derived in the preceding section. The vegetation canopy consists of many rows and we want to relate the scattering properties of a single row to the scattering properties of the whole canopy. A slab (row) of periodically distributed scatterers is conservative in terms of the number and directions of its Bragg modes. In other words, if the wave is incident upon a slab from one of the Bragg mode directions associated with the waves transmitted by the previous slab, the number of new Bragg modes will remain the same as for the previous slab.Therefore in a cascaded arrangement of identical slabs, the directions of multiple bounces between the slabs are quantized and limited to the directions associated with a single slab. Each Bragg mode direction can be considered as a port of a multi-port system and network theory can be utilized to characterize the behavior of the cascaded slabs. Figure 3.8 illustrates an example of such a slab when L, the period of the scatterers, is 1.25λ. with superscripts denoting the slab number and subscripts denoting the port number, the plane waves incident from ports u_4^1, u_5^1, or u_6^1 will be scattered only into the

12 prescribed directions shown in Figure 3.8. Due to the symmetry of Bragg modes, incident waves from any other Bragg-mode directions will be scattered into the same directions constituted by ports 4, 5, and 6. Therefore, a 12-port network can completely represent the scattering behavior of the example in Figure 3.8. If R_{ij} represents the scattering amplitude of the plane wave scattered into port i due to a plane wave incident at port j on the same side of the slab, and T_{ij} is defined similarly for the wave scattered into the other side of the slab, then $[R_s]$ and $[T_s]$, the reflection and transmission coefficient matrices, are given by:

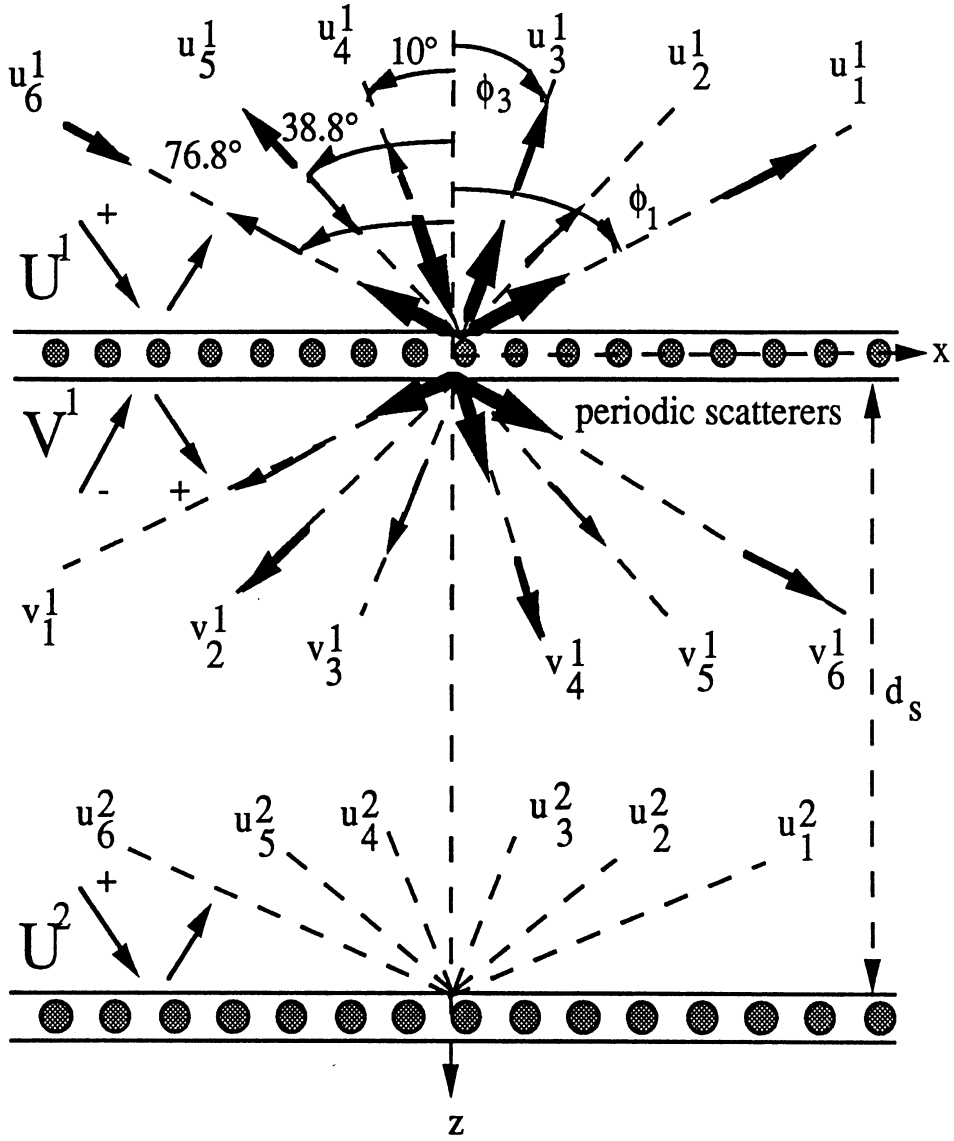

Figure 3.8 An example of a multi-port network for an array of periodically distributed scatterers next to a slab of air

$$[R_s] = \begin{bmatrix} R_{11} & R_{12} & R_{13} & \cdot\ \cdot & R_{1n} \\ R_{21} & R_{22} & R_{23} & \cdot\ \cdot & R_{2n} \\ R_{31} & R_{32} & R_{33} & \cdot\ \cdot & R_{3n} \\ \cdot & \cdot & \cdot & \cdot\ \cdot & \cdot \\ \cdot & \cdot & \cdot & \cdot\ \cdot & \cdot \\ R_{n1} & R_{n2} & R_{n3} & \cdot\ \cdot & R_{nn} \end{bmatrix} \tag{3.46}$$

and

$$[T_s] = \begin{bmatrix} T_{11} & T_{12} & T_{13} & \cdot\ \cdot & T_{1n} \\ T_{21} & T_{22} & T_{23} & \cdot\ \cdot & T_{2n} \\ T_{31} & T_{32} & T_{33} & \cdot\ \cdot & T_{3n} \\ \cdot & \cdot & \cdot & \cdot\ \cdot & \cdot \\ \cdot & \cdot & \cdot & \cdot\ \cdot & \cdot \\ T_{n1} & T_{n2} & T_{n3} & \cdot\ \cdot & T_{nn} \end{bmatrix} \tag{3.47}$$

where n is the total number of Bragg modes at each side of the slab.

With reference to Figure 3.8, the $[U^1]$ fields on one side of the first slab are related to the $[V^1]$ fields on the other side of the slab by a scattering matrix [S'],

$$\begin{bmatrix} U^{1+} \\ U^{1-} \end{bmatrix} = [S'] \begin{bmatrix} V1^{+} \\ V^{1-} \end{bmatrix} \tag{3.48}$$

whose elements are given by

$$[S'] = \begin{bmatrix} [T_s]^{-1} & -[T_s]^{-1}[R_s] \\ [R_s][T_s]^{-1} & [T_s] - [R_s][T_s]^{-1}[R_s] \end{bmatrix} \tag{3.49}$$

The fields $[V^1]$ of the first slab can be related to fields $[U^2]$ of the second slab by the phase shifting matrix $[\phi]$, such that $[V^1] = [\phi]\,[U^2]$, with

$$[\phi] = \begin{bmatrix} [\phi_1] & [0] \\ [0] & [\phi_2] \end{bmatrix} \tag{3.50}$$

The diagonal matrix $[\phi_1]$ is defined by:

$$[\phi_1] = \begin{bmatrix} e^{-ik_0 d_s \cos\phi_1} & 0 & \cdots & 0 \\ 0 & e^{-ik_0 d_s \cos\phi_2} & \cdots & 0 \\ \vdots & \vdots & \cdots & \vdots \\ 0 & 0 & \cdots & e^{-ik_0 d_s \cos\phi_n} \end{bmatrix} \tag{3.51}$$

and $[\phi_2]$ is the complex conjugate of $[\phi_1]$. Then,the overall ABCD matrix, [S] representing the combination comprised of a row of periodically distributed scatterers next to a slab of air can be represented by:

$$[S] = \begin{bmatrix} [T_s]^{-1}[\phi_1] & -[T_s]^{-1}[R_s][\phi_2] \\ [R_s][T_s]^{-1}[\phi_1] & [T_s][\phi_2] - [R_s][T_s]^{-1}[R_s][\phi_2] \end{bmatrix} \tag{3.52}$$

Finally, for a periodic array of n slabs, the total ABCD matrix, $[S_n]$, of the cascaded structure is:

$$[S_n] = [S]^n = \begin{bmatrix} [S_{n_{11}}] & [S_{n_{12}}] \\ [S_{n_{21}}] & [S_{n_{22}}] \end{bmatrix} \tag{3.53}$$

for a plane wave incident on the j^{th} port of the first slab, the total transmission and reflection coefficients of the resultant medium at ports i can be obtained from

$$T_{t_{ij}} = \left\{ \left[S_{n_{11}} \right]^{-1} \right\}_{ij} \tag{3.54}$$

and

$$R_{t_{ij}} = \left\{ \left[S_{n_{21}} \right] \left[S_{n_{11}} \right]^{-1} \right\}_{ij} \tag{3.55}$$

All multiple coherent wave scattering between the stalks has been taken into account in the above derivation. It should be noted that if the spacing between the slabs d_s does not satisfy the condition $d_s << \lambda_0$, then some of the non-propagating Bragg modes should also be included in the formulation.

3.6 Transmission of a Non-Uniform Wave Through Cascaded Slabs

The field $\bar{U}$ radiated by an antenna aperture located in the z=0 plane (Figure 3.9), can be expressed in terms of its angular spectrum representation [Collin, 1985]:

$$\bar{U}(x, y, z) = \frac{1}{4\pi^2} \int_{-\infty}^{+\infty} \int \bar{G}(k_x, k_y) e^{ik_x x + ik_y y + ik_z z} dk_x dk_y \tag{3.56}$$

where $\bar{G} = g_x \hat{x} + g_y \hat{y} + g_z \hat{z} = \bar{G}_t + g_z \hat{z}$, and $\bar{G}_t$ is the two-dimensional Fourier Transform of the tangential field $\bar{U}_a(x,y,0)$ over the antenna's aperture,

$$\bar{G}_t = \iint_{S_a} \bar{U}_a(x, y, 0)\, e^{-ik_x x - ik_y y}\, dx\, dy \tag{3.57}$$

By invoking the divergence relationship, g_z can be obtained from

$$g_z = \frac{-\bar{k}_t . \bar{G}_t}{k_z} = \frac{-k_x g_x - k_y g_y}{\sqrt{k_0^2 - k_x^2 - k_y^2}} \tag{3.58}$$

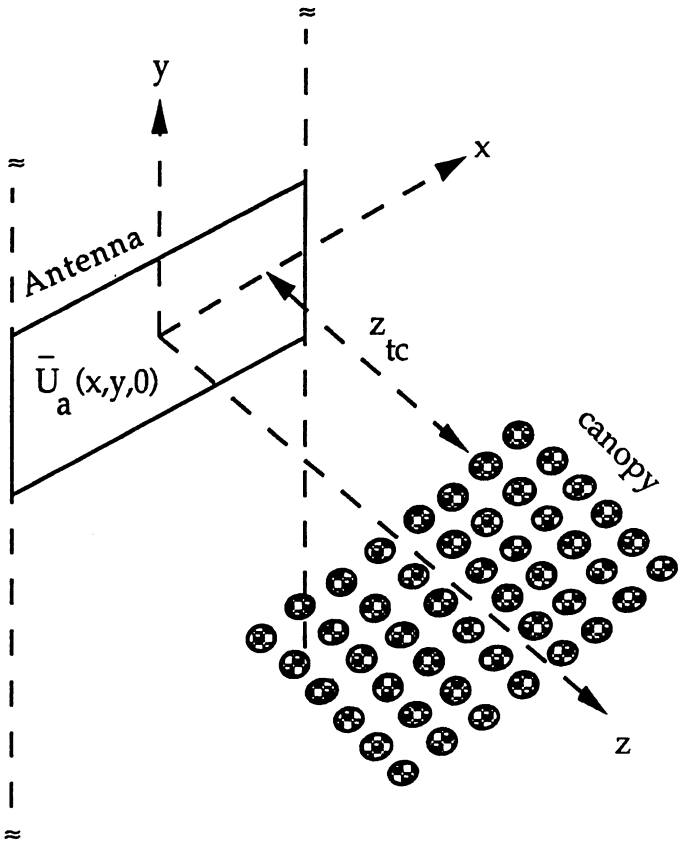

Figure 3.9 Antenna aperture with the illumination field $\bar{U}_a(x,y)$.

The integral (3.56) can be evaluated asymptotically to give

$$\bar{U}(\bar{r}) \approx \frac{ik_0 \cos\theta_0}{2\pi r} e^{ik_0 r} \bar{G}(k_0 \sin\theta\cos\phi, k_0 \sin\theta\sin\phi) \qquad (3.59)$$

where θ and ϕ are spherical coordinate angles, and $r = \sqrt{x^2 + y^2 + z^2}$. Equation (3.59) states that the diffraction pattern of the aperture field is directly related to the Fourier transform of the aperture field with

$$k_x = k_0 \sin\theta\cos\phi \qquad \text{and} \qquad k_y = k_0 \sin\theta\sin\phi \qquad (3.60)$$

Since we are dealing with a two-dimensional solution of the wave propagation problem, the antenna aperture can be assumed to be an infinite strip with no field variation along the y-direction ($\frac{\partial}{\partial y} = 0$). Then, the integration over y in equation (3.56) yields 2π and the wave pattern incident on the canopy can be represented by the two-dimensional antenna angular spectrum as:

$$\bar{U}^{inc} = \frac{1}{2\pi} \int_{-\infty}^{+\infty} \bar{A}(k_x) e^{ik_z z + ik_x x} dk_x \qquad (3.60)$$

where $\bar{A}(k_x)$ is a complex function (two-dimensional analogue of $\bar{G}(k_x,k_y)$) representing the one-dimensional Fourier transform of the field distribution on the transmitting antenna aperture. $\bar{A}(k_x)$ is in the y-direction and represents the electric field for a vertically polarized wave and the magnetic field for a horizontally polarized wave. Since it is assumed that there is no field variation in the y-direction, the two-dimensional g_z is found to be zero through the divergence relationship. The above representation of $\bar{U}^{inc}$ shows that the incident wave is the sum of an infinite number of plane waves travelling in the $(k_z \hat{z} + k_x \hat{x})$ direction,

each having an amplitude $\frac{\bar{A}(k_x)}{2\pi}$. The field transmitted through the cascaded slabs is the product of the incident wave and the total transmission coefficient of the medium. Since the incident wave is the sum of an infinite number of plane waves travelling in different directions, the transmitted wave will be the superposition of all transmitted plane waves with amplitudes $\frac{\bar{A}(k_x)\bar{T}_t(k_x)}{2\pi}$, where $\bar{T}_t(k_x)$ is the total transmission coefficient of the cascaded slabs for the incident angle $\phi_0 = \tan^{-1}(\frac{k_x}{k_z})$ which is represented by (3.54).

At the transmit antenna, the incident field is equal to the Fourier transform of $\bar{A}(k_x)$. If we shift the reference from the antenna aperture to the edge of the canopy at a distance z_{tc} away (Figure 3.9), then the incident field at that point becomes equal to the Fourier transform of the function

$$\bar{F}(k_x) \equiv \bar{A}(k_x) e^{ik_z z_{tc}} \tag{3.61}$$

The total transmitted wave can now be obtained by taking the inverse Fourier transform of the product of $\bar{F}(k_x)$ and the total transmission coefficient of the medium, $\bar{T}_t(k_x)$. Thus

$$\bar{U}^{tr} = \frac{1}{2\pi} \int_{-\infty}^{+\infty} \bar{F}(k_x) \bar{T}(k_x) e^{ik_x x} dk_x \tag{3.62}$$

The reflected wave pattern can be derived in a similar fashion. This equation suggests that if $\bar{T}_t(k_x)$ is a narrower function than $\bar{F}(k_x)$ in the k_x domain, the incident wave widens as it propagates through the medium, which is consistent with the beam-

widening observation noted in the experimental observations. The function $\bar{F}(k_x)$ may be represented by:

$$\bar{F}(k_x) = \int_{-\infty}^{+\infty} \bar{f}(x)\, e^{-ik_x x}\, dx \tag{3.63}$$

where $\bar{f}(x)$ is the incident wave pattern at the edge of the canopy. Assuming a one dimensional uniform field distribution at the aperture of the transmitting antenna, $\bar{f}(x)$ can be asymptotically approximated by:

$$\bar{f}(x) = \frac{1}{\sqrt{\rho}} e^{ik_0 \rho \cos\phi} \frac{\sin(\alpha k_0 \sin\phi)}{\alpha k_0 \sin\phi} \hat{y} \tag{3.64}$$

where α is a function of the antenna size, frequency, and polarization, ϕ is the angle measured from the boresight direction of the transmitting antenna, and ρ is the distance the wave travels at the angle ϕ from transmitter to the edge of the canopy. Using the measured data, α can be estimated such that the simulated reference pattern is the same as that of the measured reference field. As an example, Figure (3.10) is the plot of $\bar{F}(k_x)$ versus k_x at 1.5 GHz for vertical polarization.

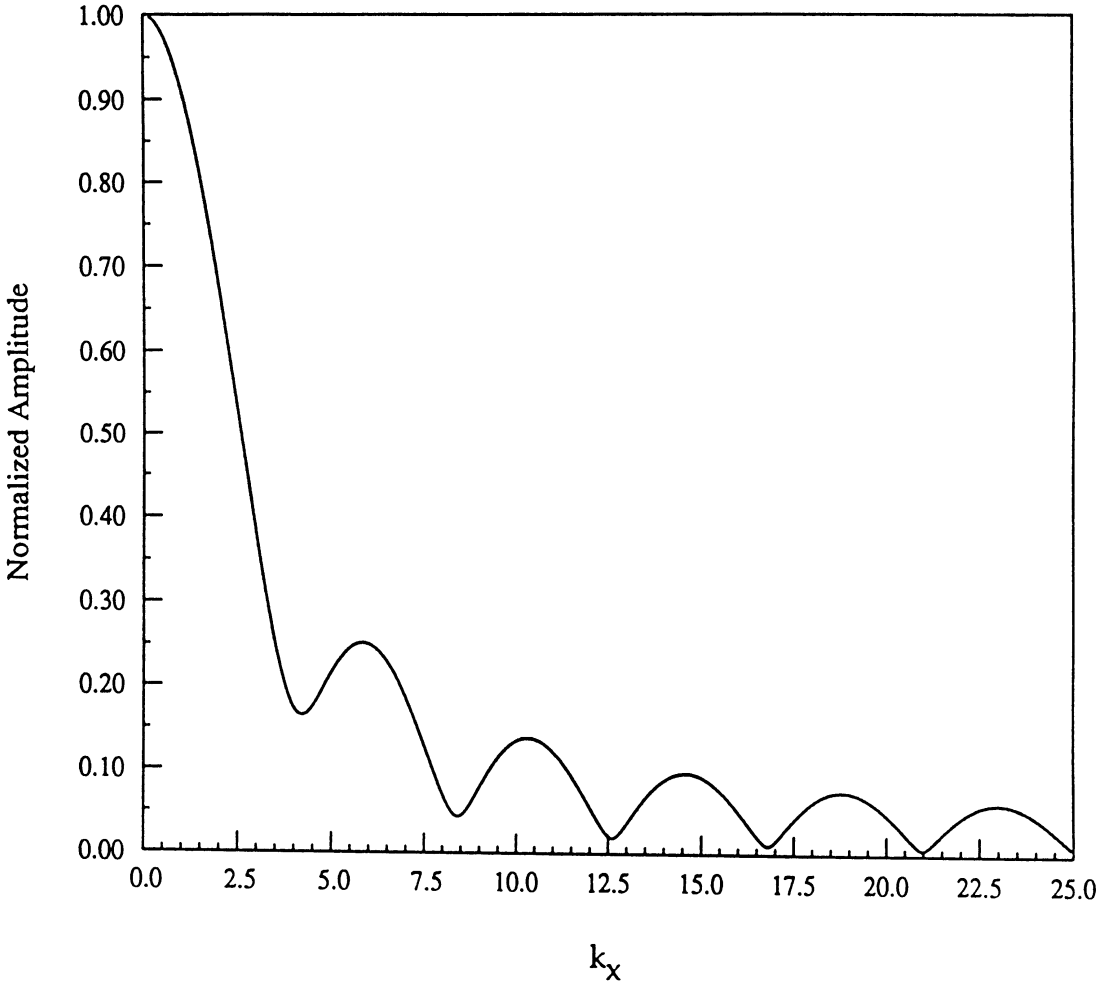

Figure 3.10 Spectrum of $\bar{F}(k_x)$ versus k_x at 1.5 GHz for vertical polarization.

3.7 Comparison with Experimental Data for a Defoliated Canopy

The model introduced in the preceding section (WPSM) was applied to configurations for which the experimental data is available. Figure 3.11 compares the resultant amplitude and phase of the simulation of seven rows of stalks with measured data at 1.5 GHz for vertical polarization. Parts (a) and (b) are the measured amplitude and phase and parts (c) and (d) are the simulated results. Part (e) is the simulation solutions of $\bar{T}(k_x)$ and part (f) is $\bar{T}(k_x)\bar{F}(k_x)$, i.e. the product of part (e) and Figure 3.10. The canopy parameters that were used are:

Row spacing = d_s = 77.3 cm,

Plant spacing = L = 25 cm,

Diameter of the stalks = 2r = 1.75 cm,

Permittivity of the stalks = $\varepsilon_s = 36 + i10$.

The simulation results are in good agreement with the experimental measurements for the overall pattern, attenuation level, and the peak to peak variation of power that is exhibited by the measurements. The simulated phase complies with the measured data in predicting that the field in the canopy leads the reference field at 1.5 GHz. Figure 3.12 displays the same calculation for horizontal polarization at L-band. Both the pattern and the attenuation level of the simulation are in excellent agreement with the measured data. The phase calculation reconfirms that the canopy phase at horizontal polarization, unlike the vertical polarization, lags the reference phase. It should also be noted that the simulation underestimates the attenuation level by about 2 dB for horizontal polarization. This is attributed to the fact that the stalks in the canopy are not perfectly vertical and the component of the field parallel to the cylinders is attenuated by an amount proportional to the attenuation for vertical polarization.

Results similar to those shown in Figures 3.11 and 3.12 were also obtained for the case where the canopy was reduced to one-half by cutting and removing every other plant in each row, resulting in a plant separation of 50 cm. Because of the greater separation, the number of Bragg modes is doubled in comparison with the full-density case. Figures 3.13 and 3.14 display the comparisons between measurement and the simulation for the half density case at 1.5 GHz. From Figure 3.13, it can be seen that the model can predict the attenuation level and its frequency of variation, but not the peak to peak variation for vertical polarization. This discrepancy is due to the fact that the high amplitude of $\bar{T}(k_x)$ coincides with the null of $\bar{F}(k_x)$ of the simulation. In reality, the illumination field at the antenna aperture is not perfectly uniform and its spectrum has minima, but not nulls as in the simulation. The horizontal-polarization power and phase calculations are in excellent agreement with the data and within the error range of the measurements (Figure 3.14). The same calculations were performed at 4.75 GHz and the Figures 3.15 and 3.16 compare the measured data with the simulation for vertical and horizontal polarizations respectively. Again good agreement between the measured data and the simulation is observed. At C-band, unlike L-band, the canopy propagation phase lags the reference phase at both polarizations which is confirmed by both the experiment and the theoretical simulation.

In general, the behavior of the wave in the stalk canopy (with no leaves) is completely characterized by the WSPM when used in conjunction with the Bragg mode technique. It is concluded that wave propagation in such man-made canopies is a coherent process and incoherent random-media techniques are not capable of explaining scattering in such environments.

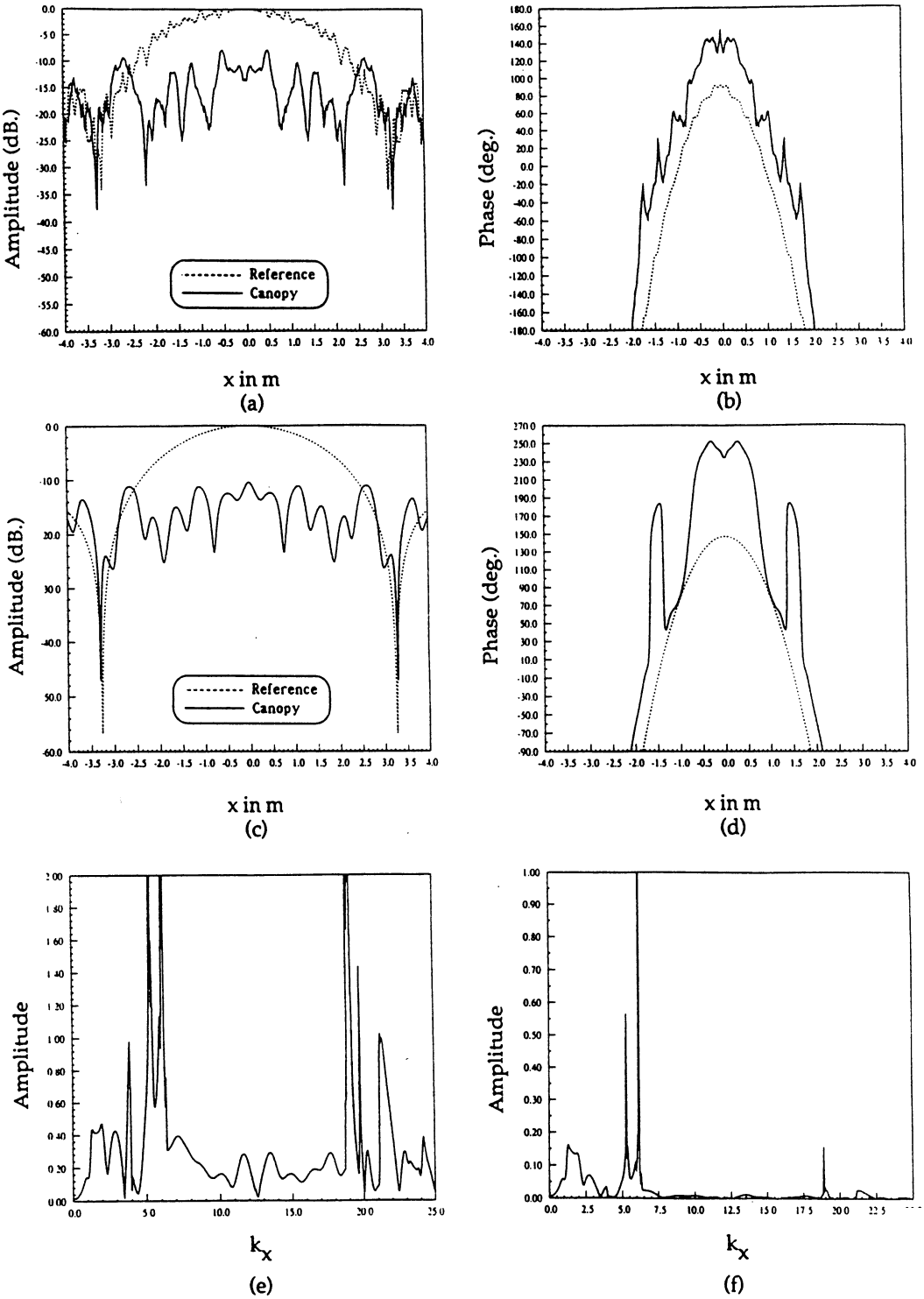

Figure 3.11 Comparison between measurement and simulation for seven rows of stalks at L-band illuminated by a vertically polarized incident field; (a) measured power, (b) measured phase, (c) simulated power, (d) simulated phase, (e) $\bar{T}(k_x)$, and (f) $\bar{T}(k_x)\,\bar{F}(k_x)$.

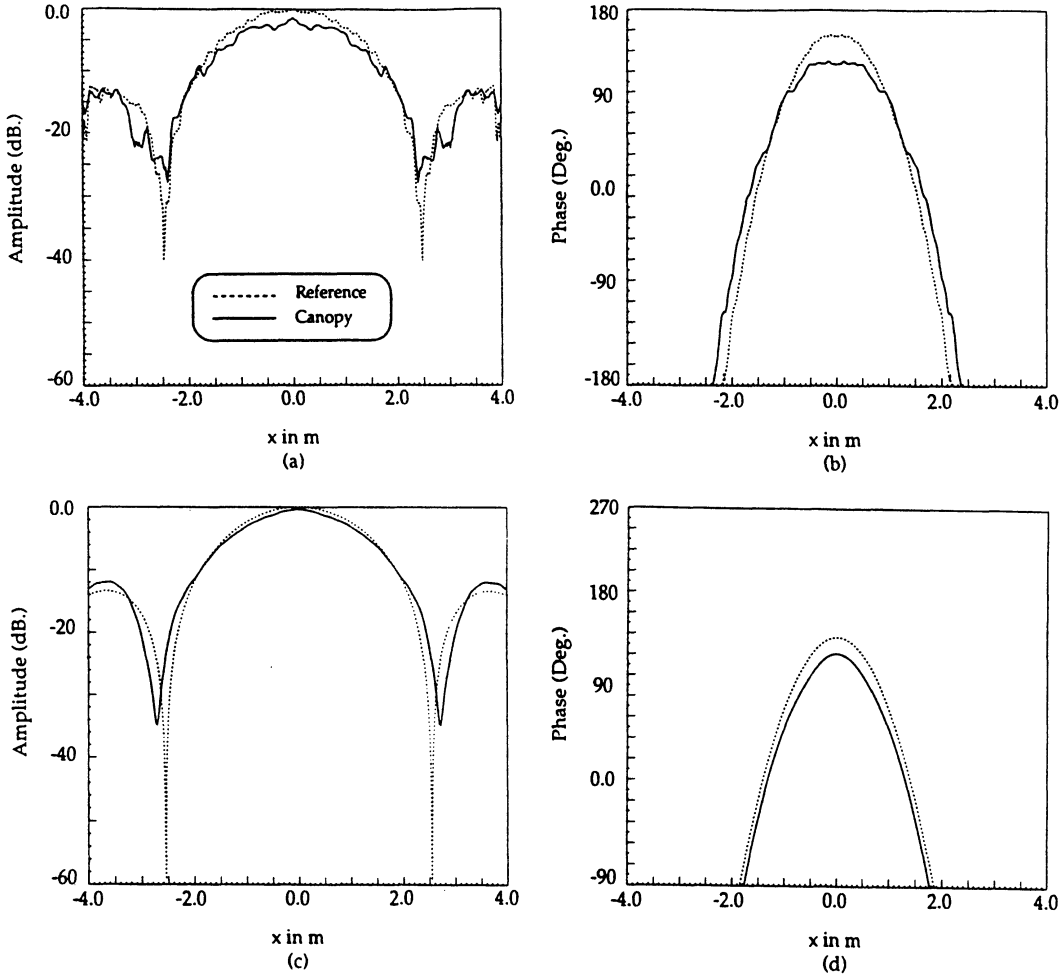

Figure 3.12 Comparison between measurement and simulation for seven rows of stalks at L-band illuminated by a horizontally polarized incident field; (a) measured power, (b) measured phase, (c) simulated power, and (d) simulated phase.

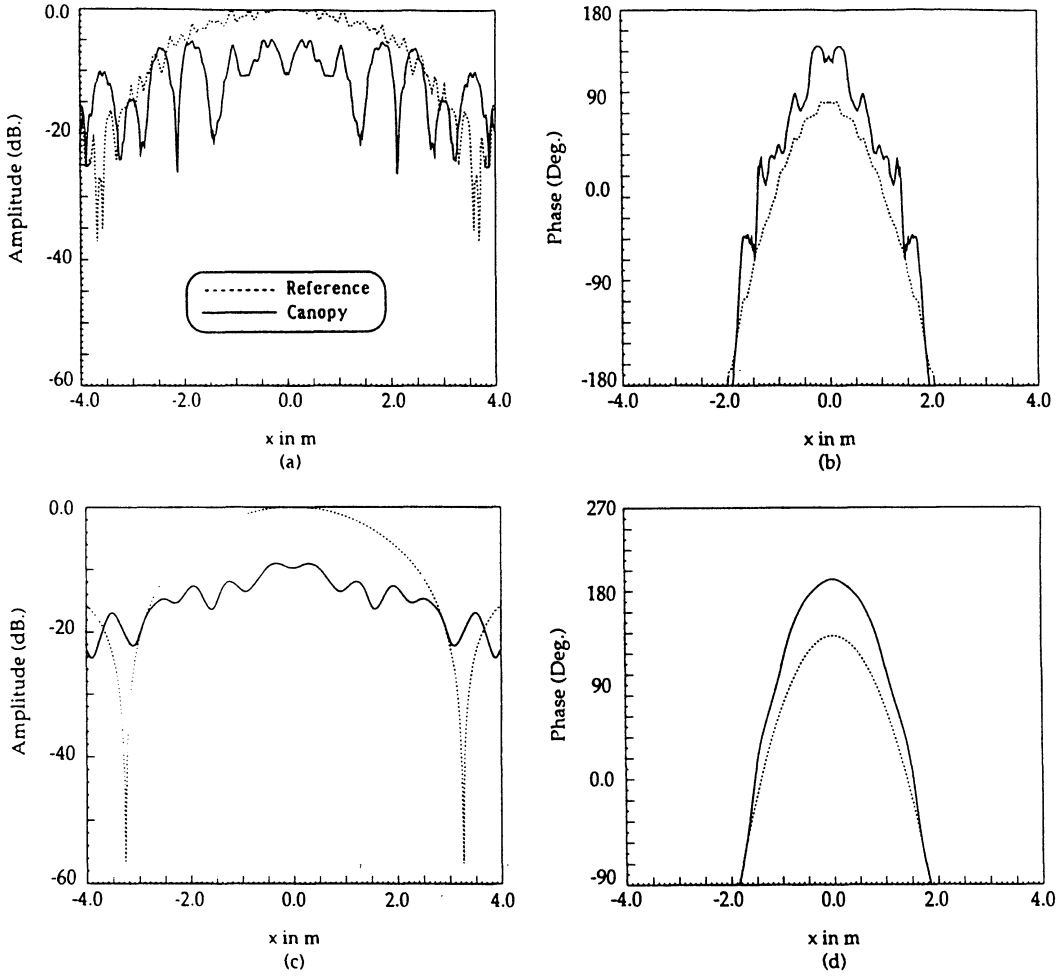

Figure 3.13 Comparison between measurement and simulation for seven rows of stalks reduced to half density at L-band and illuminated by a vertically polarized incident field; (a) measured power, (b) measured phase, (c) simulated power, and (d) simulated phase.

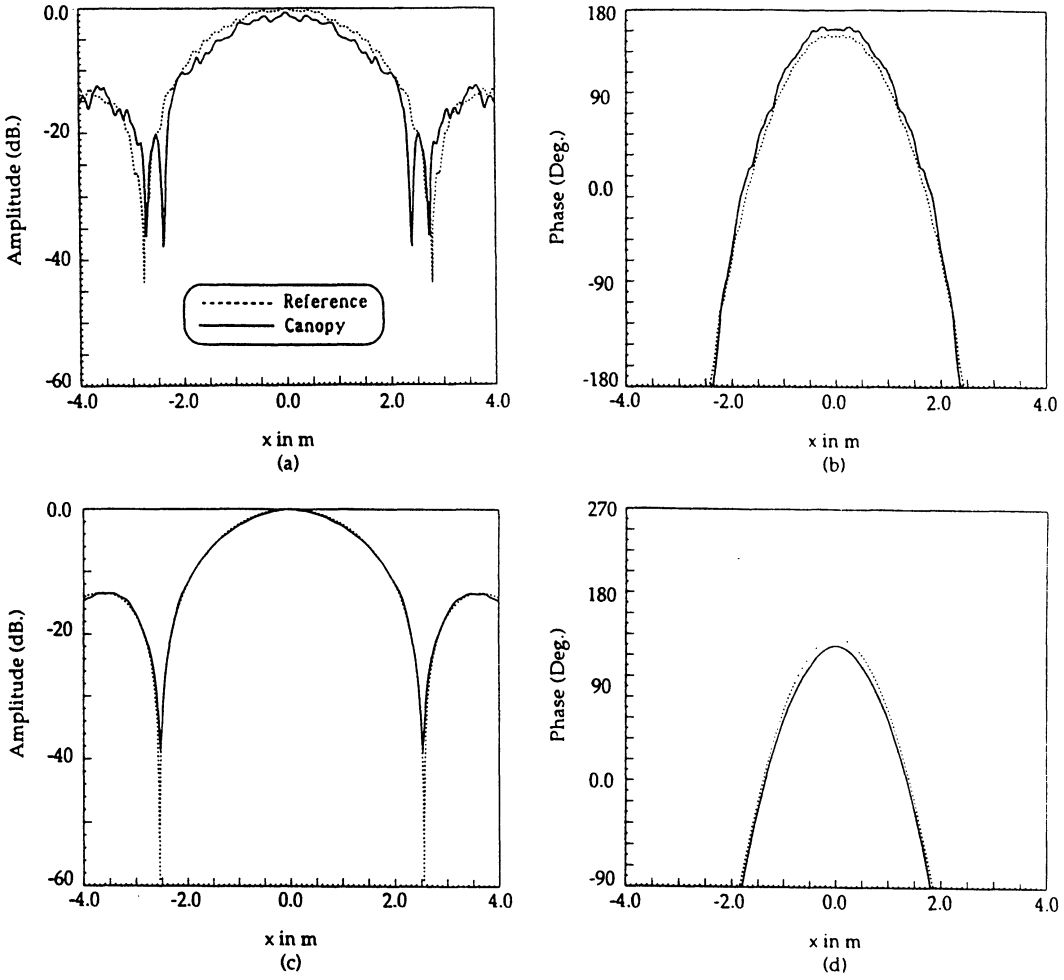

Figure 3.14 Comparison between measurement and simulation for seven rows of stalks reduced to half density at L-band and illuminated by a horizontally polarized incident field; (a) measured power, (b) measured phase, (c) simulated power, and (d) simulated phase.

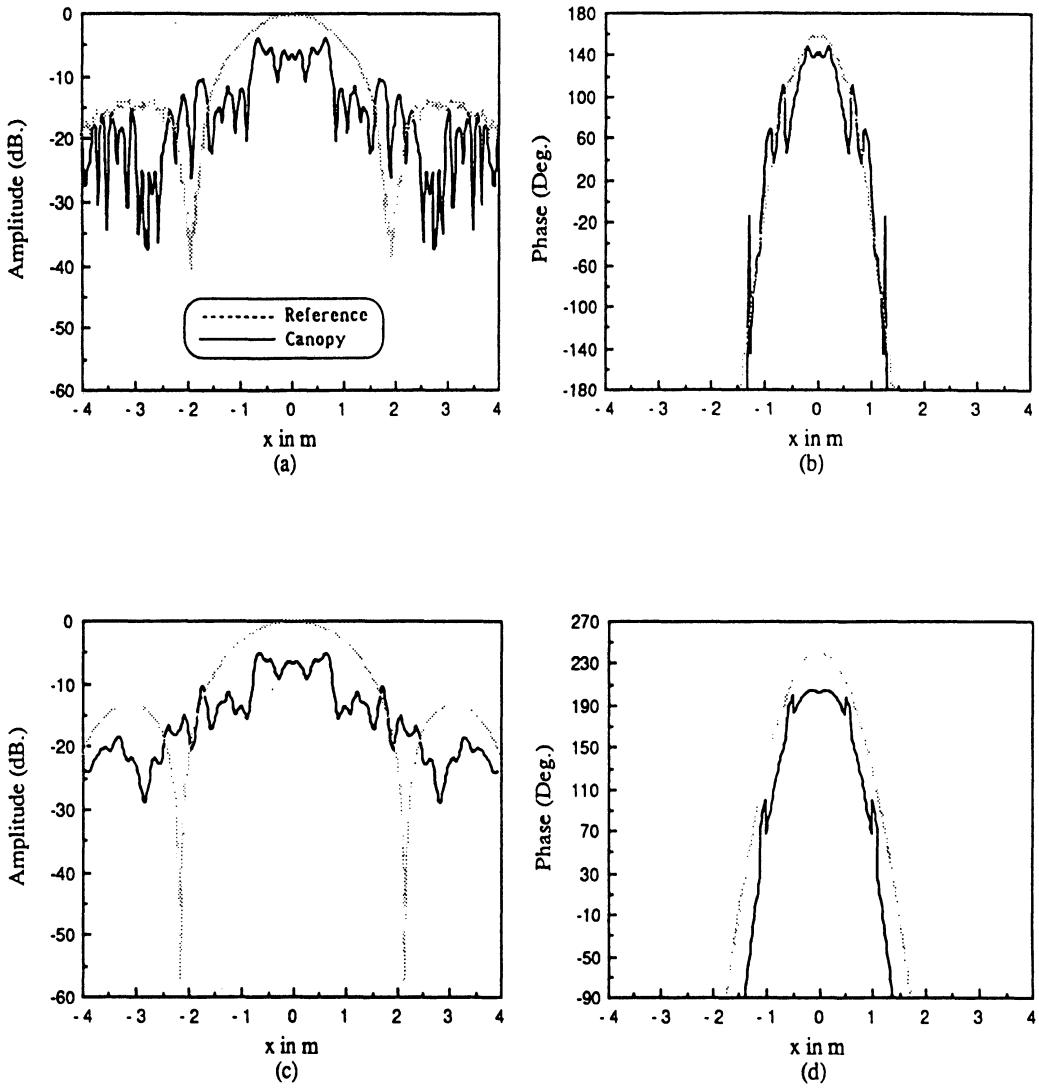

Figure 3.15 Comparison between measurement and simulation for seven rows of stalks at C-band illuminated by a vertically polarized incident field; (a) measured power, (b) measured phase, (c) simulated power, and (d) simulated phase.

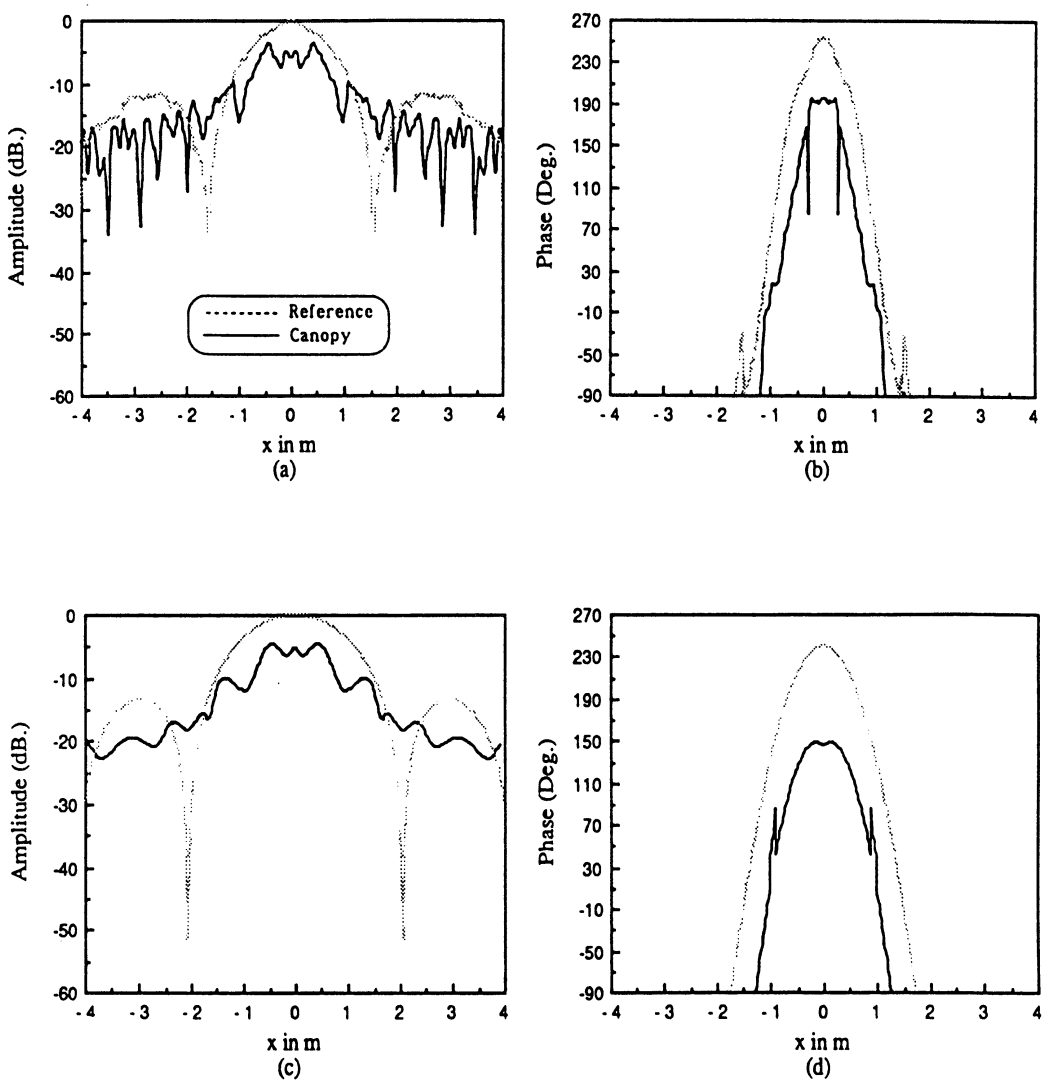

Figure 3.16 Comparison between measurement and simulation for seven rows of stalks at C-band illuminated by a horizontally polarized incident field; (a) measured power, (b) measured phase, (c) simulated power, and (d) simulated phase.

3.8 Sensitivity Analysis of the Bragg-Mode Technique

The goal of the canopy model is to establish the behavior we would observe for plane-wave incidence upon the canopy, and WSPM has been developed to confirm the validity of the model by establishing means for comparing the measured data with the calculations. Since the Bragg mode technique is a coherent process, it is expected that distances (or frequency variation) have major effects on the propagation of waves through the canopy. A sample of a sensitivity analysis for vertical polarization will be presented in this section. Figure 3.17 displays the effect of changing stalk parameters (permittivity, and diameter) on the loss suffered by the wave. Parts (a) and (b) depict the amplitude of the transmitted wave versus row spacing for two different stalk dielectric constants and stalk diameters, respectively. In the figure, m indicates the Bragg mode number (3.11), ε_s is the stalk dielectric constant, and dc is the diameter of the stalks. Row spacing can change the attenuation level for a wave incident at seven rows of a stalk canopy by as much as 50 dB. Small variations in dielectric constant and diameter of the stalks do not play a major role in the total attenuation level. Figure 3.18 depicts the attenuation level versus the number of rows for six different row spacings. The loss level goes through a cycle as the row spacing changes and can vary up to 200 dB for 40 rows depending on row spacing. Observation of Figures 3.17 and 3.18, display the high sensitivity of the model to distances compared to the wavelength. Therefore, a small variation in the frequency will change the wave attenuation by the canopy to a great degree. Since WSPM is a coherent model, the effect of the approximation in the solution of the Bragg-mode scattering amplitudes are also studied. Figure 3.19 (a) compares the solutions of the seven rows of stalks when the exact and approximate scattering amplitudes are applied. The general patterns of the solutions are similar, but do not predict the same attenuation level at an equivalent row spacing. In order to confirm that this discrepancy is the result of the phase inaccuracy, the same plot in given

in Figure 3.19 (b) where the exact phase is used in conjunction with the approximate amplitude. It can be seen that both the approximate attenuation level and pattern are in good agreement with the exact solution. Since plant spacing in terms of the wavelength increases as frequency increases, the approximate solution should yield better phase results at higher frequencies, or, similarly, for canopies with larger stalk separations.

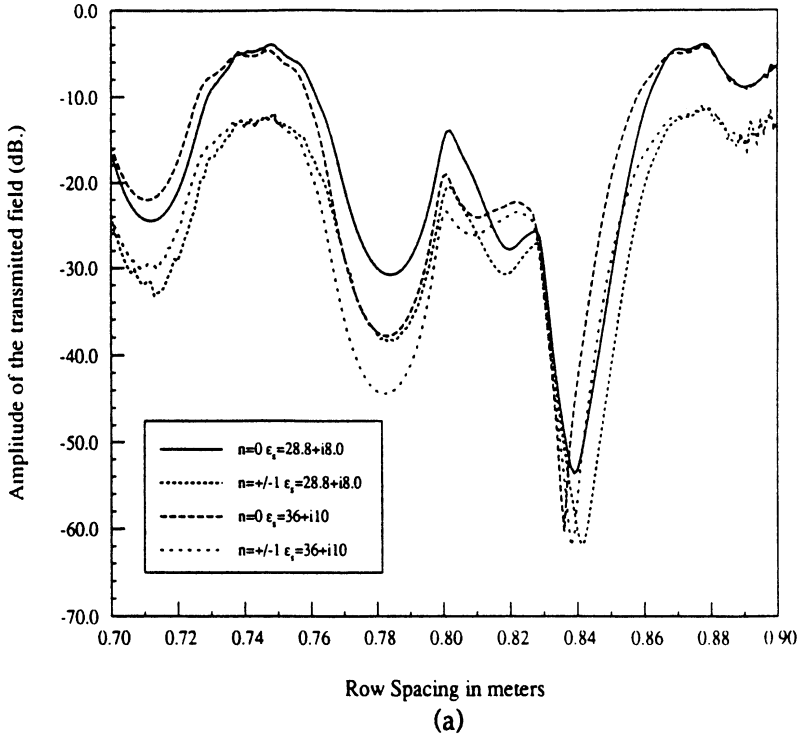

(a)

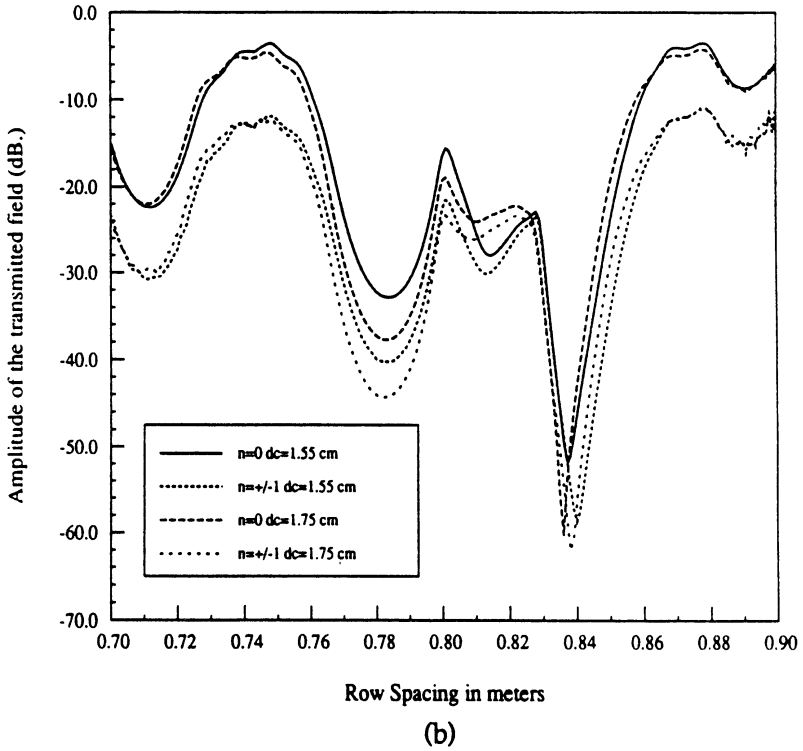

(b)

Figure 3.17 Amplitude of the vertically transmitted field versus row spacing for seven rows of stalks at L-band; (a) at two different dielectric constant, (b) at two different stalk diameter.

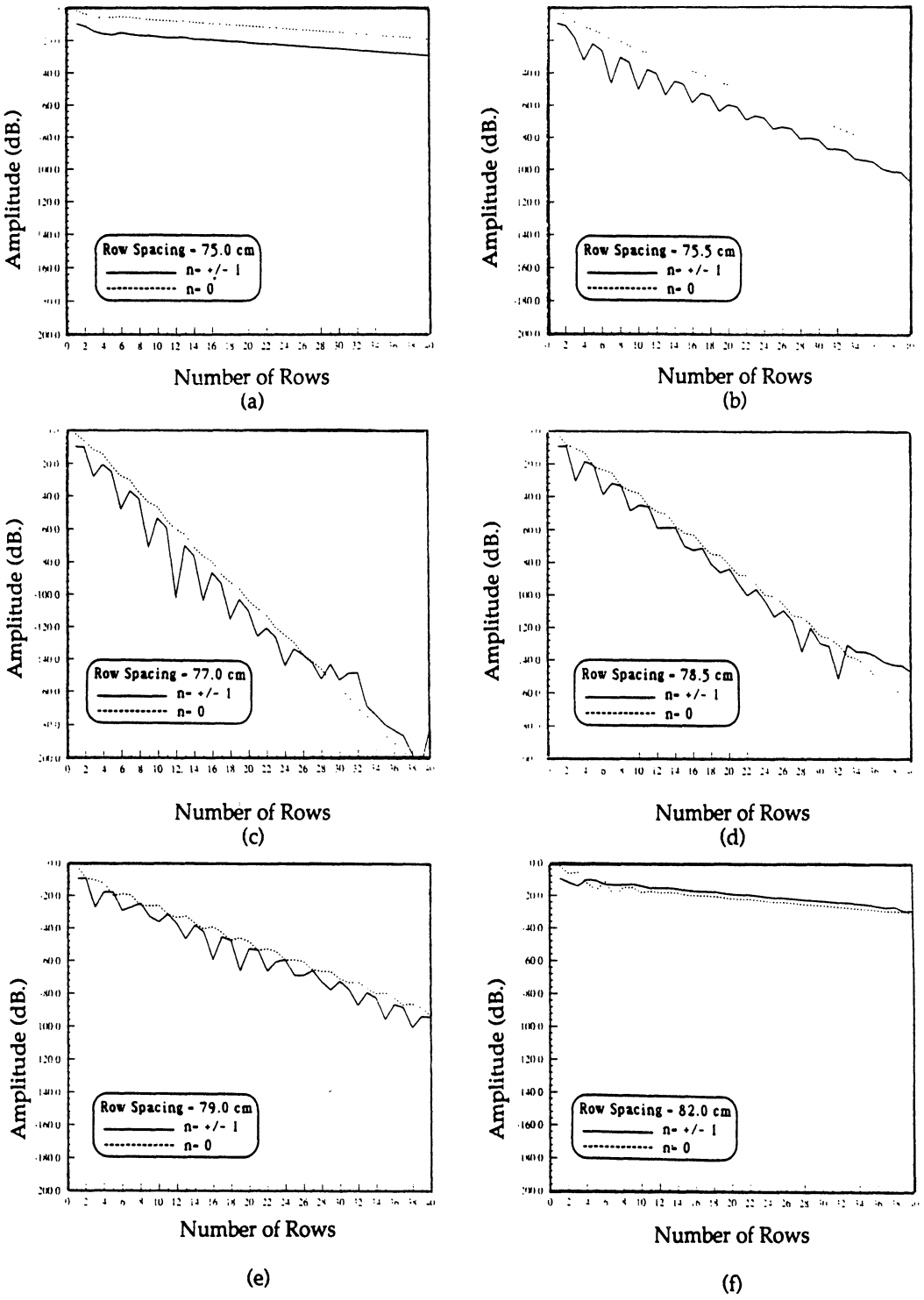

Figure 3.18 Amplitude of the vertically transmitted wave versus number of rows at six different row spacings.

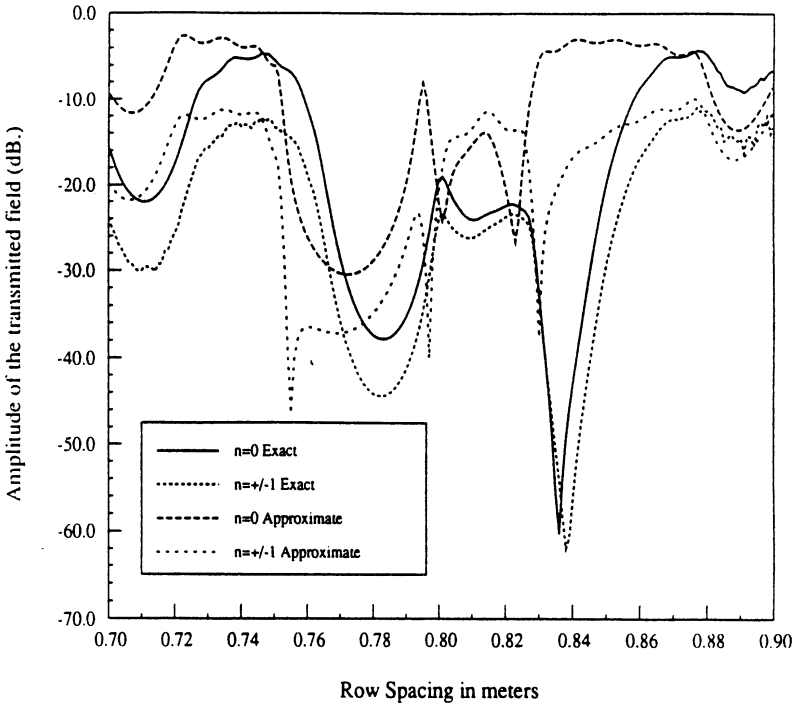

(a)

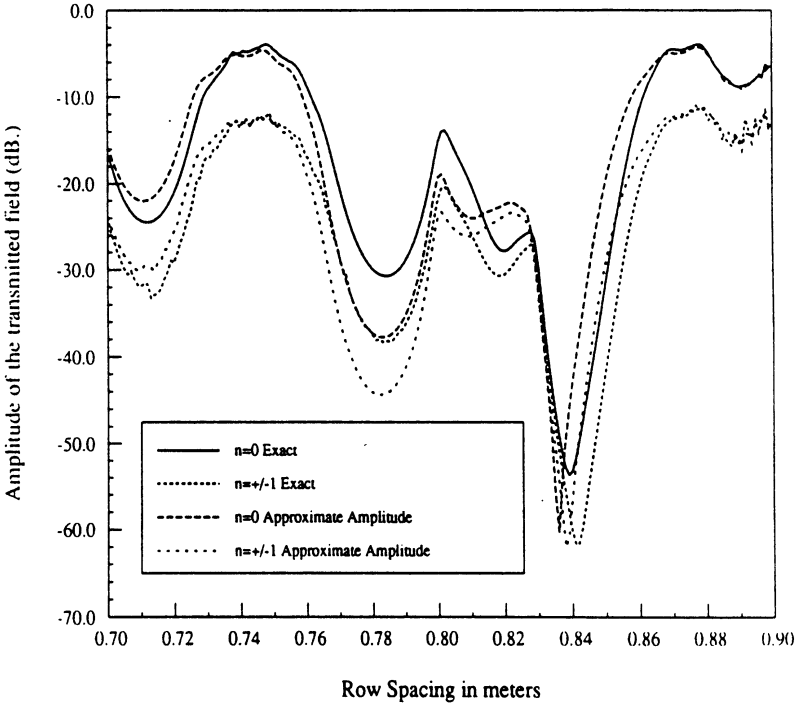

(b)

Figure 3.19 Comparison of the amplitude of the vertically transmitted field at L-band for seven rows of stalks using (a) approximate phase solution, (b) exact phase solution.

3.9 Propagation Model for a Canopy of Stalks with Leaves

At wavelengths much longer than the dimensions of a leaf (1.5 GHz), the leaves in a canopy exhibit weak scattering properties, and their presence serve primarily to alter the effective dielectric constant of the background medium surrounding the stalks. If leaves are treated as randomly oriented disks with volume fraction υ_l, the equivalent dielectric constant of the medium is given by the mixing model [de Loor, 1968; Ulaby, *et al.*, 1986]:

$$\varepsilon_a = 1 + \frac{\upsilon_l}{3}(\varepsilon_l - 1)\left(2 + \frac{1}{\varepsilon_l}\right) \tag{3.65}$$

where ε_l is the dielectric constant of the leaf material, for which expressions relating to the leaf moisture content are available (see equation 2.2). Therefore, by using the value of ε_a in calculation of k_a in equation (3.45) and substituting this value for k_0 in equation (3.51) the effect of leaves at low frequencies is considered. This model was applied to the seven rows of stalks with leaves at 1.5 GHz with the same stalk parameters of section 3.7 and $\varepsilon_l = 28 + i8$, and $\upsilon_l = 7.5 \times 10^{-4}$. Figures 3.20 and 3.21 compare the model results with measured data for vertical and horizontal polarizations, respectively. The pattern, oscillation, and attenuation levels are in very good agreement with the measured data. It should be noted that for vertical polarization, the field transmitted through the stalk canopy leads the reference field, but the opposite is true for the leaf canopy. Therefore, these two phenomena tend to cancel each other's effect when both stalks and leaves are present in the canopy, which is supported by both the simulation and the measured data. The apparent inconsistency for vertical polarization phase is within measurement accuracy. The simulation did not produce satisfactory results at C-band which indicates that the corn leaves are not weak scatterers

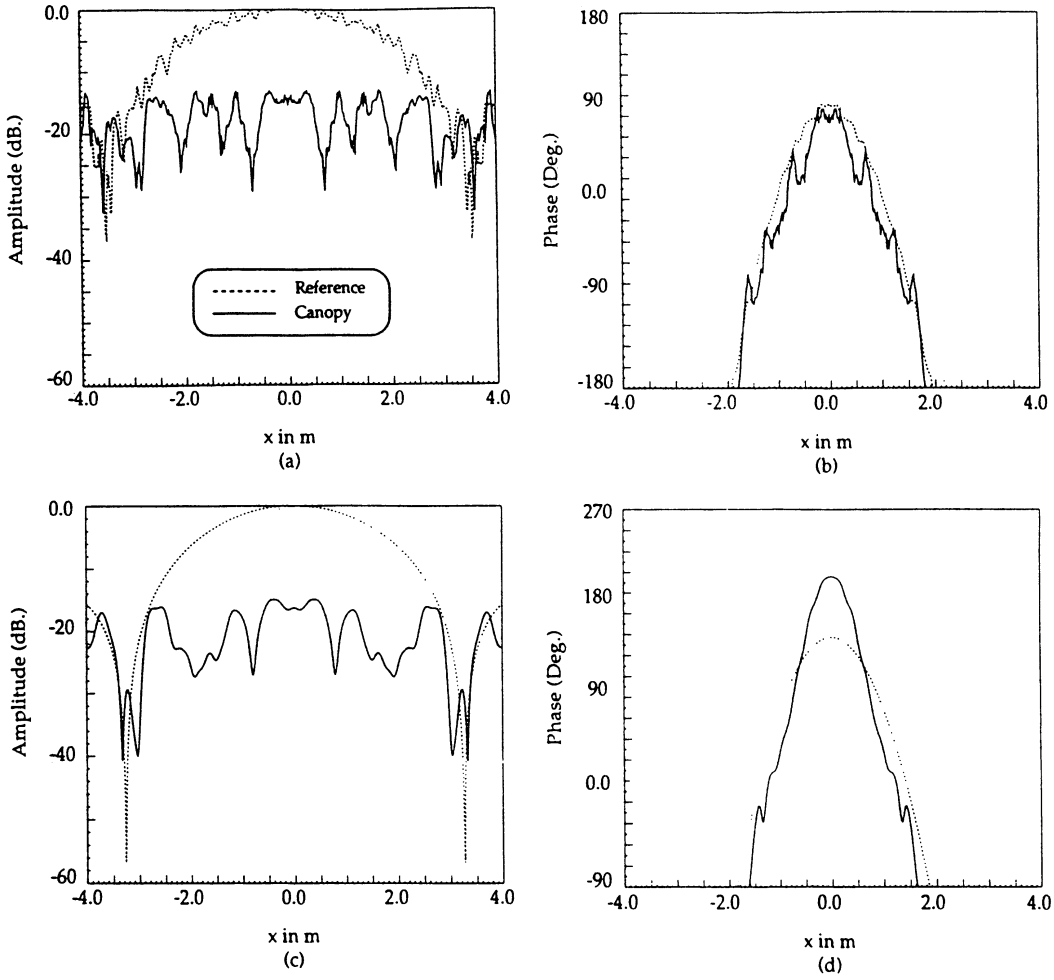

Figure 3.20 Comparison between measurement and simulation for seven rows of a full canopy of both stalks and leaves illuminated by a vertically polarized incident field at 1.5 GHz; (a) measured power, (b) measured phase, (c) simulated power, (d) simulated phase.

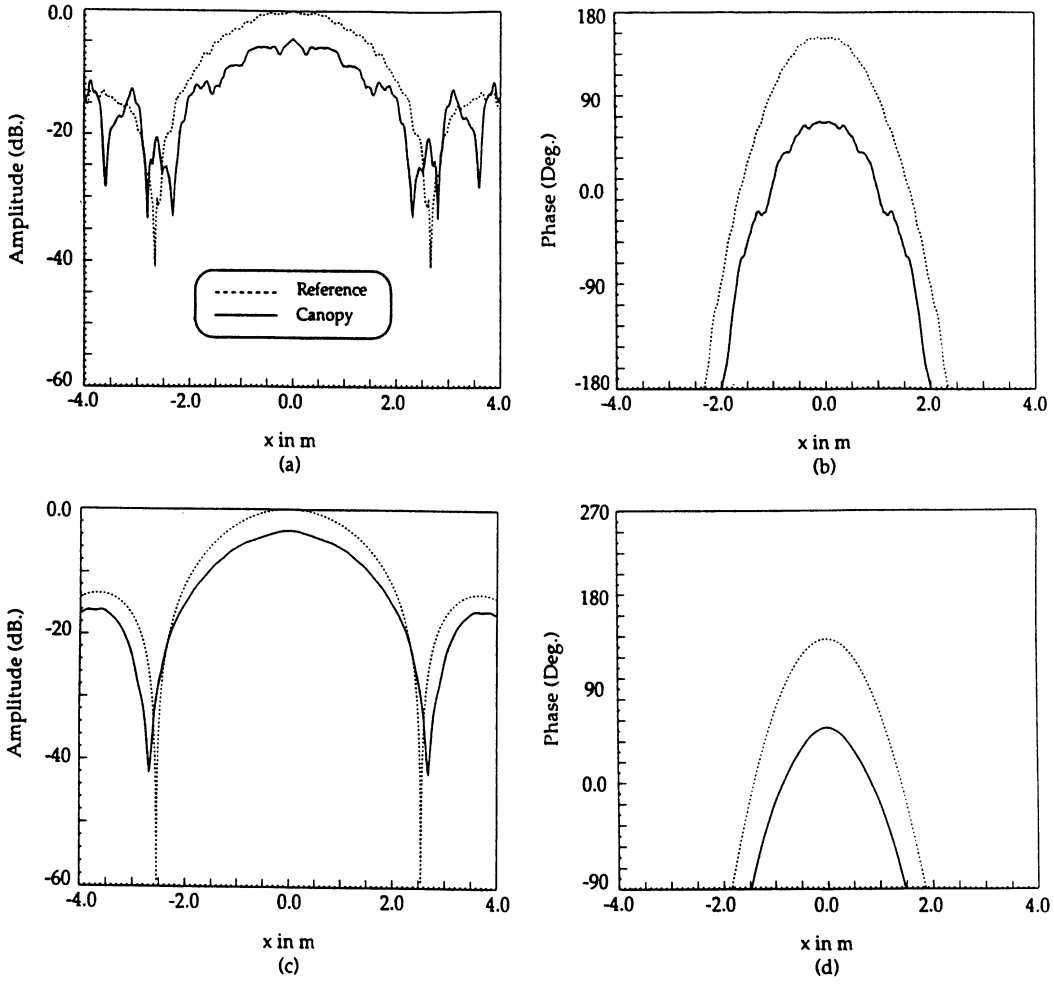

Figure 3.21 Comparison between measurement and simulation for seven rows of a full canopy of both stalks and leaves illuminated by a horizontally polarized incident field at 1.5 GHz; (a) measured power, (b) measured phase, (c) simulated power, (d) simulated phase.

and the scattering loss by the leaves should be taken into account in the development of the model. This phenomena is due to the fact that the leaf surface dimensions are comparable to the wavelength at 4.75 GHz.

3.10 Conclusion

The propagation model developed in this chapter is a deterministic field approach to the solution of wave propagation through man-made vegetation canopy comprised of stalks and leaves. Both multiple, coherent, wave scattering by the stalks and intrinsic absorption by the leaves are accounted for in the derivation. Excellent agreement between theory and experiment is obtained for canopies with and without leaves at 1.5 GHz and 4.75 GHz. Very good agreement is obtained for the full canopy (stalks and leaves) at L-band, but the inclusion of the leaves could not be accounted for at C-band. In order to extend the frequency range coverage of this model to higher frequencies, it will be necessary to account for scattering by the leaves explicitly. Inclusion of the leaves at C-band destroys the coherent scattering observed in this chapter and will necessitate the use of an appropriate incoherent scattering model that incorporates the size and orientation distributions of the leaves.

CHAPTER IV

INCOHERENT WAVE PROPAGATION THROUGH PERIODIC VEGETATION CANOPIES

4.1 Introduction

In chapter III, coherent wave scattering through a man-made vegetation canopy was studied. It was concluded that in a corn like canopy, when the surface dimensions of leaves are much smaller than a wavelength, leaves behave as weak scatterers and contribute mostly to absorption loss, hence, stalks are the main cause of multiple scattering in the canopy. Domination of the stalks in the scattering process, combined with the periodicity of plants in each row and rows in the whole canopy was the cause of coherent multiple scattering in the medium. As the frequency of operation increases, the leaves' dimensions become comparable to the wavelength and their scattering amplitude becomes comparable to that of the stalks. Consequently, scattering by leaves becomes important in the scattering process in the canopy, and due to leaves' random distribution, incoherent wave scattering takes over the coherent wave scattering that was considered previously. As a result, the plant periodicity in each row is over shadowed by presence of the leaves and only row periodicity in the medium affects the propagating wave.

The goal of this chapter is to formulate a model that can adequately characterize incoherent horizontal wave propagation in a medium comprised of a one-dimensional periodic row structure with known periodicity. A two-dimensional periodic radiative

transfer model is developed for a medium containing vertical stalks, represented by smooth cylinders, and leaves, represented by infinitesimally thin resistive strip. In section 4.2 a brief review of the radiative transfer technique and the development of the radiative transfer equation for the two-dimensional medium will be presented. Solution of the radiative transfer equation for a two-dimensional periodic random medium is pursued in two ways: (1) iterative, and (2) a new numerical technique based on the discrete-ordinate approximation and Taylor series expansion (DOT). Sections 4.3 and 4.4 discuss the iterative and DOT solutions of the radiative transfer equation, respectively. In section 4.5 the extinction and phase function for stalks, and in section 4.6 the extinction and phase function for leaves will be provided. Section 4.7 contains comparisons between the results of the theoretical model and the experimental data of section 3.2.

4.2 Radiative Transfer Technique

The radiative transfer technique examines the radiation intensity in a medium that is able to absorb, emit, and scatter electromagnetic radiation. The technique was first introduced by Schuster in an attempt to explain the appearance of absorption and emission lines in stellar spectra [Schuster, 1905]. The subject is further investigated by astrophysicists and physicists for the problem of diffusion in neutrons [Davison, 1957; Chandrasekhar, 1960; Case and Zweifel, 1967]. Recently, many investigators have utilized the technique to explain the wave vegetation interactions for remote sensing purposes [Fung and Ulaby, 1978; Fung, 1982; Tsang *et al.*, 1985].

Generally, two approaches are used in dealing with the problem of scattering in a medium. First, the wave theory, such as in chapter III, where the wave propagation is formulated *via* Maxwell's equations and scattering and absorption characteristics of the medium is studied. Radiative transfer theory, on the other hand does not start with Maxwell's equation. It begins with the radiative transfer equations that govern the

propagation of energy through the scattering medium. It assumes that there is no correlation between fields and therefore, the addition of intensities rather than the addition of fields is considered.

In radiative transfer theory, the quantity of interest is the specific intensity $\bar{I}(\bar{r},\hat{s})$, which is defined as the power per unit area and per unit solid angle propagating along $\hat{s}$, and which is a function of position in the random medium, $(\bar{r})$. In applying transport theory to the electromagnetic problem, the specific intensity $\bar{I}(\bar{r},\hat{s})$ usually is defined by a four - component vector. For a monochromatic elliptically polarized plane wave with electric field vector

$$\bar{E} = (E_v \hat{v}_i + E_h \hat{h}_i) e^{i k_0 r} \tag{4.1}$$

and unit vertical and horizontal polarization vectors $\hat{v}_i$ and $\hat{h}_i$, I is defined through the modified stokes parameters:

$$\bar{I} = \begin{bmatrix} I_v \\ I_h \\ U \\ V \end{bmatrix} = \frac{1}{\eta} \begin{bmatrix} |E_v|^2 \\ |E_h|^2 \\ 2\,\mathrm{Re}(E_v E_h^*) \\ 2\,\mathrm{Im}(E_v E_h^*) \end{bmatrix} \tag{4.2}$$

The vector radiative transfer equation, which simply expresses the conservation of energy in a unit volume of the medium (Fig. 4.1), is given by

$$\nabla . \bar{I}\,(r, \hat{s}) = - \bar{\bar{\kappa}}\,(r, \hat{s})\,\bar{I}\,(r, \hat{s}) + \int_{\Omega} \bar{\bar{P}}\,(r, \hat{s}, \hat{s}')\,\bar{I}\,(r, \hat{s}')\,d\Omega \tag{4.3}$$

where $\bar{\bar{\kappa}}(r,\hat{s})$ and $\bar{\bar{P}}(r,\hat{s},\hat{s}')$ are, respectively, the extinction and phase matrices of the medium. The extinction matrix represents the losses due to absorption and scattering by particles per unit volume and, in general, is a function of position and direction of propagation.

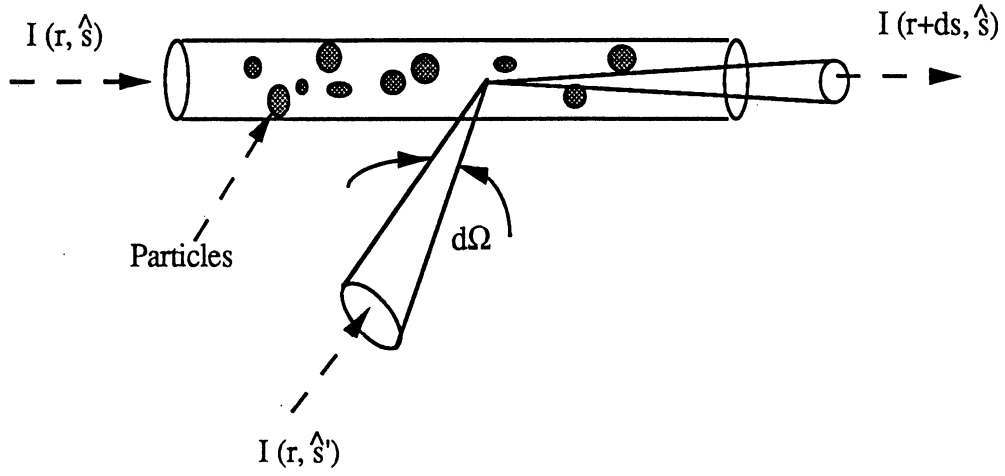

Figure 4.1 Radiative energy transfer for specific intensity $\bar{I}(r,\hat{s})$ incident upon a cylindrical column of particles.

For a plane wave illumination on a single particle, the scattered field assumes the form

$$\bar{E}_s = \frac{e^{ik_0 r}}{r} \bar{\bar{S}} . \bar{E}_i \qquad (4.4)$$

where $\bar{\bar{S}}$ is the scattering matrix of the particle. Identifying the elements of the extinction matrix as the attenuation rates in coherent wave propagation, the extinction matrix is given by [Ishimaru and Cheung, 1980]:

$$\bar{\bar{K}} = \begin{bmatrix} -2\,\mathrm{Re}(M_{vv}) & 0 & -\mathrm{Re}(M_{vh}) & -\mathrm{Im}(M_{vh}) \\ 0 & -2\,\mathrm{Re}(M_{hh}) & -\mathrm{Re}(M_{hv}) & -\mathrm{Im}(M_{hv}) \\ -2\,\mathrm{Re}(M_{hv}) & -2\,\mathrm{Re}(M_{vh}) & -\mathrm{Re}(M_{vv}) - \mathrm{Re}(M_{hh}) & +\mathrm{Im}(M_{vv}) - \mathrm{Im}(M_{hh}) \\ 2\,\mathrm{Im}(M_{hv}) & -2\,\mathrm{Im}(M_{vh}) & -\mathrm{Im}(M_{vv}) + \mathrm{Im}(M_{hh}) & -\mathrm{Re}(M_{vv}) - \mathrm{Re}(M_{hh}) \end{bmatrix} \tag{4.5}$$

where the attenuation rates, M_{ij}, are defined as:

$$M_{ij} = \frac{i\,2\pi N}{k_0} < S_{ij}(\theta, \phi; \theta, \phi) > \qquad i, j = v, h \tag{4.6}$$

In equation (4.6), N is the number of particles per unit volume, and S_{ij} $(\theta,\phi; \theta,\phi)$ is the forward scattering amplitude of individual particles. The angular bracket denotes average to be taken over the orientation and size distribution of the particles.

Phase matrix, $\bar{\bar{P}}(\hat{s},\hat{s}')$, of the medium relates the scattered intensity in the direction $\hat{s}$ to the incidence intensity from the direction $\hat{s}'$and is defined by

$$\bar{\bar{P}}\,(\hat{s},\hat{s}') = N < \bar{\bar{L}}\,(\hat{s},\hat{s}',\hat{s}_p) > \tag{4.7}$$

where the Stokes matrix, $\bar{\bar{L}}$, relates the scattered modified Stokes vector $\bar{I}^s$ to the incident modified Stokes vector $\bar{I}^i$ for a single particle of orientation $\hat{s}_p$, and < > is ensemble average over the size and orientation of the particles in the medium. The Stokes matrix, $\bar{\bar{L}}$, is given by [Ulaby *et al.* ,1986]

$$\bar{\bar{L}} = \begin{bmatrix} |S_{vv}|^2 & |S_{vh}|^2 \\ |S_{hv}|^2 & |S_{hh}|^2 \\ 2\,\mathrm{Re}(S_{vv}S_{hv}^*) & 2\,\mathrm{Re}(S_{vh}S_{hh}^*) \\ 2\,\mathrm{Im}(S_{vv}S_{hv}^*) & 2\,\mathrm{Im}(S_{vh}S_{hh}^*) \end{bmatrix}$$

$$\begin{bmatrix} \mathrm{Re}(S_{vh}^*S_{vv}) & -\mathrm{Im}(S_{vh}^*S_{vv}) \\ \mathrm{Re}(S_{hh}^*S_{hv}) & -\mathrm{Im}(S_{hh}^*S_{hv}) \\ \mathrm{Re}(S_{vv}S_{hh}^* + S_{vh}S_{hv}^*) & -\mathrm{Im}(S_{vv}S_{hh}^* - S_{vh}S_{hv}^*) \\ \mathrm{Im}(S_{vv}S_{hh}^* + S_{vh}S_{hv}^*) & \mathrm{Re}(S_{vv}S_{hh}^* - S_{vh}S_{hv}^*) \end{bmatrix} \qquad (4.8)$$

If the extinction and phase matrices of a particular medium are known, then by applying the boundary conditions, the solution of the radiative transfer equation (4.3) can be obtained either iteratively or numerically [Tsang *et al.*, 1985; Ulaby *et al.*, 1986].

As discussed previously, in a man-made vegetation canopy, such as a corn field, the plants are arranged in a row-structured fashion as shown in Fig. 4.2. In formulating the problem, we assume that there is no variation along the z-direction and treat the medium as a two-dimensional one. We further assume that the canopy structure is statistically periodic in the y-direction and homogeneous in planes perpendicular to the periodic direction (i.e., in the x-z plane). Each period of this structure includes a slab of corn plants adjacent to a slab of air. The stalks are uniformly planted along the row direction (x-axis) with leaves filling the space around the stalks. The leaves may have a distribution along the y-direction.

Referring to Fig. 4.2, for a plane wave incidence, there would be no variations with respect to variables x and z, and therefore (4.3) is simplified to

$$\hat{s}\cdot\hat{y}\,\frac{d\,\bar{I}(y,\hat{s})}{dy} = -\bar{\bar{\kappa}}(y,\hat{s})\,\bar{I}(y,\hat{s}) + \int_{\Omega}\bar{\bar{P}}(y,\hat{s},\hat{s}')\,\bar{I}(y,\hat{s}')\,d\Omega \qquad (4.9)$$

Since scatterers are infinite in the z-direction and the incidence direction is normal to $\hat{z}$, then

$$\hat{s} = \cos\phi\,\hat{x} + \sin\phi\,\hat{y} \quad \text{and} \quad d\Omega = d\phi \tag{4.10}$$

noting that the intensity is redefined by power per unit length per unit angle. Thus, the radiative transfer equation for this problem takes the following form:

$$\sin\phi\,\frac{d\,\bar{I}\,(y,\phi)}{dy} = -\,\bar{\bar{\kappa}}\,(y,\phi)\,\bar{I}\,(y,\phi) + \int_0^{2\pi} \bar{\bar{P}}\,(y,\phi,\phi')\,\bar{I}\,(y,\phi')\,d\phi' \tag{4.11}$$

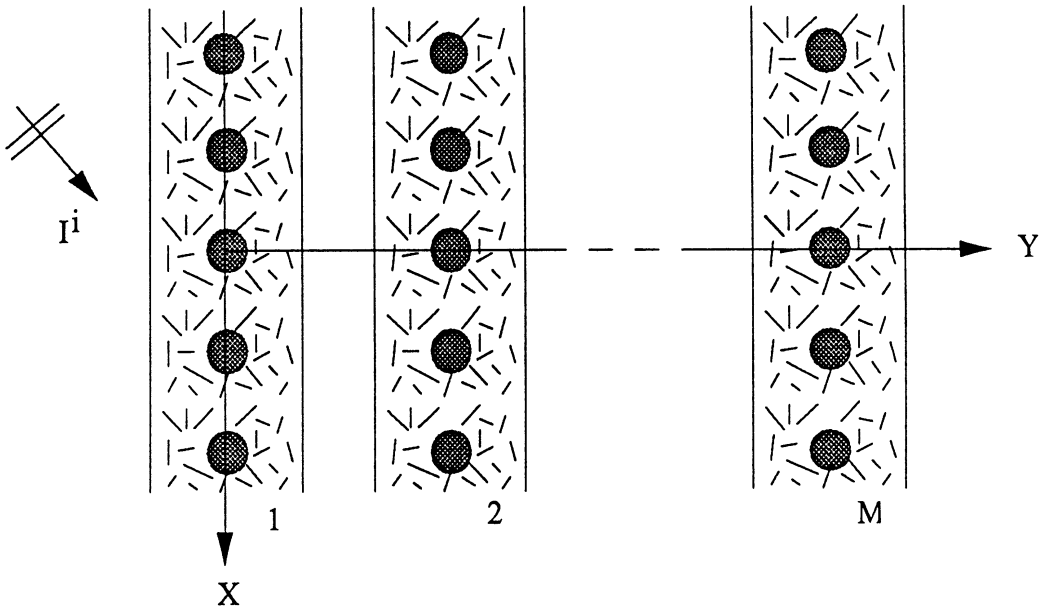

Figure 4.2 Top view of a row structured periodic canopy. Each period consist of a row of vegetation next to a slab of air.

In the above formulation of the mean field intensity in a two-dimensional random medium by radiative transfer, the scattered intensity by a unit cross-sectional area of the random medium into direction ϕ_s is related to the intensity incident upon the unit area from direction ϕ_i by the phase matrix $\bar{\bar{P}}(y, \phi_s, \phi_i)$. Also, the extinction matrix $\bar{\bar{\kappa}}(y, \phi)$ characterizes the loss of intensity due to absorption and scattering by the unit area. To relate the extinction and phase matrices of the medium to the constituent particles in the two-dimensional canopy, we ignore near-field interactions between particles and only consider single-scattering interactions, which is a reasonable approach for low-density media (the volume fraction of the vegetation material in a canopy seldom exceeds 1%). The field scattered by a two-dimensional object whose generating axis is parallel to the z-direction and is illuminated by a plane wave is given by

$$\bar{E}_s = \frac{e^{ik_0\rho - i\frac{\pi}{4}}}{\sqrt{\rho}} \bar{\bar{S}} . \bar{E}_i \tag{4.12}$$

where $\bar{\bar{S}}$ is the scattering matrix of the object. Since in two-dimensional problems, vertically and horizontally polarized fields are decoupled, the scattering matrix becomes diagonal, i.e.

$$\bar{\bar{S}} = \begin{bmatrix} S_{vv} & 0 \\ 0 & S_{hh} \end{bmatrix} \tag{4.13}$$

Using a similar definition for the scattered Stokes vector as given by (4.2), modified by $\frac{1}{\rho}$, and using (4.12), it can be shown that the Stokes matrix $\bar{\bar{L}}$ is given by

$$\bar{\bar{L}} = \begin{bmatrix} |S_{vv}|^2 & 0 & 0 & 0 \\ 0 & |S_{hh}|^2 & 0 & 0 \\ 0 & 0 & \mathrm{Re}(S_{vv}S_{hh}^*) & -\mathrm{Im}(S_{vv}S_{hh}^*) \\ 0 & 0 & \mathrm{Im}(S_{vv}S_{hh}^*) & \mathrm{Re}(S_{vv}S_{hh}^*) \end{bmatrix} \tag{4.13}$$

Because the radiative transfer formulation is based on conservation of energy, the Stokes vectors are added incoherently. Thus, the phase matrix must be obtained from the Stokes matrix averaged over the particle type, size, and orientation-angle distributions. If m types of particles exist in the canopy and each has N_j particles per unit area, then

$$\bar{\bar{P}}(y, \phi, \phi') = < \sum_{j=1}^{m} N_j \bar{\bar{L}}_j > \tag{4.14}$$

The extinction matrix of the canopy can also be obtained by applying the optical theorem for the two-dimensional particles. Using definition (4.12) for the scattering matrix, it can be shown that the extinction cross section is related to the forward scattering amplitude by [Van Bladel, 1985]

$$\sigma_e^p = -\sqrt{\frac{8\pi}{k_0}}\, \mathrm{Re}[S_{pp}(\phi, \phi)] \qquad p = v \text{ or } h \tag{4.15}$$

Because no cross coupling occurs between the V- and H-polarized waves propagating in a two-dimensional medium, the extinction matrix (4.5) can be shown to have the following form:

$$\underline{\underline{\kappa}} = \begin{bmatrix} \sum_{j=1}^{m} N_j \langle \sigma_e^v \rangle & 0 & 0 & 0 \\ 0 & \sum_{j=1}^{m} N_j \langle \sigma_e^h \rangle & 0 & 0 \\ 0 & 0 & 2 \sum_{j=1}^{m} N_j \langle \sigma_e^v + \sigma_e^h \rangle & \kappa_{34} \\ 0 & 0 & \kappa_{43} & \frac{1}{2} \sum_{j=1}^{m} N_j \langle \sigma_e^v + \sigma_e^h \rangle \end{bmatrix}$$

(4.16)

where

$$\kappa_{34} = -\kappa_{43} = -\sqrt{\frac{2\pi}{k_0}} \sum_{j=1}^{m} N_j \langle \mathrm{Im}[S_{vv}(\phi, \phi) - S_{hh}(\phi, \phi)] \rangle$$

From (4.14) and (4.16) it is obvious that the first two components of the Stokes vectors are decoupled from each other and from the other Stokes components. Hence, the vector radiative transfer equation reduces to uncoupled scalar equations for I_v and I_h. Since the total energy is carried by the first two components only, we just consider the solution to scalar radiative transfer equations for these components. It is worth noting that the scattering matrix (for the two-dimensional particles) is a function of ϕ_s - ϕ_i (where ϕ_i and ϕ_s are the incident and scattered azimuth angles) and the particle orientation ϕ_p. Hence in the case of uniform particle distributions, the extinction coefficient of the medium becomes independent of the incidence and scattering angles, and the phase function becomes a function of ϕ_s - ϕ_i only.

The radiative transfer equation (4.11) is an integro-differential equation with nonhomogeneous boundary conditions. If we assume that the air-canopy boundaries are diffuse, there would be no reflections at boundaries and the intensity would be continuous across each boundary. Also the intensity should approach zero as y approaches infinity. Solution to this equation in analytical form is very difficult, if not impossible. However, under certain conditions, approximate solutions or efficient numerical solutions are attainable. In the next two sections, an iterative solution and a numerical solution to the radiative transfer equation will be presented.

4.3 Iterative Solution

For a canopy condition where extinction is dominated by absorption, that is the albedo $\alpha = \frac{\sigma_s}{\sigma_{ext}} << 1$, the iterative method is the standard approach used to solve the radiative transfer equation (R.T.E.). In this approach, first the contribution of the phase function to the intensity is ignored (i.e. $P_{v,h}(\phi,\phi') = 0$) so the equation reduces to a first-order homogeneous ordinary differential equation which can be solved easily. Then the solution of this equation (the zeroth-order solution) will be substituted back into the R.T.E. to obtain the first-order solution. By continuing this process, solutions to any desired order can be obtained in principle. To set the formulation in a form amenable for boundary conditions, common practice is to separate the intensity in the random medium into two functions $I^+(y,\phi)$ and $I^-(y,\phi)$ corresponding to positive and negative going intensities, respectively. In this form, ϕ ranges from 0 to π, and the R.T.E. becomes

$$\sin\phi\,\frac{dI^{+}(y,\phi)}{dy} = -\kappa(y)I^{+}(y,\phi) + \int_0^{\pi}[P(y,\phi,\phi')I^{+}(y,\phi') + P(y,\phi,\phi'+\pi)I^{-}(y,\phi'+\pi)]\,d\phi' \tag{4.17}$$

$$-\sin\phi\,\frac{dI^{-}(y,\phi)}{dy} = -\kappa(y)I^{-}(y,\phi) + \int_0^{\pi}[P(y,\phi+\pi,\phi')I^{+}(y,\phi') + P(y,\phi+\pi,\phi'+\pi)I^{-}(y,\phi'+\pi)]\,d\phi' \tag{4.18}$$

But $P(\phi,\phi') = P(\phi - \phi')$ which is a periodic function with period 2π, i.e. $P(\alpha) = P(\alpha + 2\pi)$, thus

$$P(\phi+\pi,\phi'+\pi) = P(\phi-\phi') \triangleq P^{+}(\phi-\phi') \qquad 0 \le \phi,\phi' \le \pi \tag{4.19}$$

$$P(\phi+\pi,\phi') = P(\phi,\phi'+\pi) = P(\pi+\phi-\phi') \triangleq P^{-}(\phi-\phi') \qquad 0 \le \phi,\phi' \le \pi \tag{4.20}$$

To get the zeroth-order solution, $P(\phi - \phi')$ must be set to zero, then

$$\sin\phi\,\frac{dI_0^{+}(y,\phi)}{dy} = -\kappa(y)I_0^{+}(y,\phi) \tag{4.21}$$

$$-\sin\phi\,\frac{dI_0^{-}(y,\phi)}{dy} = -\kappa(y)I_0^{-}(y,\phi) \tag{4.22}$$

If the incident wave is a plane wave in direction ϕ_i, then

$$I^{+}(0,\phi) = I^{i}\delta(\phi-\phi_i) \tag{4.23}$$

and the zeroth order solutions are given by

$$I_0^+(y, \phi) = I^i \, e^{-\csc\phi_i \, \tau(y)} \, \delta(\phi - \phi_i) \tag{4.24}$$

$$I_0^-(y, \phi) = 0 \tag{4.25}$$

where

$$\tau(y) = \int_0^y \kappa(\xi) \, d\xi \tag{4.26}$$

Now by substituting back (4.24) and (4.25) into (4.17), the first-order solution for the positively going intensity can be obtained to be

$$I_1^+(y, \phi) = \left[e^{-\csc\phi_i \, \tau(y)} \delta(\phi - \phi_i) + \csc\phi \, e^{-\csc\phi \, \tau(y)} \int_0^y P^+(y', \phi - \phi_i) e^{(\csc\phi - \csc\phi_i)\tau(y')} dy' \right] I^i \tag{4.27}$$

Equation (4.27) can be simplified by noting that $\kappa(y)$ and $P(y,\phi-\phi')$ are periodic in y. Defining the integral over one period, L, of $\kappa(\xi)$ by T, i.e.,

$$T = \int_0^L \kappa(\xi) \, d\xi \tag{4.28}$$

and also assuming that the observation point is in the $(N+1)^{th}$ row, then by subdividing the integral in (4.27) into summation of integrals over multiples of a period, I_1^+ becomes

$$I_1^+(y,\phi) = \Bigg[e^{-\csc\phi_i\,\tau(y)}\delta(\phi-\phi_i) + \csc\phi\; e^{-\csc\phi\;\tau(y)} \left(\sum_{n=0}^{N-1} \int_{nL}^{(n+1)L} P^+(y',\phi-\phi_i)\, e^{(\csc\phi-\csc\phi_i)\,\tau(y')}\, dy' + \int_{NL}^{y} P^+(y',\phi-\phi_i)\, e^{(\csc\phi-\csc\phi_i)\,\tau(y')}\, dy' \right) \Bigg] I^i \tag{4.29}$$

Noting the fact that

$$\int_0^{nL} \kappa(\xi)\, d\xi = nT \tag{4.30}$$

and also defining $\tau_p(y)$ as

$$\tau_p(y) = \int_{nL}^{y} \kappa(\xi)\, d\xi \tag{4.31}$$

equation (4.29) can be written as

$$I_1^+(y,\phi) = \Bigg[e^{-\csc\phi_i\,\tau(y)}\delta(\phi-\phi_i) + \csc\phi\; e^{-\csc\phi\;\tau(y)} \left(\sum_{n=0}^{N-1} \int_{nL}^{(n+1)L} P^+(y',\phi-\phi_i)\, e^{(\csc\phi-\csc\phi_i)\,[nT+\tau_p(y')]}\, dy' + \int_{NL}^{y} P^+(y',\phi-\phi_i)\, e^{(\csc\phi-\csc\phi_i)\,[nT+\tau_p(y')]}\, dy' \right) \Bigg] I^i \tag{4.32}$$

Since the medium is periodic in y, then

$$P^{\pm}(y + nL, \phi - \phi') = P^{\pm}(y, \phi - \phi') \tag{4.33}$$

Also defining

$$F^{\pm}(x, \phi, \phi_i) = \int_0^x P^{\pm}(\zeta, \phi - \phi_i)\, e^{(\pm \csc\phi - \csc\phi_i)\,\tau(\zeta)} d\zeta, \quad 0 \le x \le L \tag{4.34}$$

equation (4.32) can be further simplified to

$$\begin{aligned} I_1^+(y, \phi) = \Big[& e^{-\csc\phi_i \tau(y)} \delta(\phi - \phi_i) + \csc\phi\, e^{-\csc\phi\, \tau(y)} \\ & \left(\sum_{n=0}^{N-1} e^{(\csc\phi - \csc\phi_i) nT} F^+(L, \phi, \phi_i) \right. \\ & \left. e^{(\csc\phi - \csc\phi_i) NT} F^+(y - NL, \phi, \phi_i) \right) \Big] I^i \end{aligned} \tag{4.35}$$

Summation over n can be carried out in closed form and the final result of I_1^+ can be shown to be

$$\begin{aligned} I_1^+(y, \phi) = & e^{-(NT + \csc\phi_i \tau(y - NL)} \delta(\phi - \phi_i) I^i + \csc\phi\, e^{-\csc\phi\, \tau(y - NL)} \\ & \left[\frac{e^{-NT\csc\phi} - e^{-NT\csc\phi_i}}{1 - e^{-T(\csc\phi - \csc\phi_i)}} F^+(L, \phi, \phi_i) + e^{-NT\csc\phi_i} F^+(y - NL, \phi, \phi_i) \right] I^i \end{aligned}$$

(4.36)

The first-order solution for the intensity travelling in the negative directions can be obtained by noting that $I_1^-(Y_0, \phi) = 0$, where Y_0 is a distance after which there is no canopy, thus

$$I_1^-(y, \phi) = \left[\csc \phi \, e^{-\csc\phi \, \tau(y)} \int_y^{Y_0} P^+(y', \phi - \phi_i) e^{(\csc\phi - \csc\phi_i)\tau(y')} dy' \right] I^i \quad (4.37)$$

In a manner similar to that of the positive going intensity, the final solution of the negative going intensity can be obtained by assuming that Y_0 is some integer multiple of a period (i.e., $Y_0 = ML$) and is given by

$$I_1^-(y, \phi) = \csc \phi \, e^{\csc\phi \, \tau(y - NL)} \left[\frac{1 - e^{-(\csc\phi - \csc\phi_i)(M-N)T}}{1 - e^{-T(\csc\phi - \csc\phi_i)}} F^-(L, \phi, \phi_i) + e^{NT\csc\phi_i} [F^-(L, \phi, \phi_i) - F^-(y - NL, \phi, \phi_i)] \right] I^i \quad (4.38)$$

Higher order solutions can be obtained by substituting (4.36) and (4.38) into (4.17) and (4.18). However, obtaining the solutions in a closed form seems difficult. Therefore the higher order solutions must be computed numerically. If the observation point is not in between a row (i.e. y = NL), the first-order solutions can be further simplified to

$$I_1^+(y, \phi) = \left\{ e^{-NT}\delta(\phi - \phi_i) + \csc \phi \left[\frac{e^{-NT\csc\phi} - e^{-NT\csc\phi_i}}{1 - e^{-T(\csc\phi - \csc\phi_i)}} F^+(L, \phi, \phi_i) \right] \right\} I^i \quad (4.39)$$

$$I_1^-(y, \phi) = \csc \phi \left[\frac{1 - e^{-(\csc\phi - \csc\phi_i)(M-N)T}}{1 - e^{-T(\csc\phi - \csc\phi_i)}} + e^{NT\csc\phi_i} \right] F^-(L, \phi, \phi_i)] I^i \qquad (4.40)$$

4.4 Numerical Solution (DOT)

If the albedo of the medium is not much smaller than one, the iterative solution does not converge rapidly. In such a case we have to resort to an appropriate numerical method. One such technique is the discrete ordinate eigen-analysis method in which the continuum propagation direction of the intensity within the medium is discretized into finite number of directions [Tsang *et al.*, 1984]. By this approximation the integro-differential equation can be cast into a system of first-order differential equations. For cases where the medium has homogeneous extinction and phase functions, the system of linear differential equations can be solved by the eigen-analysis method. For the general case, however, this method cannot be applied. The extinction and phase functions of the row-structured canopy as discussed earlier are periodic and an alternative approach must be pursued.

In what follows a new numerical technique for the solution of the radiative transfer equation with inhomogeneous extinction and phase functions will be introduced. This method is specifically very efficient for problems with periodic extinction and phase functions. We discretize the direction of propagation and subdivide each row into many thin slabs, then we relate the input-output intensity of each thin slab by keeping the first term of the Taylor series expansions of functions. Finally by multiplying the resultant transmission matrix of individual slabs, the overall transmission matrix can be obtained. This method henceforth will be referred to as discrete ordinate Taylor expansion (DOT) method.

Starting from (4.17) and (4.18), and numerically approximating the integrals, the following coupled system of differential equations can be obtained

$$\frac{d\bar{I}^{+}(y)}{dy} = -\bar{\bar{K}}(y)\,\bar{I}^{+}(y) + \bar{\bar{P}}^{+}(y)\,\bar{I}^{+}(y) + \bar{\bar{P}}^{-}(y)\,\bar{I}^{-}(y) \tag{4.41}$$

$$\frac{d\,\bar{I}^{-}(y)}{dy} = \bar{\bar{K}}(y)\,\bar{I}^{-}(y) - \bar{\bar{P}}^{-}(y)\,\bar{I}^{+}(y) - \bar{\bar{P}}^{+}(y)\,\bar{I}^{-}(y) \tag{4.42}$$

where $\bar{\bar{P}}^{\pm}(y)$ is a 2n x 2n matrix whose elements are defined using the following approximation

$$\csc\phi_i \int_0^{\pi} p^{\pm}(y, \phi_i, \phi')\, I^{\pm}(y, \phi')\, d\phi' \cong \sum_{j=-n}^{n} [P^{\pm}]_{ij}(y)\, I^{\pm}(y, \phi_j) \tag{4.43}$$

and $\bar{\bar{K}}(y)$ is a diagonal matrix with

$$[K]_{ii}(y) = \csc\phi_i\, \kappa(\phi_i, y) \tag{4.44}$$

Equations (4.41) and (4.42) are valid for all of the thin slabs. Suppose thickness of each slab (Δ) is chosen thin enough so that the functions in equations (4.41) and (4.42) can be approximated by their Taylor series expansion around the values of y at the left boundary of the slabs up to the first term. That is, for the m^{th} slab we have

$$\begin{aligned} &\bar{I}^{\pm}(y) \cong \bar{a}^{\pm}_m + \bar{b}^{\pm}_m (y - y_m), \\ &\bar{\bar{K}}(y) \cong \bar{\bar{K}}_m + \bar{\bar{K}}'_m (y - y_m), \text{ and} \\ &\bar{\bar{P}}(y) \cong \bar{\bar{P}}_m + \bar{\bar{P}}'_m (y - y_m). \end{aligned} \tag{4.45}$$

After substituting (4.45) into (4.41) and (4.42) and rearranging the terms of equal power in y, the following algebraic equations for the coefficients are obtained

$$\bar{b}_m^+ = -(\bar{\bar{K}}_m + \bar{\bar{P}}_m^+)\bar{a}_m^+ + \bar{\bar{P}}_m^- \bar{a}_m^- \tag{4.46}$$

$$\bar{b}_m^- = (\bar{\bar{K}}_m - \bar{\bar{P}}_m^-)\bar{a}_m^- - \bar{\bar{P}}_m^- \bar{a}_m^+ \tag{4.47}$$

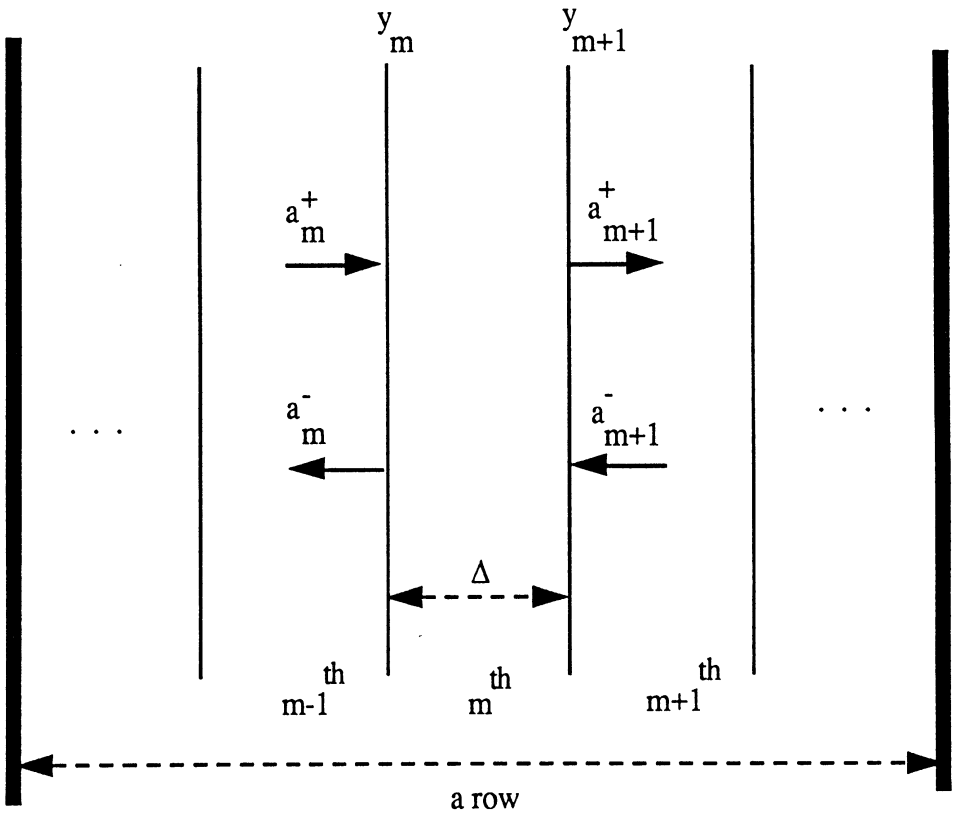

Figure 4.3 Configuration showing a row of vegetation consisting of M slabs. Also depicting the incidence and reflected intensities on the m^{th} slab. Thickness of each slab is Δ.

The intensity in the $(m+1)^{th}$ slab is related to the intensity of the m^{th} slab by (see Fig. 4.3)

$$\underline{\bar{a}}^{\pm}_{m+1} = \underline{\bar{a}}^{\pm}_{m} + \underline{\bar{b}}^{\pm}_{m}\,\Delta \tag{4.48}$$

Using (4.48) in (4.47), the intensity on the right-hand side can be related to the intensity on the left hand side of the m^{th} slab by

$$\begin{bmatrix} \underline{\bar{a}}^{+}_{m+1} \\ \underline{\bar{a}}^{-}_{m+1} \end{bmatrix} = \begin{bmatrix} \bar{\bar{I}} - \Delta(\bar{\bar{K}}_m - \bar{\bar{P}}^{+}_{m}) & \Delta\,\bar{\bar{P}}^{-}_{m} \\ -\Delta\,\bar{\bar{P}}^{-}_{m} & \bar{\bar{I}} + \Delta(\bar{\bar{K}}_m - \bar{\bar{P}}^{+}_{m}) \end{bmatrix} \begin{bmatrix} \underline{\bar{a}}^{+}_{m} \\ \underline{\bar{a}}^{-}_{m} \end{bmatrix} \tag{4.49}$$

where $\bar{\bar{I}}$ is the unit matrix. The matrix in (4.49), which relates the input-output of the thin slab ($\bar{\bar{T}}_m$), will be referred to as the transmission matrix. The transmission matrix of a row comprised of M thin slabs is given by

$$\bar{\bar{T}}_{row} = \prod_{m=1}^{M} \bar{\bar{T}}_{m} \tag{4.50}$$

which relates the input and output intensities of a single row. If there are N rows of the canopy under consideration the overall transmission matrix can be obtained from

$$\bar{\bar{T}} = \left[\bar{\bar{T}}_{row}\right]^{N} \triangleq \begin{bmatrix} \bar{\bar{T}}_{11} & \bar{\bar{T}}_{12} \\ \bar{\bar{T}}_{21} & \bar{\bar{T}}_{22} \end{bmatrix} \tag{4.51}$$

The overall transmission matrix for large values of N can be calculated by diagonalizing the matrix. Suppose $\bar{\bar{T}}_{row}$ can be diagonalized, i.e.,

$$\bar{\bar{T}}_{row} = \bar{\bar{Q}}\,\bar{\bar{\Lambda}}\,\bar{\bar{Q}}^{-1} \tag{4.52}$$

where $\bar{\bar{Q}}$ is a diagonal matrix whose columns are eigen-vectors of $\bar{\bar{T}}_{row}$, and $\bar{\bar{\Lambda}}$ is a diagonal matrix whose enteries are the eigenvalues of $\bar{\bar{T}}_{row}$. Thus

$$\left[\bar{\bar{T}}_{row}\right]^{N} = \bar{\bar{Q}}\,\bar{\bar{\Lambda}}^{N}\,\bar{\bar{Q}}^{-1} \tag{4.53}$$

where $\bar{\bar{\Lambda}}^{N}$ is a diagonal matrix whose entries are the eigenvalues of $\bar{\bar{T}}_{row}$ raised to the N^{th} power. Noting that there is no intensity incident on the $(M+1)^{th}$ boundary, (i.e., $\bar{a}^{-}_{M+1} = 0$), the reflected and transmitted intensities, respectively, are given by

$$\bar{I}^{r} = -\left[\bar{\bar{T}}_{22}\right]^{-1}\left[\bar{\bar{T}}_{21}\right]\bar{I}^{i} \tag{4.54}$$

$$\bar{I}^{t} = \left[\left[\bar{\bar{T}}_{22}\right] - \left[\bar{\bar{T}}_{12}\right]\left[\bar{\bar{T}}_{22}\right]^{-1}\left[\bar{\bar{T}}_{21}\right]\right]\bar{I}^{i} \tag{4.55}$$

4.5 Extinction and Phase Function for Stalks

As mentioned previously, stalks are modeled as infinitely long, vertically oriented homogeneous dielectric cylinders. The cylinder is one of the few geometries for which an exact electromagnetic scattering solution exists. If a plane wave propagating in a direction denoted by ϕ_i is illuminating an infinitely long dielectric cylinder with radius r_0 whose axis coincides with the z-axis, it can be shown that the bistatic scattering matrix elements can be represented by [Ruck *et al.*, 1970]:

$$S_{vv} = \sum_{n=0}^{\infty} C_n^V \cos\, n(\phi_s - \phi_i) \tag{4.56}$$

$$S_{hh} = \sum_{n=0}^{\infty} C_n^H \cos\, n(\phi_s - \phi_i) \tag{4.57}$$

In equations (4.56) and (4.57) ϕ_s denotes the scattering direction and

$$C_n^V = \sqrt{\frac{2}{\pi k_0}}\,(-1)^{n+1}\alpha_n \frac{\sqrt{\varepsilon}\,J_n(x_0)J_n'(x_1) - J_n'(x_0)J_n(x_1)}{\sqrt{\varepsilon}\,H_n^{(1)}(x_0)J_n'(x_1) - H_n^{(1)'}(x_0)J_n(x_1)} \tag{4.58}$$

$$C_n^H = \sqrt{\frac{2}{\pi k_0}}\,(-1)^{n+1}\alpha_n \frac{J_n(x_0)J_n'(x_1) - \sqrt{\varepsilon}\,J_n'(x_0)J_n(x_1)}{H_n^{(1)}(x_0)J_n'(x_1) - \sqrt{\varepsilon}\,H_n^{(1)'}(x_0)J_n(x_1)} \tag{4.59}$$

where

$$x_0 = k_0 r_0, \quad \text{and}$$
$$x_1 = k_0 \sqrt{\varepsilon}\, r_0. \tag{4.60}$$

ε is the relative dielectric constant of the cylinders and

$$\alpha_n = \begin{cases} 1 & n = 0 \\ 2 & n \neq 0 \end{cases} \tag{4.61}$$

Since the cylinders are vertically oriented and azimuthally symmetric, evaluation of the extinction and phase function does not involve particle orientation averaging. Using (4.56) and (4.57) in (4.14) and (4.16) gives the phase and extinction functions of the stalks.

4.6 Extinction and Phase Function for Leaves

Leaves in this two-dimensional model are considered as long thin dielectric strips. The thickness and dielectric constant of leaves are usually such that they can be modeled as resistive sheets at centimeter wavelengths [Senior *et al.*, 1987; Sarabandi *et al.*, 1988]. At high frequencies, where the width of a leaf is large compared to the wavelength, the physical optics approximation can be used to find the scattered field. Otherwise numerical techniques such as the method of moments should be employed instead. Consider a resistive strip of width w illuminated by a plane wave as shown in Fig. 4.4 where the orientation and incidence angles, measured from the x-axis, are denoted by ϕ_l and ϕ_i respectively. Depending on the polarization, the incident field is assumed to have the following form

$$\bar{E}^i = \hat{z}\, e^{ik_0(x\cos\phi_i + y\sin\phi_i)} \tag{4.62}$$

for V-polarization and

$$\bar{H}^i = Y_0 \hat{z} e^{i k_0 (x \cos \phi_i + y \sin \phi_i)} \tag{4.63}$$

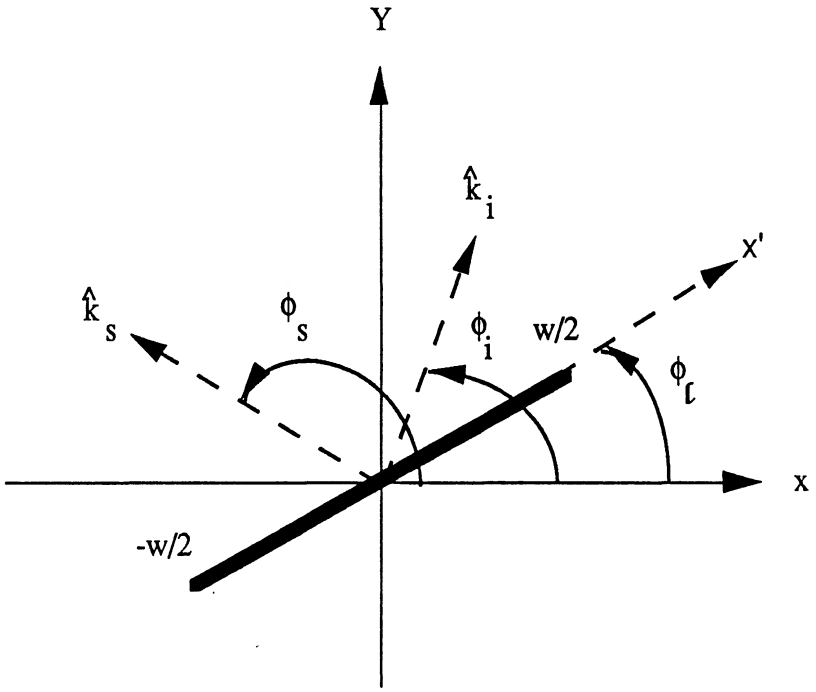

Figure 4.4 geometry of a resistive strip depicting the orientation, incidence, and scattered angles.

for H-polarization. Following the procedure outlined by Senior *et al.* [1987], the physical optics currents for V- and H-polarized incidence waves are given by

$$J_z = \Gamma^V\left(\frac{\pi}{2} - |\phi_i - \phi_l|\right) J_z^{PC} \tag{4.64}$$

$$J_{x'} = \Gamma^H\left(\frac{\pi}{2} - |\phi_i - \phi_l|\right) J_{x'}^{PC} \tag{4.65}$$

where J^{PC} refers to the physical optics current that would exist on the surface of the resistive sheet had it been a perfect conductor. Γ^V and Γ^H are the reflection coefficients for the resistive sheet for horizontal and vertical polarization and are given by

$$\Gamma^V\left(\frac{\pi}{2} - |\phi_i - \phi_l|\right) = \left[1 + \frac{2R}{Z_0}\cos\left(\frac{\pi}{2} - |\phi_i - \phi_l|\right)\right]^{-1} \tag{4.66}$$

$$\Gamma^H\left(\frac{\pi}{2} - |\phi_i - \phi_l|\right) = -\left[1 + \frac{2R}{Z_0}\sec\left(\frac{\pi}{2} - |\phi_i - \phi_l|\right)\right]^{-1} \tag{4.67}$$

where Z_0 is the free space characteristic impedance and R is the resistivity of the leaf given by

$$R = \frac{i Z_0}{k_0 \tau (\varepsilon - 1)} \tag{4.68}$$

In (4.68) τ and ε are the thickness and dielectric constant of the leaf. Noting that the physical optics currents J_z^{PC} and $J_{x'}^{PC}$ are

$$J_z^{PC} = -2Y_0 \sin\left(\left|\phi_i - \phi_l\right|\right) e^{ik_0 \cos(\phi_i - \phi_l) x'} \tag{4.69}$$

$$J_{x'}^{PC} = +2Y_0 e^{ik_0 \cos(\phi_i - \phi_l) x'} \tag{4.70}$$

and using the far field approximation, the scattered field due to the physical optics currents J_z and $J_{x'}$ can be obtained from

$$E_z^s = -Z_0 \sqrt{\frac{k_0}{8\pi}} \frac{e^{ik_0\rho - \frac{i\pi}{4}}}{\sqrt{\rho}} \int_{-w/2}^{w/2} J_z(\zeta) e^{-ik_0 \zeta \cos(\phi_s - \phi_l)} d\zeta \tag{4.71}$$

$$H_z^s = \sqrt{\frac{k_0}{8\pi}} \frac{e^{ik_0\rho - \frac{i\pi}{4}}}{\sqrt{\rho}} \sin\left|\phi_s - \phi_l\right| \int_{-w/2}^{w/2} J_{x'}(\zeta) e^{-ik_0 \zeta \cos(\phi_s - \phi_l)} d\zeta \tag{4.72}$$

Finally, after evaluating the integrals, the scattered field for V- and H-polarizations are

$$E_z^s = \sqrt{\frac{k_0}{2\pi}} \frac{e^{ik_0\rho - \frac{i\pi}{4}}}{\sqrt{\rho}} \frac{\sin\left|\phi_i - \phi_l\right|}{1 + \frac{2R}{z_0} \sin\left|\phi_i - \phi_l\right|} \left\{\frac{w \sin X}{X}\right\} \tag{4.73}$$

$$H_z^s = Y_0 \sqrt{\frac{k_0}{2\pi}} \frac{e^{ik_0\rho - \frac{i\pi}{4}}}{\sqrt{\rho}} \frac{\sin\left|\phi_s - \phi_l\right|}{1 + \frac{2R}{z_0} \csc\left|\phi_i - \phi_l\right|} \left\{\frac{w \sin X}{X}\right\} \tag{4.74}$$

with

$$X = \frac{k_0 w}{2}\left[\cos(\phi_i - \phi_l) - \cos(\phi_s - \phi_l)\right] \tag{4.75}$$

Hence,

$$\overline{\overline{S}} = \sqrt{\frac{k_0}{2\pi}}\, w \begin{bmatrix} \dfrac{\sin\left|\phi_i - \phi_l\right|}{1 + \dfrac{2R}{z_0}\sin\left|\phi_i - \phi_l\right|}\dfrac{\sin X}{X} & 0 \\ 0 & \dfrac{\sin\left|\phi_s - \phi_l\right|}{1 + \dfrac{2R}{z_0}\csc\left|\phi_i - \phi_l\right|}\dfrac{\sin X}{X} \end{bmatrix} \tag{4.76}$$

The averaging over the orientation angle ϕ_l involved in the derivations of the extinction and phase matrices cannot be evaluated analytically; hence, the integrals should be calculated numerically. The physical-optics approximation is valid as long as the width of the strips is large compared to the wavelength, and if the material is lossy, this approximation provides reasonable results for values of w as small as λ_0.

For cases where the width of the strips is not large compared to the wavelength, numerical techniques, such as the method of moments, may be used to find the scattered field. However, use of such computational techniques to compute the phase and the extinction matrices from the scattered field would be prohibitive in terms of computational time. In what follows, we demonstrate an efficient procedure for numerical computation of the extinction and phase matrices. The integral equations for the induced currents on the

resistive sheet, as shown in Fig. 4.4, for V- and H-polarizations are respectively given by [Sarabandi, 1990]

$$RJ_z(x') = e^{ik_0\cos(\phi_i-\phi_l)x'} - \frac{k_0 z_0}{4}\int_{-w/2}^{w/2} J_z(\zeta)\,H_0^{(1)}(k_0|x'-\zeta|)\,d\zeta \quad (4.77)$$

$$\begin{aligned} RJ_{x'}(x') = &-\sin|\phi_i-\phi_l|\,e^{ik_0\cos(\phi_i-\phi_l)x'} \\ &-\frac{k_0 z_0}{4}\int_{-w/2}^{w/2} J_{x'}(\zeta)\left(1+\frac{\partial^2}{k_0^2\partial x'^2}\right)H_0^{(1)}(k_0|x'-\zeta|)\,d\zeta \end{aligned} \quad (4.78)$$

where $H_0^{(1)}$ is the Hankel function of the first kind and zeroth order. These integral equations can be cast into a linear system of equations by applying the method of moments and point matching technique. By solving the linear system of equations an approximate solution for the currents can be obtained. Having found the induced currents, the scattered fields can be obtained from (4.71) and (4.72). The approximate form of the scattering matrix assuming that the strip is divided into M small sections takes the following form

$$\bar{\bar{S}} = -Z_0\sqrt{\frac{k_0}{8\pi}} \begin{bmatrix} \sum_{m=1}^{M} J_m^z e^{-ik_0 x_m\cos(\phi_s-\phi_l)} & 0 \\ 0 & \sin|\phi_s-\phi_l|\sum_{m=1}^{M} J_m^{x'} e^{-ik_0 x_m\cos(\phi_s-\phi_l)} \end{bmatrix} \quad (4.79)$$

where x_m is the coordinate of the m^{th} cell in the x' coordinate system and J_m is the value of the current for the m^{th} cell. The matrix approximation of (4.77) and (4.78) can be written as

$$\bar{\bar{Z}}_{V,H}\,\bar{J}_{z,x'} = \bar{V}_{V,H} \tag{4.80}$$

where Z_V and Z_H are the impedance matrices and V_V and V_H are the excitation vectors whose elements are

$$V_m^V = e^{ik_0\cos(\phi_i-\phi_l)x_m} \tag{4.81}$$

$$V_m^H = -\sin|\phi_i-\phi_l|e^{ik_0\cos(\phi_i-\phi_l)x_m} \tag{4.82}$$

From (4.80)-(4.82) the induced current supported by each cell is given by

$$J_m^z = \sum_{l=1}^{m}\left[\bar{\bar{Z}}_V^{-1}\right]_{ml} e^{ik_0\cos(\phi_i-\phi_l)x_l} \tag{4.83}$$

$$J_m^{x'} = -\sum_{l=1}^{m}\left[\bar{\bar{Z}}_H^{-1}\right]_{ml}\sin|\phi_i-\phi_l|\,e^{ik_0\cos(\phi_i-\phi_l)x_l} \tag{4.84}$$

Finally by substituting back (4.83) and (4.84) into (4.79), the scattering amplitudes of the scattered field can be derived to be

$$S_{vv}(\phi_i, \phi_s, \phi_l) = -Z_0\sqrt{\frac{k_0}{8\pi}} \sum_{m=1}^{M} \sum_{l=1}^{M} \left[\overline{\overline{Z}}_V^{-1}\right]_{ml} e^{ik_0[\cos(\phi_i - \phi_l)x_l - \cos(\phi_s - \phi_l)x_l]} \tag{4.85}$$

$$S_{hh}(\phi_i, \phi_s, \phi_l) = -Z_0\sqrt{\frac{k_0}{8\pi}} \sum_{m=1}^{M} \sum_{l=1}^{M} \left[\overline{\overline{Z}}_H^{-1}\right]_{ml} \sin|\phi_i - \phi_l| \sin|\phi_s - \phi_l| e^{ik_0[\cos(\phi_i - \phi_l)x_l - \cos(\phi_s - \phi_l)x_l]} \tag{4.86}$$

Suppose the orientation angle distribution of the leaves is uniform in the interval $(0, 2\pi)$, then the ensemble average of S_{vv} and S_{hh} in the forward direction ($\phi_s = \phi_i$) is

$$\begin{aligned} \langle S_{vv} \rangle &= -Z_0\sqrt{\frac{k_0}{8\pi}} \sum_{m=1}^{M} \sum_{l=1}^{M} \left[\overline{\overline{Z}}_V^{-1}\right]_{ml} \\ &\quad \frac{1}{2\pi} \int_0^{2\pi} e^{ik_0 \cos(\phi_i - \phi_l)(x_l - x_m)} d\phi_l \\ &= -Z_0\sqrt{\frac{k_0}{8\pi}} \sum_{m=1}^{M} \sum_{l=1}^{M} \left[\overline{\overline{Z}}_V^{-1}\right]_{ml} J_0(k_0|x_l - x_m|) \end{aligned} \tag{4.87}$$

$$\begin{aligned} \langle S_{hh} \rangle &= -Z_0\sqrt{\frac{k_0}{8\pi}} \sum_{m=1}^{M} \sum_{l=1}^{M} \left[\overline{\overline{Z}}_H^{-1}\right]_{ml} \\ &\quad \frac{1}{2\pi} \int_0^{2\pi} \sin^2(\phi_i - \phi_l) e^{ik_0[\cos(\phi_i - \phi_l)(x_l - x_m]} d\phi_l \\ &= -Z_0\sqrt{\frac{k_0}{8\pi}} \sum_{m=1}^{M} \sum_{l=1}^{M} \left[\overline{\overline{Z}}_H^{-1}\right]_{ml} \\ &\quad \left[\frac{1}{2} J_0(k_0|x_l - x_m|) \pm \frac{1}{2} J_2(k_0|x_l - x_m|)\right] \end{aligned} \tag{4.88}$$

where J_0 and J_2 are the Bessel function of the zeroth and second order, respectively, and the + or - sign must be used according to the sign of $(x_l - x_m)$. Therefore, the extinction coefficient of leaves for vertical and horizontal polarization, respectively, are

$$\kappa_L^V = Z_0 N_L \sum_{m=1}^{M} \sum_{l=1}^{M} \mathrm{Re}\left[\left[\bar{\bar{Z}}_V^{-1}\right]_{ml}\right] J_0(k_0 |x_l - x_m|) \tag{4.89}$$

$$\kappa_L^H = Z_0 N_L \sum_{m=1}^{M} \sum_{l=1}^{M} \mathrm{Re}\left[\left[\bar{\bar{Z}}_H^{-1}\right]_{ml}\right] \left[\frac{1}{2} J_0(k_0 |x_l - x_m|) \pm \frac{1}{2} J_2(k_0 |x_l - x_m|)\right] \tag{4.90}$$

where N_L is the number of the leaves per unit area. Inspection of (4.89) and (4.90) reveals that the extinction coefficients are independent of the incidence angle.

For evaluation of the phase matrix we note that

$$\langle |S_{vv}|^2 \rangle = \frac{Z_0^2 k_0}{8\pi} \sum_{m=1}^{M} \sum_{l=1}^{M} \sum_{n=1}^{M} \sum_{j=1}^{M} \left[\bar{\bar{Z}}_V^{-1}\right]_{ml} \left[\bar{\bar{Z}}_V^{-1}\right]_{nj}^{*} \frac{1}{2\pi} \int_0^{2\pi} e^{ik_0[\cos(\phi_i - \phi_l)(x_l - x_n) - \cos(\phi_s - \phi_l)(x_m - x_j)]} d\phi_l \tag{4.91}$$

The integral in (4.91) can be represented as

$$\frac{1}{2\pi} \int_0^{2\pi} e^{ik_0[\cos(\phi_i - \phi_l)(x_l - x_n) - \cos(\phi_s - \phi_l)(x_m - x_j)]} d\phi_l = \frac{1}{2\pi} \int_0^{2\pi} e^{ik_0 q \cos(\phi_l - \gamma)} d\phi_l \tag{4.92}$$

where

$$q = \sqrt{(x_l - x_n)^2 + (x_m - x_j)^2 - 2(x_l - x_n)(x_m - x_j)\cos(\phi_i - \phi_s)} \quad (4.93)$$

$$\gamma = \tan^{-1} \frac{(x_l - x_n)\sin(\phi_s - \phi_i)}{(x_l - x_n)\cos(\phi_s - \phi_i) - (x_m - x_j)} \quad (4.94)$$

The solution to the definite integral in (4.92) is

$$\frac{1}{2\pi} \int_0^{2\pi} e^{i k_0 q \cos(\phi_l - \gamma)} d\phi_l = J_0(k_0 q) \quad (4.95)$$

Therefore, the phase function for the V-polarization becomes

$$P_{VV} = N_L \frac{Z_0^2 k_0}{8\pi} \sum_{m=1}^{M} \sum_{l=1}^{M} \sum_{n=1}^{M} \sum_{j=1}^{M} \left[\bar{\bar{Z}}_V^{-1}\right]_{ml} \left[\bar{\bar{Z}}_V^{-1}\right]_{nj}^{*} J_0(k_0 q) \quad (4.96)$$

Following a similar procedure for H-polarization and using the following integral identities,

$$\frac{1}{2\pi} \int_0^{2\pi} \cos^2(\phi_l - \alpha)\, e^{i k_0 q \cos(\phi_l - \gamma)} = \cos(4\gamma - 2\alpha) J_4(k_0 q) - \frac{1}{2} J_0(k_0 q) \quad (4.97)$$

and

$$\frac{1}{2\pi}\int_0^{2\pi}\cos(\phi_1-\alpha)\,e^{ik_0q\cos(\phi_1-\gamma)}=-\cos(2\gamma-\alpha)\,J_2(k_0q) \tag{4.98}$$

the phase function for the H-polarization can be shown to be

$$\begin{aligned}P_{HH}=N_L\frac{Z_0^2k_0}{8\pi}\sum_{m=1}^{M}\sum_{l=1}^{M}\sum_{n=1}^{M}\sum_{j=1}^{M}\left[\bar{\bar{Z}}_H^{-1}\right]_{ml}\left[\bar{\bar{Z}}_H^{-1}\right]^*_{nj}\\ \left[\frac{1}{2}\cos 2(\phi_s-\phi_i)J_0(k_0q)+\right.\\ 2\cos(\phi_s-\phi_i)\cos(2\gamma-(\phi_s-\phi_i))\,J_2(k_0q)+\\ \left.\cos(4\gamma-2(\phi_s-\phi_i))J_4(k_0q)\right]\end{aligned} \tag{4.99}$$

Equations (4.96) and (4.99) show that the phase functions are independent of the incidence and scattering angles and are only dependent on the difference angle (ϕ_s - ϕ_i).

4.7 Comparison with Experimental Data

In order to use the iterative and DOT solutions for practical applications, the validity of the developed model should be checked against experimental data. The horizontal propagation measurements, presented in section 3.2, can be used for this purpose. A summary of the measured canopy parameters are given in Table 4.1. Before proceeding with the comparison of the theory with experimental data, it is useful to examine the behavior of the phase function of cylinders and resistive strips. Using the data of Table 4.1, the phase functions of a single cylinder and a single resistive strip (i.e., $N_{S,L}$ = 1) at 4.75 GHz were calculated as a function of (ϕ_s-ϕ_i) and are presented in Fig. 4.5. It can be seen that considering the number of leaves and stalks in the canopy, the phase function of leaves becomes comparable in amplitude to the phase function of stalks at C-band. Hence, leaves play as important a role in the scattering process as stalks, which was also observed

in the experimental data. Referring to Fig. 4.5b, it can be concluded that the physical optics solution is in good agreement with the exact solution derived by the method of moments at 4.75 GHz. It should be mentioned that in computation of the phase function by the method of moments, the size of the cells (segments) does not have to be as small as the size that is required for accurate computation of the scattering amplitude (usually $\lambda/15$). This is due to the fact that the averaging process over the magnitude of the scattering amplitude in the calculation of the phase function washes out the fine features of the scattering amplitude.

	λ	ε_t	ε_s
f=1.5 GHz	20 cm	28+ i 8	33+ i 10
f=4.75 GHz	6.3 cm	26+ i 8	31+ i 10

Leaf: w = 5 cm τ = 0.25 mm

Stalk: d = 1.75 cm

Row spacing = 80 cm

Number of plants per square meter = 6.2

Number of leaves per plant = 13

Table 4.1 Canopy parameters used in the calculation of the theoretical results

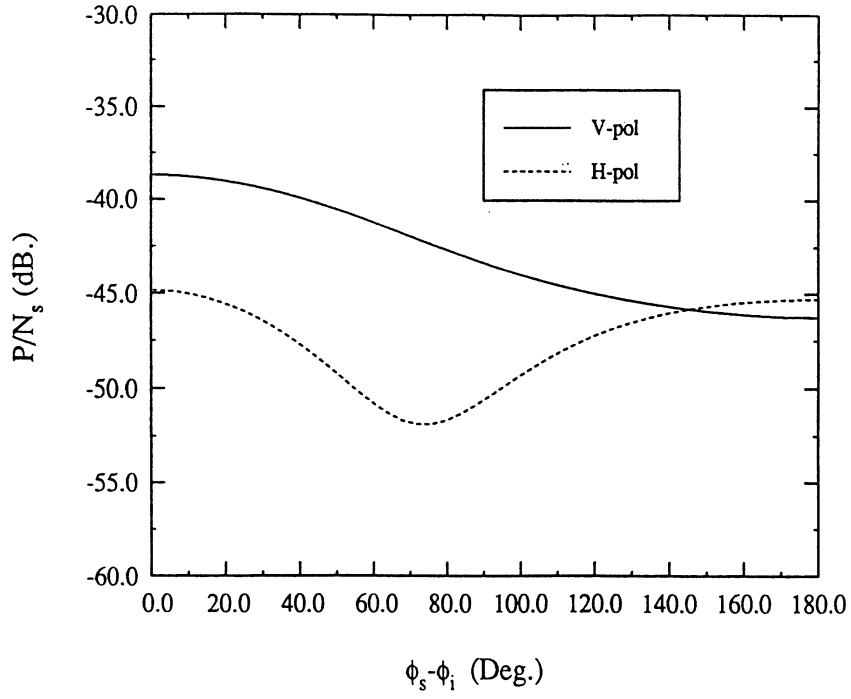

(a)

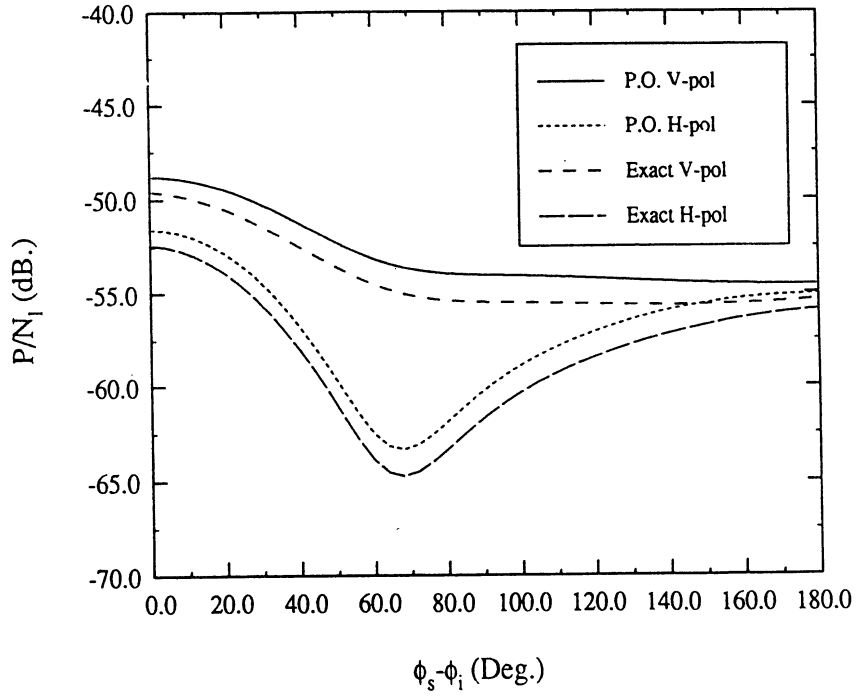

(b)

Figure 4.5 Calculated phase function of a single (a) cylinder, (b) resistive strip as a function of phase difference, ϕ_S-ϕ_i, at 4.75 GHz for the parameters of Table 4.1.

Figure 4.6 shows comparisons between the phase function of a single strip calculated by the physical optics method and the result obtained by using the method of moments. The phase functions is calculated as a function of w/λ using the parameters of Table 4.1. It can be seen that the physical-optics solution is a good approximation for calculation of the leaves' phase function at C-band. But, at lower frequencies, the exact solution derived by the method of moments must be used (i.e., at L-band). Therefore, in the calculation of the phase function for leaves, the exact solution at 1.5 GHz, and the physical optics solution at 4.75 GHz are used. For a plane wave incident normally on seven rows of a full corn canopy, the bistatic scattering coefficient was calculated and is presented in Fig. 4.7. The result of the iterative and DOT solutions are comparable at both L- and C-bands. The first order solution underestimates the DOT solution by up to 3 dB. It can be concluded that both methods produce similar results for corn-like canopies at frequencies in the L- to C-band range. The coherent component of the calculated transmitted wave is also given in Table 4.2.

	V-polarization		H-polarization	
	First order	DOT	First order	DOT
L-band	-24.1	-22.7	-2.7	-2.2
C-band	-30.8	-27.3	-18.6	-16.8

Table 4.2 Coherent component of the transmitted wave (in dB), when a plane wave of unit magnitude is incident normally on seven rows of a corn canopy.

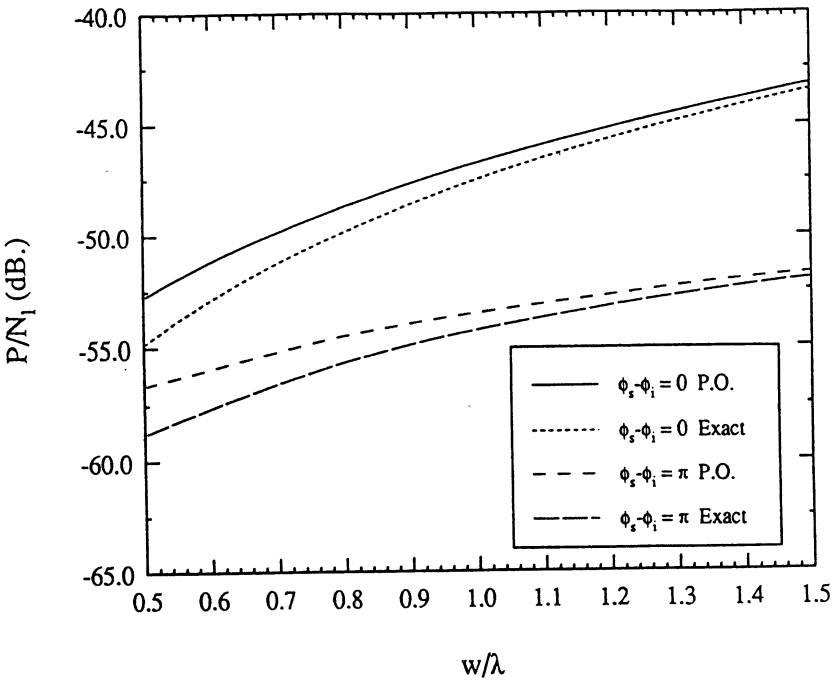

(a)

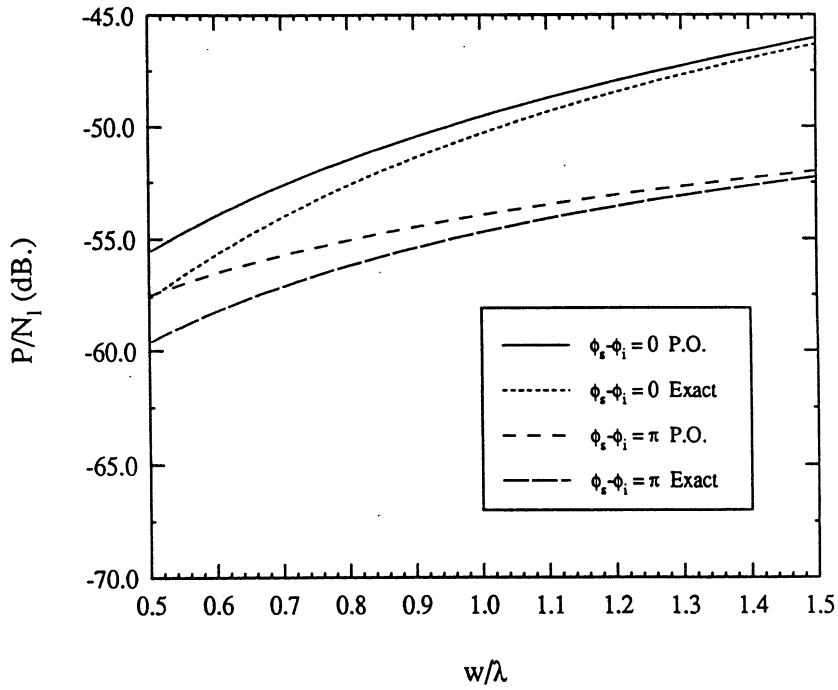

(b)

Figure 4.6 Calculated phase function of a single resistive strip as a function of w/λ, using the iterative and DOT methods with the parameters of Table 4.1 for (a) V-polarization, and (b) H-polarization.

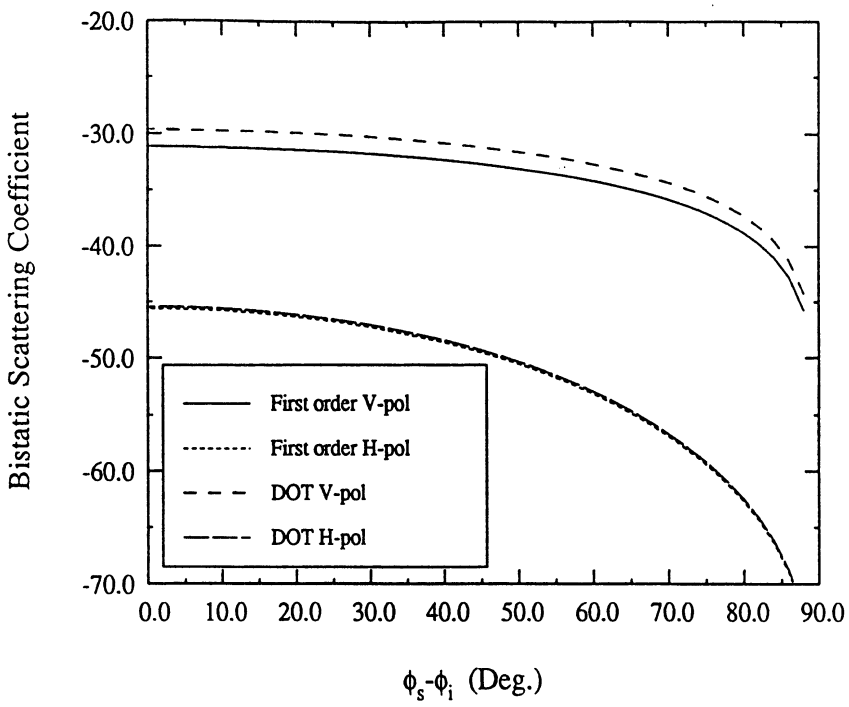

(a)

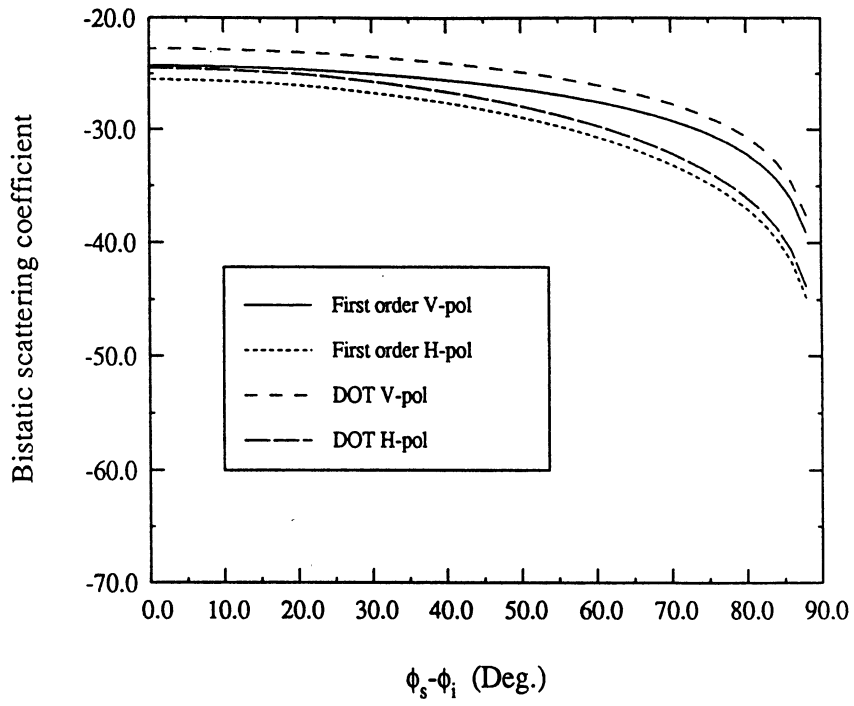

(b)

Figure 4.7 Calculated bistatic scattering coefficient for a plane wave incident normally on seven rows of a corn canopy, using both iterative and DOT methods at (a) L-band, (b) C-band.

As it was discussed in section 3.2, measurements of the magnitudes of wave patterns transmitted horizontally through seven rows of a corn canopy were made at 1.5 GHz (L-band) and 4.75 GHz (C-band) for both vertical and horizontal polarizations. We can now compare the simulated results of the iterative and DOT solutions with the experimental data. Equation (3.64) was used to simulate the incidence wave patterns. In calculation, each row was subdivided into sections of 1.95-cm wide slabs for L-band and 1.77 cm-wide slabs at C-band, where stalks are only present in the central slab and leaves are uniformly distributed in all slabs. Figures 4.8 and 4.9 compare the result of simulation with the experimental data for stalks at 1.5 and 4.75 GHz, respectively. It should be noted that the radiative transfer technique produces the statistical average of the transmitted wave pattern and the experimental wave patterns are not averaged over many measurements. It can be seen that both the first-order iterative solution and the DOT solution produce satisfactory wave patterns at both L- and C-band frequencies. Figures 4.10 and 4.11 depict similar results when leaves are also present. Good agreement between the experimental data and the theory is obtained for a vertically polarized wave, but poor agreement is achieved for the horizontal polarization. The model underestimates the propagation loss for horizontally polarized waves. This shortcoming is due to the fact that leaves are modeled as vertically oriented strips, whereas in reality, leaves are also oriented in non-vertical directions. Therefore, the simulated propagation loss is not accurate for H-polarization.

4.8 Conclusion

In this chapter, a two-dimensional radiative transfer model for horizontal wave propagation through a random medium with inhomogeneous particle distribution was developed. Solution of the radiative transfer equation was pursued both iteratively and by a new method based on the discrete-ordinate approximation and the taylor series expansion (DOT). As an example, a corn canopy was considered where stalks were represented as

infinitely long, vertically oriented dielectric cylinders, and leaves were represented by vertically oriented thin resistive strips. An efficient numerical procedure was developed to compute the extinction and phase function of particles with arbitrary cross section. This model was used to compute the extinction and phase function of the leaves at L-band and the physical optics approximation was used to calculate the extinction and phase function of the leaves at C-band. It is shown that the models agree with the experimental data for a canopy of stalks at both polarizations. The model also predicts the propagation characteristic of a vertically polarized transmitted wave through a full corn canopy, but underestimated the horizontal propagation loss due to the fact that leaves were modeled as vertically oriented resistive strips. Overall, the model can be used to study the electromagnetic interaction with a random medium with inhomogeneous particle distribution of arbitrary cross section when their longitudinal dimension is much larger than their cross sectional dimensions for horizontal propagation through periodic vegetation canopies. The performance of the model for leaves at horizontal polarization will improve as the frequency of the operation increases. This is due to the fact that the leaves' phase function for vertical and horizontal propagation become comparable in magnitude by increasing the frequency of operation.

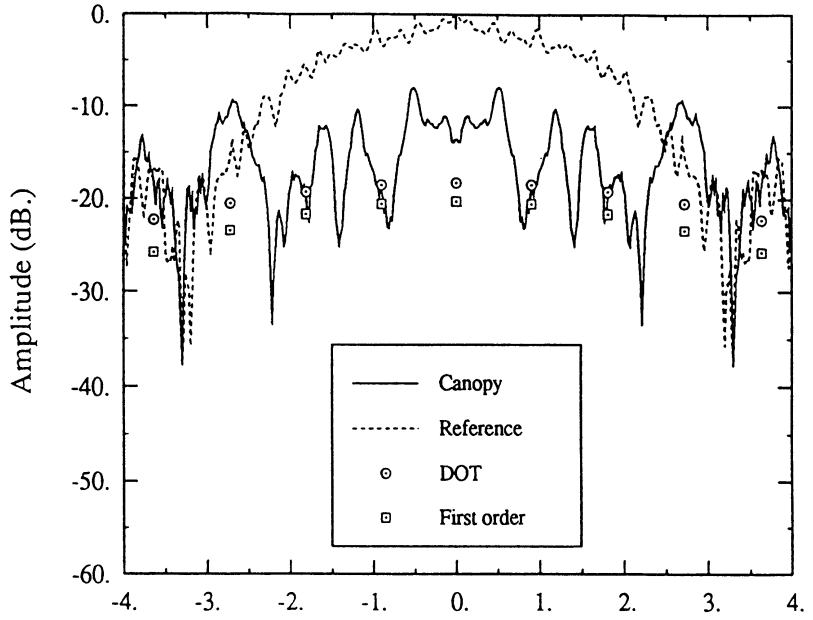

(a)

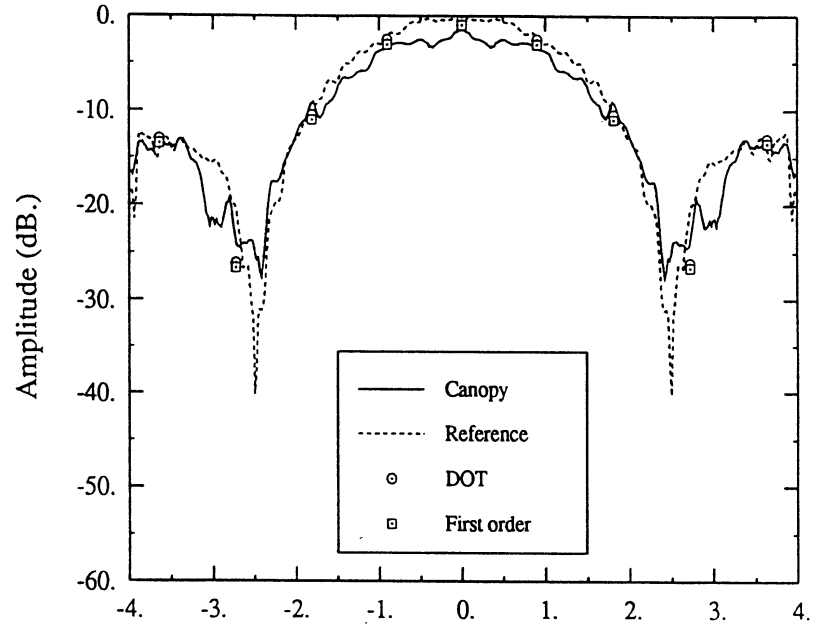

(b)

Figure 4.8 Comparison between the theoretical and experimental transmitted wave patterns for seven rows of stalks at L-band at (a) V-polarization, and (b) H-polarization.

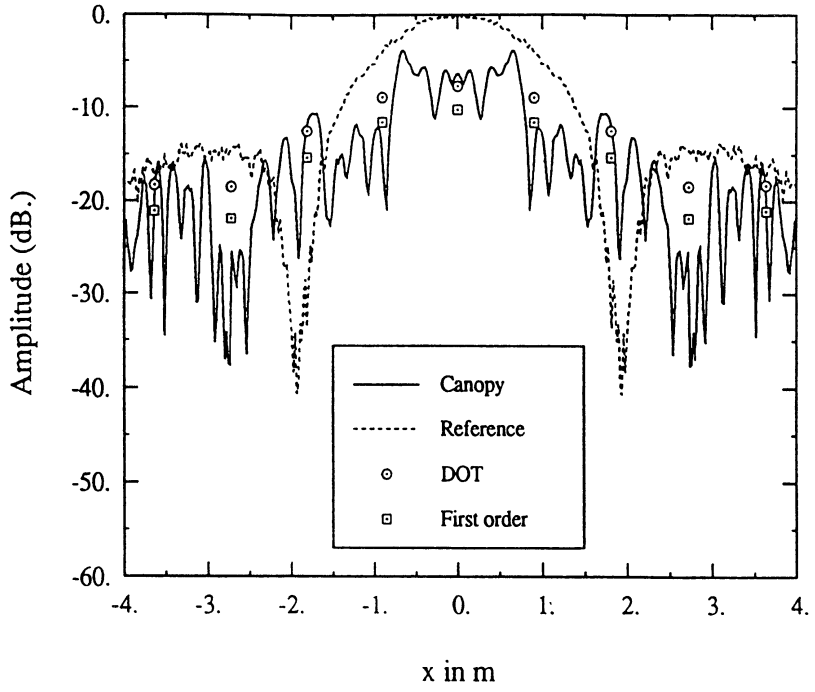

(a)

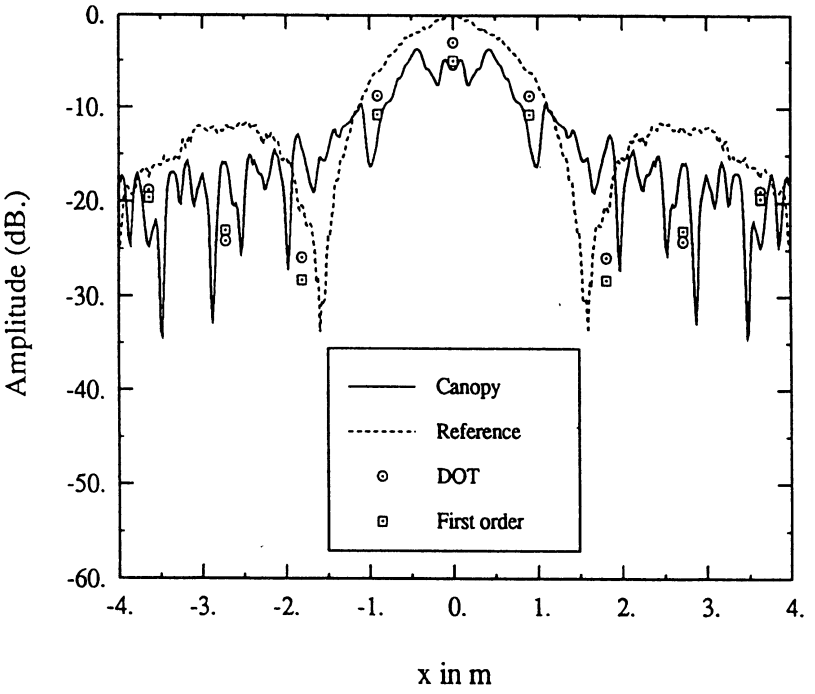

(b)

Figure 4.9 Comparison between the theoretical and experimental transmitted wave patterns for seven rows of stalks at C-band at (a) V-polarization, and (b) H-polarization.

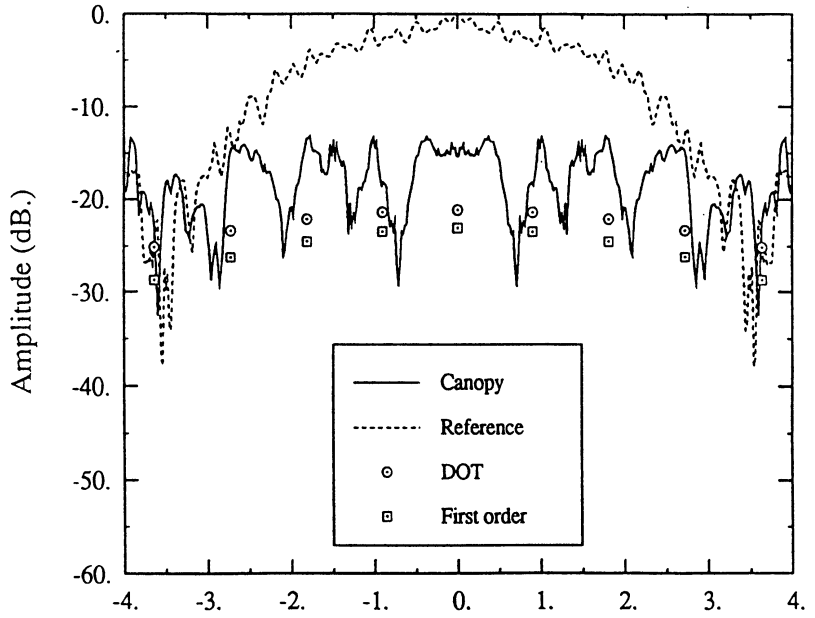

(a)

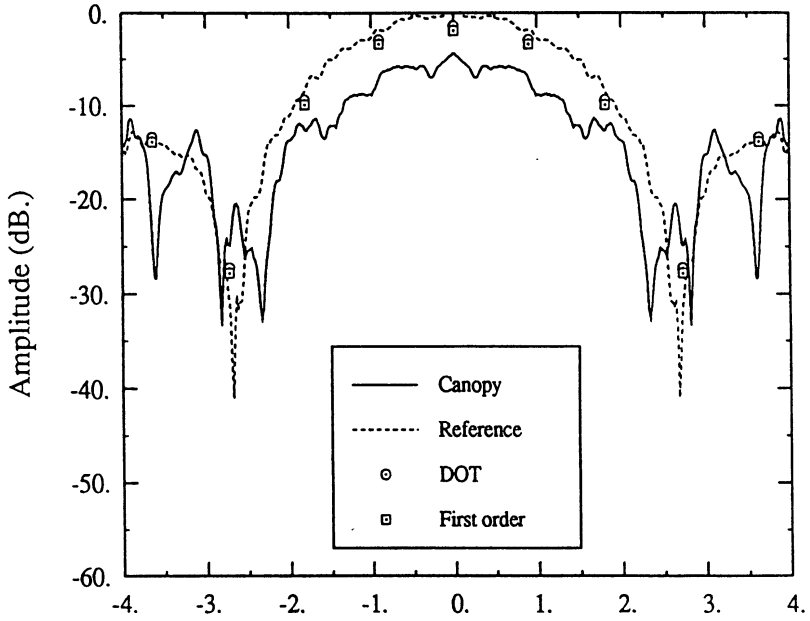

(b)

Figure 4.10 Comparison between the theoretical and experimental transmitted wave patterns for seven rows of stalks and leaves at L-band at (a) V-polarization, and (b) H-polarization.

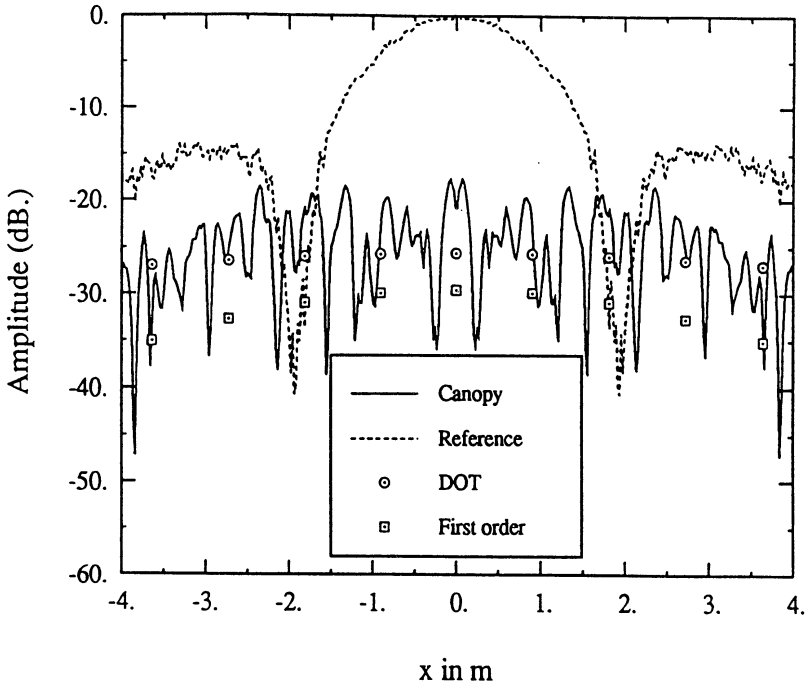

(a)

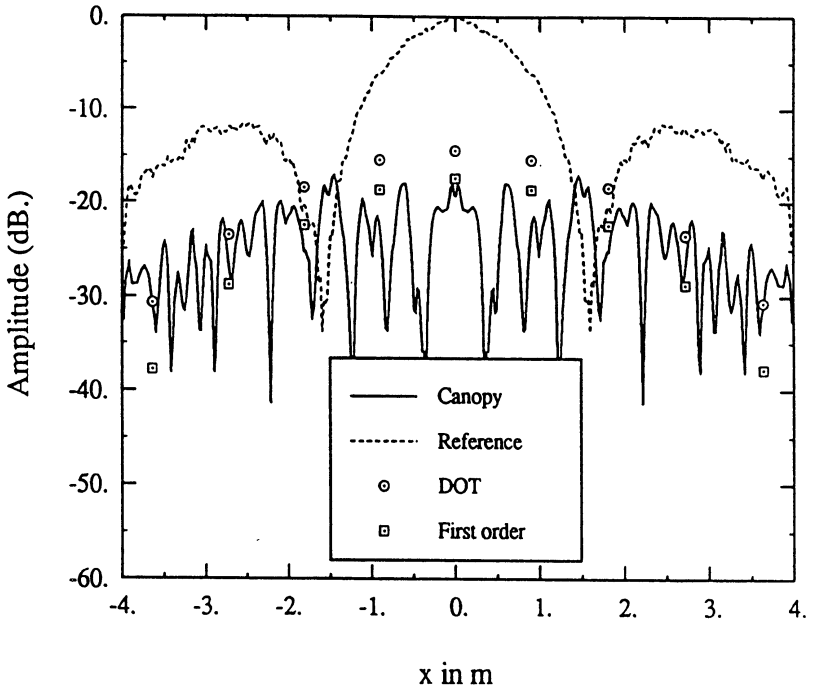

(b)

Figure 4.11 Comparison between the theoretical and experimental transmitted wave patterns for seven rows of stalks and leaves at C-band at (a) V-polarization, and (b) H-polarization.

CHAPTER V

CONCLUSIONS AND RECOMMENDATIONS

5.1 Summary

This thesis examines the problem of microwave propagation through semi-deterministic media such as man-made vegetation canopies. The reason for classifying the earth's vegetation cover into natural terrain and man-made canopies is beacuse of the orderly structure associated with man-made vegetation covers. Location, spacing, and density of plants in a natural vegetation cover tend to be random in character, whereas in man-made vegetation canopies, such as agricultural fields, orchards, and artificial forests, location, spacing, and density of plants are deterministic quantities. Since many cultural vegetation canopies are planted in a row arrangement, a series of experiments were performed on corn canopies to investigate the possible effects that the semi-deterministic arrangement of plants may have on microwave propagation through the canopy. The first set of experiments were performed at oblique incidence angles on a corn canopy. The second set of experiments examined horizontal propagation through corn canopies along different directions. Through these experimentations, it was concluded that for short, man-made canopies, such as a corn field, the canopy behaves like a non-deterministic vegetation cover and random medium techniques for modelling the wave propagation are applicable. For horizontal propagation through the man-made canopy, the periodicity of plants in each row and rows in the whole canopy necessiated propagation models that take the deterministic properties of the canopy into the consideration. Two distinctive cases were

observed. For a canopy of stalks, or when leaves are in the Rayleigh region of the operating frequency, a coherent multiple scattering phenomenon was observed taking place in the canopy. At the frequency regimes where leaves are not weak scatterers, multiple scattering contributions in the canopy were no longer coherently related, eventhough, the periodicity of rows had certain effects on the propagating wave.

In chapter II, a model that characterized wave propagation in a random medium was presented. The model takes both the absorption and scattering losses of the canopy constituents into account and is capable of predicting the average propagation phase changes that the wave experiences. Stalks were modeled as infinitely long dielectric cylinders at all frequencies, but for leaves two frequency domains were considered. In the Rayleigh region, dielectric mixing models were used to represent leaves and in the high frequency region, the physical optics approximation and resistive sheet models were used in modeling the leaves. The models proved useful in characterizing the wave propagation at oblique incidence angles for corn canopies in the L- to X-band region.

Chapter III presented a deterministic model that could effectively explain the coherent multiple scattering phenomenon that is observed due to the presence of stalks. The model is a two-dimensional wave approach and network theory was used to characterize the cascaded row arrangement of the canopy. The periodicity of stalks in each row was modeled through Bragg-mode theory and approximate expressions for the scattering amplitude of each Bragg-mode was presented for deployment in the model. The presence of leaves in the Rayleigh region was modeled by dielectric mixing formulas which was further incorporated into the coherent model. The model has also the advantage of predicting the propagation power and phase patterns of the transmitted wave. Overall, the coherent model proved to be satisfactory for a canopy of stalks and for a full canopy when the leaf dimensions are much smaller than a wavelength.

In chapter IV, the problem of incoherent wave propagation in a periodic vegetation medium was studied. A two-dimensional radiative transfer model for a periodic random

medium was developed. Both the iterative solution of the transfer equation, and a new efficient numerical technique (DOT) were presented. Stalks were modeled as infinitely long dielectric cylinders, and leaves were modeled as thin infinitely long dielectric strips. Comparison between theory and experimental data showed that the model behaves reasonably well for stalks. For a vertically polarized wave, the leaf model proved to be satisfactory, but it did not produce satisfactory results for a horizontally polarized propagating wave.

5.2 Future Work and Recommendations

The models presented in this thesis provided some insight into the problem of wave propagation in man-made vegetation canopies. Development of the theoretical models were based on the experimental data. Therefore, the need for more experimentation on different man-made vegetation canopies is evident. In chapter II, it was concluded that at oblique incidence angles, a random medium approach is applicable when considering microwave propagation in a corn canopy. But, for example, in artificial forests with tall trees, this may not be true. Additional experimental data is needed to reach the conclusion that random medium models are applicable at oblique incidence angles for all man-made vegetation canopies.

Models for leaves in the intermediate frequencies (i.e., when the leaf dimensions are less but comparable to λ) are also needed for incorporation in the volume scattering models. At this point, leaf models are only applicable in the Rayleigh or physical-optics regions.

Three-dimensional radiative transfer models are also needed to take the scattering by leaves into consideration for horizontal polarization. This, however, will definitely make the model more complicated and computationally less efficient.

BIBLIOGRAPHY

BIBLIOGRAPHY

Allen, C. T., and F. T. Ulaby, "Modeling the polarization dependence of the attenuation in vegetation canopies," Proceedings of IGARSS'84 Symposium, August 1984.

Attema, E. P. W., and F. T. Ulaby, "Vegetation modeled as a water cloud," *Radio Sci.*, vol. 13, pp. 357-364, 1978.

Attema, E. P. W., and J. Van Kuilenburge, "Short range scatterometry," *Proceedings of the URSI Commission II Specialist Meeting on Microwave Scattering and Emission from Earth*, Berne, switzerland, pp. 177-183, 1974.

Batlivala, P. P., and F. T. Ulaby, "Feasibility of monitoring soil moisture using active microwave remote sensing," Remote Sensing Laboratory Technical Report 264-12, University of Kansas Center for Research, Inc., Lawrence, KS, 1977.

Brisco, B., and R. Protz, "Corn field identification accuracy using airborne radar imagery," *Can. J. Rem. Sens.*, vol. 6, pp. 14-25, 1980.

Brown, G. S., and W. J. Curry, "A theory and model for wave propagation through foliage," *Radio Sci.*, vol. 17, no. 5, pp. 1027-1036, 1982.

Bush, T., and F. T. Ulaby, "An evaluation of radar as a crop classifier," *Rem. Sens. Environ.*, vol. 7, pp. 15-36, 1978.

Case, K. M., and P. F. Zweifel, Linear Transport Theory, Addison-Wesley, Reading Mass., 1967.

Chandrasekhar, S., Radiative Transfer, Dover Publications, New York, 1960.

Collin, R. E., Antennas and Radiowave Propagation, The McGraw-Hill Book Company, 1985.

Davison, B., Neutron Transport Theory, Oxford University Press, London, 1958.

de Loor, G. P., "Dielectric properties of heterogeneous mixtures containing water," J. Microwave Power, vol. 3, pp. 67-73, 1968.

Dobson, M. C., and F. T. Ulaby, "Soil textural effects on radar response to soil moisture," Remote Sensing Laboratory Technical Report 264-30, University of Kansa Center for Research, Inc., Lawrence, KS, 1979.

El-Rayes, M. A., and F. T. Ulaby, "Microwave dielectric spectrum of vegetation-part I: experimental observations," IEEE Trans. Geosci. Remote Sensing, vol. GE-25, no. 5, pp. 550-557, Sep. 1987.

Engheta, N., and C. Elachi, "Radar scattering from a diffuse vegetation layer over a smooth surface," *IEEE Trans. Geosci. Remote Sensing.*, vol. GE-20, no. 2, pp. 212-216, April 1982.

Eom, J. J., and A. K. Fung, "A scatter model for vegetation up to Ku-band," *Remote Sensing Environ.*, vol. 15, pp. 185-200, 1984.

Eyton, R. J., R. Li, and F. T. Ulaby, "Combined Radar and Landsat Multitemporal Crop Calassification," Remote Sensing Laboratory Technical Report 360-10, University of Kansas Center for Research, Inc. Lawrence, Kansas, February 1979.

Fung, A. K., " Scattering from a vegetation layer," *IEEE Transs. Geosci. Electron.*, vol. 17, no. 1, pp. 1-6, 1979.

Fung, A. K., and F. T. Ulaby, "A scatter model for leafy vegetation," *IEEE Trans. Geosci. Electron.*, vol. GE-16, pp. 281-286, 1978.

Harrington R. F., and J. R. Mautz, "An impedance sheet approximation for thin dielectric shells," *IEEE Trans. Antennas Propag.*, vol. 23, pp. 531-534, 1975.

Ishimaru, A., and R. L. Cheung, "Multiple scattering effects on wave propagation due to rain," Ann. Telecommunications, vol. 35, pp. 373-378, 1980.

Ishimaru, A., Wave Propagation and Scattering in Random Media, vols. 1,2, Academic, New York, 1978.

Karam, M. A., A. K. Fung, and Y. M. Antar, "Scattering models for vegetation samples," *Proceeding of IEEE Geosci. Remote Sensing Symposium*, vol. 2, pp. 1013-1018, 1987.

Kastern, H. W., and M. K. Smit, " Measurements on the backscatter of X-band radiation of seven crops, throughout the growing season," NIWARS publ. no. 47, 1977.

Kong, J. A., Electromagnetic Wave Theory, John Wiley & Son 1986.

Lang, R. H., "Electromagnetic backscattering from a sparse distribution of lossy dielectric scatterers," *Radio Sci.*, 16, 15-30, 1981.

Lang, R. H., and J. S. Sidhu, "Electromagnetic Backscattering from a layer of vegetation: a discrete approach," *IEEE Trans. Geosci. Remote Sensing*, vol. GE-21, no. 1, pp. 62-71, Jan. 1983.

Lee, J. K., and J. A. Kong, "Active microwave remote sensing of an anisotropic random-medium layer," *IEEE Trans. Geosci. Remote Sensing.*, vol. GE-23, no. 6, pp. 910-923, Nov. 1985.

Lopes, A., "Etude experimentale et theorique de l'attentuation et de la retrodiffusion des micro-ondes par un couvert de ble. Application a la teledetection," Ph.D. dissertation, l'Universite Paul Sabatier de Toulouse, 1983.

Low, Karl, "UHF measurements of seasonal field-strength variations in forests," *IEEE Trans. on Vehicular Tech.*, vol. 37, no. 3, pp. 121-124, August 1988.

Ruck, G. T., D. E. Barrick, W. D. Stuart, and C. K. Krichbaum, Radar Cross Section Handbook, Newyork: plenum 1970.

Sarabandi, K., Electromagnetic Scattering From Vegetation Canopies, Ph.D. dissertation thesis, University of Michigan, 1989.

Sarabandi, K., "Study of Periodic Dielectric Surfaces: Simulation with Anisotropic Layers and Application to High Frequency Scattering from Corrugated Convex Bodies," Article 02455-2-T, Radiation Laboratory, University of Michigan, February 1990.

Schuster, A., "Radiation through a foggy atmosphere," *Astrophys. J.*, vol. 21, pp. 1-22, 1905.

Schwering, F. K., Edmond J. Violette, Richard H. Espeland, "Millimeter-wave propagation in vegetation: experiments and theory," *IEEE Trans. Geosci. Remote Sensing*, vol. GE-26, no. 3, pp. 355-367, May. 1988.

Senior, T. B. A., and J. V. Volakis, "Sheet simulation of a thin dielectric layer," *Radio Sci.*, vol.22, no. 7, pp. 1261-1272, Dec. 1987.

Story, A. G., W. H. Johnson, and R. E. Stewart, "Remote measurement of concentration and height of heads of standing grain with microwave energy," *Trans. of the ASAE*, pp. 28-32, 1970.

Stratton, J. A., Electromagnetic Theory, McGraw-Hill Book Company, New York, 1941.

Stutzman, W. L., F. W. Colliver, and H. S. crawford, "Microwave transmission measurements for estimation of the weight of standing pine trees," *IEEE Trans. Antennas. Propagat.*, vol. AP-27, pp. 22-26, 1979.

Tsang, L., J. A. Kong, and R. T. Shin, "Radiative transfer theory for active remote sensing of a layer of nonspherical particles," *Radio Science*, vol. 19, pp. 629-642, 1984.

Tsang, L., J. A. Kong, and R. T. Shin, Theory of Microwave Remote Sensing, John Wiley & Sons, Inc., 1985.

Ulaby, F. T., and E. A. Wilson, "Microwave attenuation properties of vegetation canopies," *IEEE Trans. Geosci. Remote Sensing*, vol. GE-23, no. 5, pp. 746-753, July 1984.

Ulaby, F. T., and M. A. El-Rayes, "Microwave dielectric spectrum of vegetation-part II: dual-dispersion model," *IEEE Trans. Geosci. Remote Sensing*, vol. GE-25, no. 5, pp. 550-557, Sep. 1987.

Ulaby, F. T., and R. P. Jedlicka, "Microwave dielectric properties of plant materials," *IEEE Trans. Geosci. Remote Sensing.*, vol. GE-22, no. 4, pp. 406-415, July 1984.

Ulaby, F. T., C. T. Allen, G. W. Eger, and E. T. Kanemasu, "Relating the radar backscattering coefficient to leaf-area index," *Rem. Sens. Environ.*, vol. 14, pp. 113-133, 1984.

Ulaby, F. T., D. Held, M. C. Dobson, K. C. McDonald, and T. B. A. Senior, "Relating polarization phase difference of SAR signals to scene properties," *IEEE Trans. Geosci. Remote Sensing*, vol. GE-25, no. 1, pp. 83-92, Jan. 1987.

Ulaby, F. T., K. Sarabandi, K. McDonald, M. Whitt, and M. C. Dobson, "Michigan microwave canopy scattering model," *Int. J. Remote Sensing*, vol. 11, no. 7, pp. 1223-1252, 1990.

Ulaby, F. T., R. K. Moore, and A. K. Fung, Microwave Remote Sensing: Active and Passive, vol. 1, Addison-Wesley, Publishing Co., Reading MA, 1982.

Ulaby, F. T., R. K. Moore, and A. K. Fung, Microwave Remote Sensing: Active and Passive, vol. 2, Addison-Wesley, Publishing Co., Reading MA, 1982.

Ulaby, F. T., R. K. Moore, and A. K. Fung, Microwave Remote Sensing: Active and Passive, vol. 3, Artech House, 1986.

Van Bladel, J, Electromagnetic Fields, Hemisphere Publishing Corporation, New York, 1985.

van de Hulst, H. C., Light Scattering by Small Particles, pp. 32-33, Dover, 1981.